# Performance of Drained and Undrained Flexible Pavement Structures under Wet Conditions

# Test Data from Accelerated Pavement Test Section 543-Drained

Draft Report Prepared for
California Department of Transportation

By:

**Manuel O. Bejarano, John T. Harvey, Abdikarim Ali, Mark Russo, David Mahama, Dave Hung, and Pitipat Preedonant**

February 2004

**Pavement Research Center**
**Institute of Transportation Studies**
**University of California at Berkeley**

**TABLE OF CONTENTS**

**LIST OF FIGURES**

**LIST OF TABLES**

## EXECUTIVE SUMMARY

This report is the first in a series of four reports that describe the results of accelerated pavement tests on full-scale pavements with "wet" base conditions at the Pavement Research Center, located at the University of California Berkeley Richmond Field Station (RFS). The report contains a summary of the results and associated analysis of a pavement section comprised of three lifts of asphalt concrete, an asphalt treated permeable base (ATPB) layer, and untreated aggregate base layers on top of a prepared subgrade and designated as Section 543. The pavement section is a termed a "drained' pavement due to the inclusion of an ATPB layer between the asphalt concrete layers and the untreated aggregate base. Tests on this test section have been performed as part of the Goal 5 Accelerated Test Program for the evaluation of drained and undrained pavements under conditions of water infiltration.

The main objectives of the test program are:

- Develop data to quantitatively compare and evaluate the performance of drained and undrained asphalt concrete pavements under "wet" conditions. Wet conditions intend to simulate approximate surface water infiltration rates that would occur in a badly cracked asphalt concrete layer along the north coast of California during a wet month.
- Measure the effectiveness of the drained pavement in mitigating surface water infiltration and thereby preventing a decrease in stiffness and strength of the unbound layers.

Other objectives include:

- Quantify elastic moduli of the pavement layers,
- Quantify the stress dependence of the pavement layers, and
- Determine the mechanics of failure of the pavement structure.

Heavy Vehicle Simulator (HVS) testing was begun in May 1999 and was completed in March 2000 after the application of more than $1.1 \times 10^6$ load repetitions. At the end of the test, the pavement section had more than 20 mm of surface rutting, and a surface crack density of 2.5 m of cracks per square meter ($m^2$) of pavement.

Chapter 2 describes the test program for Section 543. Design and as-constructed thicknesses of the pavement components were as follows:

| Layer | Design Thickness | As-Constructed Thickness |
|---|---|---|
| Asphalt Rubber Hot Mix | 40 mm | 37 mm |
| Dense Graded Asphalt Concrete | 148 mm | 141 mm |
| Asphalt Treated Permeable Base | 75 mm | 69 mm |
| Aggregate Base | 182 mm | 181 mm |
| Aggregate Subbase | 215 mm | 187 mm |

The test program was conducted in four stages: Stage 1, definition of the initial condition of the section under conditions of no water infiltration; Stage 2, establishing the initial structural condition of the section under water infiltration; Stage 3, HVS trafficking under conditions of water infiltration; and Stage 4, definition of the structural condition of the section after HVS trafficking.

Data collection for Stages 1, 2, and 4 were based on the deflection measurements obtained with a Dynatest Falling Weight Deflectometer (FWD), and moisture content measurements. Stage 4 included some destructive tests to verify the results obtained during Stage 3.

Data collection for Stage 3 is summarized in Table 3. Loading, applied by dual radial tires inflated to a pressure of 720 kPa, consisted of 236,000 repetitions of a 40-kN load followed by 332,000 repetitions of an 80-kN load, followed by 629,000 repetitions of a 100-kN load. At

the termination of loading, surface rutting and fatigue cracking were visible throughout the test section. Lateral wander of the wheels was distributed across the 1-m width of the test section.

Pavement responses were obtained using Multiple Depth Deflectometers (MDD), the Road Surface Deflectometer (RSD), and the laser profilometer. Fatigue cracking was photographically recorded and analyzed using a digital image analysis procedure. Thermocouples were used to measure air and pavement temperatures at various depths in the asphalt concrete. To maintain a consistent temperature around 20ºC, a temperature control cabinet was installed. Chapter 3 summarizes the data obtained during the course of loading and associated analyses.

Section 543 rapidly failed due to surface rutting during trafficking at the 100-kN load. Failure resulted form stripping in the ATPB layer and loss of adhesion in the prime coat placed on top of the aggregate base. Stripping was caused by the high shear stresses experienced under the 100-kN load present in the ATPB layer and water infiltration, which softened the binder in the ATPB. As the binder gradually washed out of the ATPB, the ATPB started losing its stiffness and at the same time fine particles from the aggregate base infiltrated the voids in the ATPB. Results from back-calculation of FWD tests indicated that the stiffness of the ATPB was reduced to that of an untreated aggregate base. Percolation tests indicated that the permeability of the ATPB in the trafficked area was reduced from 1 cm/s to 0.001 cm/s. This prevented water from draining from the ATPB, thus contributing to the stiffness reduction.

Results of the analysis reported in Chapter 4 indicate that if integrity of the ATPB had been maintained, the section would likely have failed by fatigue cracking rather than surface rutting after about 2,300 million ESALs at a reliability level of 50 percent. Actually, only 35 million ESALs were applied to the test section based on the use of the Caltrans load equivalency

factor of 4. An analysis was also conducted on a pavement section in which the ATPB layer was replaced by an equivalent thickness of DGAC; i.e., 40 mm of DGAC was substituted for the 75 mm of ATPB. Analysis of this pavement section using the same procedure as above indicated that this equivalent section would sustain about 3,300 million ESALs prior to failure in fatigue, also at a 50 percent reliability level. Internal drainage was not included in the alternate structure to intercept water entering through the pavement surface. Entry of water from the surface can be mitigated, as noted in earlier studies, by properly compacting the asphalt concrete and using sufficient thickness to mitigate the potential for load associated cracking. In addition, by increasing the degree of compaction in the aggregate base and subbase, the contribution of rutting from these layers would be minimal, all of which would eliminate the need for the ATPB.

The analysis indicated that surface rutting in Section 543 could be attributed to the reduced stiffness of the ATPB layer. As a result, rutting occurred both in the ATPB and the aggregate base. The stiffnesses of the untreated aggregate base and subbase are dependent on the stress state. Reduced stiffness of the ATPB resulted in an increase in the stress in the aggregate base, thus contributing to its increased rutting propensity and likely contributing to the observed surface rutting as well.

If ATPB is to remain effective as a drainage layer, it will be necessary to ensure that the material does not strip and that an adequate filter be provided adjacent to the ATPB to minimize the intrusion of fines. In addition, edge and transverse drains need to be maintained in order to prevent clogging. If not, water will be retained in the ATPB resulting in the type of performance observed in this test.

Chapter 5 contains conclusions, which are briefly summarized as follows:

The ATPB failed due to stripping and the prime coat did not serve as an adequate barrier to prevent fines from the aggregate base from intruding into the ATPB. Stripping was caused by the high shear stress produced by the 100-kN load and presence of water. The ATPB layer became clogged with fines from the underlying aggregate base, thereby reducing the permeability of the ATPB layer from 1 cm/s to 0.001 cm/s. This created an increased degree of saturation within the pavement that quickly contributed to deterioration in the performance of the pavement section.

Section 543 failed initially due to surface rutting. The reduced stiffnesses in the ATPB and aggregate base contributed to the rapid increase in surface rutting. The reduced stiffnesses of these layers also resulted in increased tensile strain in the asphalt concrete layers. This in turn resulted in a rapid increase in surface cracking as well.

## 1.0 INTRODUCTION

This report presents the data from the accelerated pavement testing (APT) program conducted with the Heavy Vehicle Simulator (HVS) on test Section 543. This section is part of the APT program described in the test plan for CAL/APT Goal 5, "Performance of Drained and Undrained Flexible Pavement Structures under Wet Conditions."(*1*) This document provides detailed information on the Goal 5 program.

Three sections were available from the Goal 3 study for HVS loading as part of the Goal 5 investigation. Section 543 had a 38-mm ARHM-GG (asphalt rubber hot mix—gap graded) surface course and an ATPB (asphalt treated permeable base) drainage layer. Section 544 had a 38-mm ARHM-GG surface course and only the untreated aggregate base layer (undrained). Section 545 had a 75-mm DGAC (dense graded asphalt concrete) surface course and only the untreated aggregate base layer (undrained).

The objective for the test on Section 543 was to evaluate the performance of a typical "drained" pavement section under wet conditions. The "drained" pavement section in this case is comprised of a 75-mm layer of ATPB between the asphalt concrete and the aggregate base and a perforated pipe drainage system at the shoulder. An "undrained" pavement is a conventional pavement with a Class 2 untreated aggregate base and subbase, and without an ATPB layer.

The purpose of the ATPB layer and drainage system is to intercept water entering the pavement either through cracks in the asphalt concrete or through very permeable asphalt concrete and carry it out of the pavement before it reaches the unbound layers, where it can significantly reduce their strength and stiffness characteristics.

Wet conditions for Section 543 were intended to simulate approximate surface infiltration rates that would occur along the north coast climate region in California (*2*) during a wet month for a badly cracked asphalt concrete layer. Because the surface course of Section 543 was

initially uncracked, water was introduced through small holes drilled through the asphalt concrete and into the ATPB. This was intended to simulate water infiltrating from adjacent lanes or from water entering pavement constructed in cuts.

## 1.1 Objectives

The main objective of this test program was to evaluate the effectiveness of drained pavements in preventing a decrease in stiffness and strength of unbound materials (base, subbase, and subgrade) due to an increase in water content produced by water infiltration. Other objectives included:

- Comparison of the long term performance of drained and undrained pavements under wet conditions;
- Quantification of elastic moduli of the various pavement layers using deflections obtained from a slow moving wheel and from the falling weight deflectometer;
- Determination of the failure mechanism(s) of the pavement sections; and
- Evaluation of the effectiveness of non-destructive and partially destructive methods for assessing the pavement structural condition.

An earlier report of a laboratory study together with individual reports covering the results of HVS loading on each of the three test sections and a summary and evaluation of the results of the three sections will complete the Goal 5 study.(*3–5*)

## 1.2 Test Sequence

The sequence of HVS testing of the three test sections was 1) Section 543 (drained), 2) Section 544 (undrained), and 3) Section 545 (undrained). This report presents the results of the loading tests on Section 543.

## 1.3 Organization of Report

Chapter 2 of the report contains a description of the test program for Section 543, including the loading sequence, instrumentation, and data collection scheme. Chapter 3 presents a summary and analysis of the data collected during the test, including back-calculated moduli from deflection tests and their effectiveness to establish structural condition. Chapter 4 presents the mechanistic pavement analyses used to evaluate the comparative performance of the three test sections. Chapter 5 contains a summary of the results and conclusions.

## 2.0 TEST PROGRAM

The following sections present the test section layout, environmental conditions encountered during the test, instrumentation used to collect data, and the test program.

### 2.1 Test Section Layout

Section 543 is 8 m long by 1 m wide, divided into sixteen 0.5-m long "stations," as shown in Figure 1. The pavement was constructed with a two-percent cross slop and 0.5-percent longitudinal slope in all layers above the aggregate subbase. The design thickness, pavement layers, and as-built layer thicknesses are summarized in Table 1. The as-built pavement thicknesses were obtained from direct measurements on the non-trafficked portion of a trench dug in the section at the conclusion of HVS loading.

**Table 1 Pavement Layer Thicknesses for Section 543**

| Layer | Design Thickness (mm) | As-Constructed Thickness (mm) |
|---|---|---|
| Asphalt Rubber Hot Mix | 40 | 37 |
| Dense Graded Asphalt Concrete | 148 | 141 |
| Asphalt Treated Permeable Base | 75 | 69 |
| Aggregate Base | 182 | 181 |
| Aggregate Subbase | 215 | 187 |

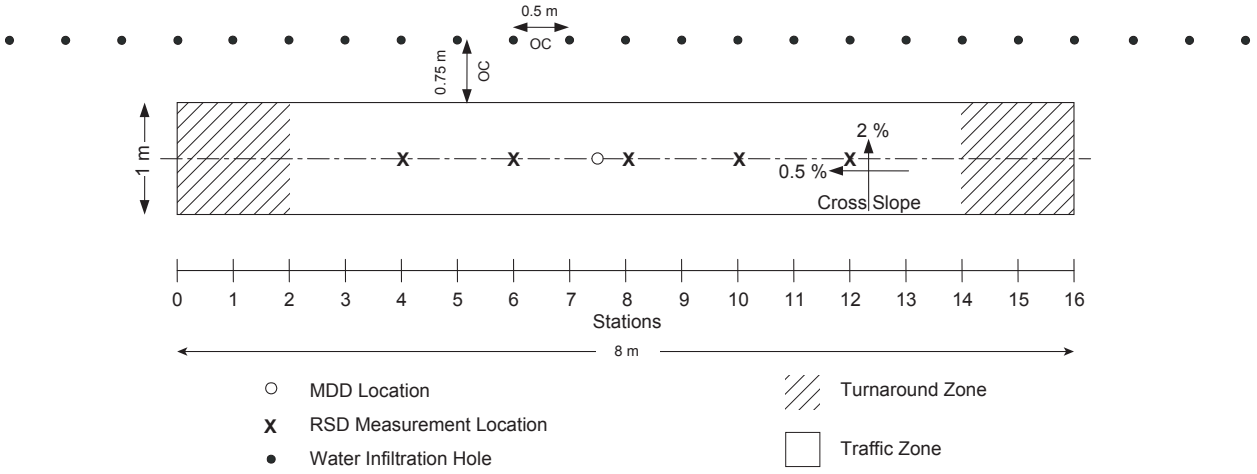


**Figure 1. Section 543 layout and locations of MDD and RSD measurements.**

## 2.2 Environmental Conditions

The accelerated pavement test was conducted under wet conditions at a pavement of about 20ºC. Water infiltration into the treated permeable base was controlled at a rate of 9.7 liters per hour over an area 7.4 m wide by 12 m long, determined to be representative of the rate of water infiltration into a pavement during an average peak week in Eureka, California of 51.3 mm rainfall.(*2*)

The water was introduced through a line of holes parallel to and upslope from the HVS test section, as shown in Figures 1 and 2. An electronic valve and timer system continuously controlled water ingress to the pavement during the test.

For the test, the actual target pavement temperature at a pavement depth of 50 mm was 20 ± 2ºC. This was maintained by a temperature control box surrounding the HVS.

## 2.3 Instrumentation

Instrumentation and measuring equipment used on Section 543 included:

- Multiple Depth Deflectometers (MDDs) to measure deflection and permanent deformation at various depths in the pavement section;
- a Road Surface Deflectometer (RSD) to measure surface deflections,
- a laser profilometer to monitor surface rutting;
- thermocouples to monitor pavement temperatures; and
- hydroprobes and tensiometers to monitor moisture content in the unbound layers.

Figure 1 shows the locations of the MDDs in the test section as well as the locations for the RSD measurements. Laser profilometer measurements were obtained at each of the numbered stations. Figure 2 contains a cross section of the pavement illustrating the locations of

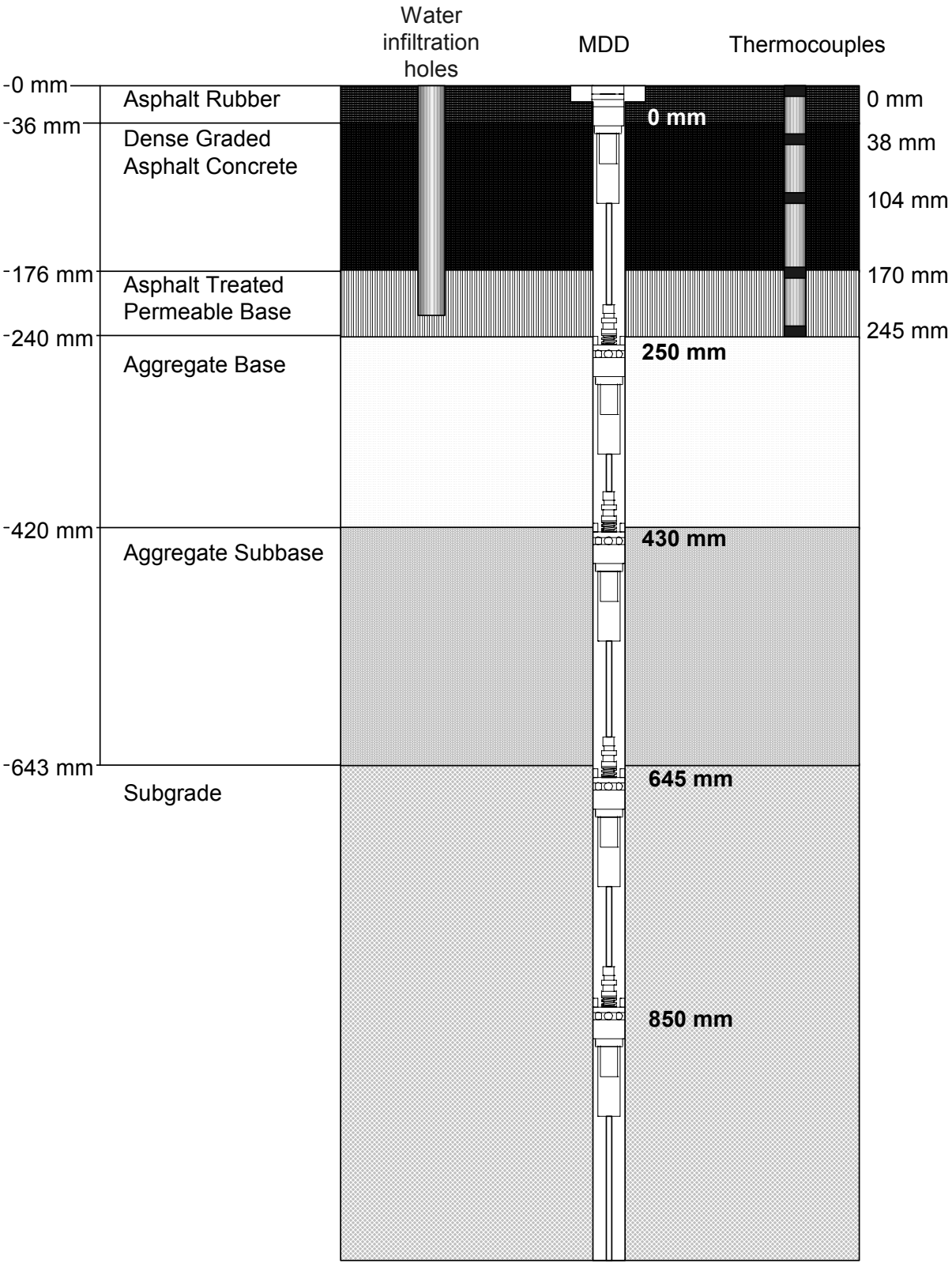


**Figure 2. Depths of MDDs, thermocouples, and water infiltration holes in Section 543.**

the MDDs, thermocouples, and the depth of the water infiltration holes. For a complete description of the instrumentation used for this study, refer to Reference (*6*).

## 2.4 Test Program

The test program consisted of four stages, as shown in Figure 3. These stages can be summarized as follows:

- Stage 1: Prior to introduction of water, water content determinations and FWD tests were conducted to establish initial moisture conditions and structural response
- Stage 2: During the water infiltration period, water content measurements and FWD tests were conducted to establish moisture conditions and the structural response before HVS testing.
- Stage 3: The pavement was subjected to HVS loading with water infiltrating the pavement. Pavement monitoring continued throughout the loading period using the instrumentation and test equipment described in Section 2.3.
- Stage 4: After HVS trafficking, a detailed forensic study was conducted which included FWD tests, trenching, and sampling of the pavement materials for laboratory tests.

### 2.4.1 Falling Weight Deflectometer Testing

FWD tests were conducted to monitor surface deflections and changes in the layer moduli of the pavement section by back-calculation procedures. Loads of 20, 40, and 60 kN were used with the deflection sensors (geophones) spaced at 0, 200, 300, 600, 900, 1200, and 1500 mm from the loading plate. Surface deflections for the various loads were normalized to a 40-kN load and back-calculated moduli were determined for this load condition.

## Section 543 Test Program Schedule

| ID | Task Name |
|---|---|
| 1 | **Stage 1: No water infiltration** |
| 2 | Section 543 |
| 3 | **Stage 2: Water infiltration** |
| 4 | Section 543 |
| 5 | **Stage 3: HVS Testing and water infiltration** |
| 6 | Section 543 |
| 7 | **Stage 4: Forensic Activities** |
| 8 | Section 543 |

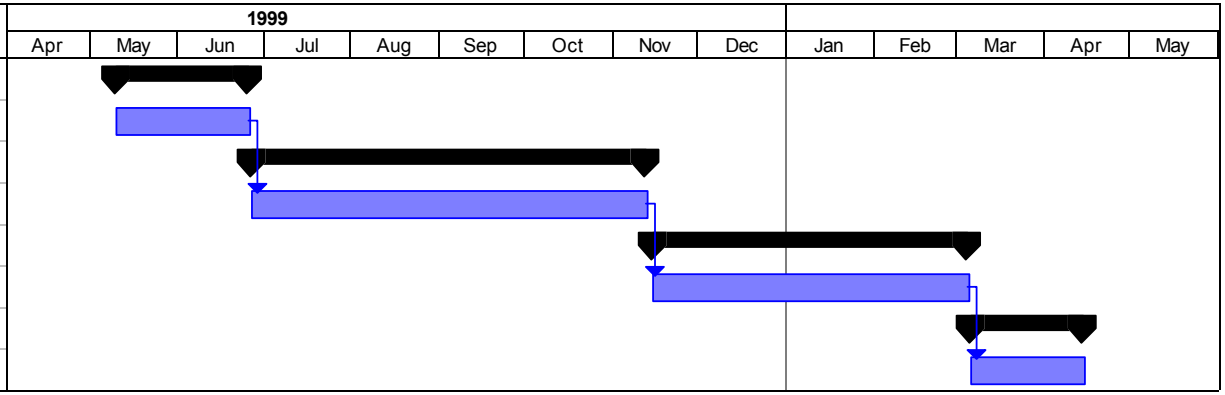


**Figure 3. Schedule for test program.**

### 2.4.2 Heavy Vehicle Simulator Trafficking

For trafficking of Section 543, the HVS was equipped with dual truck tires, representing one half of a single axle. Load was applied through two Goodyear radial tires G159 11R 22.5) inflated to a pressure of 720 kPa. Table 2 presents the trafficking loads, loading sequence, and the associated HVS load repetitions.

**Table 2 HVS Loading Sequence for Section 543**

| HVS Load (kN) | HVS Repetitions |
|---|---|
| 40 | 0 to 236,588 |
| 80 | 236,588 to 568,356 |
| 100 | 568,356 to 1,197,685 |

The test wheel trafficked the entire length of the 8-m long test section. Lateral wander over the 1-m width of the test section was programmed to simulate representative traffic wander in a typical highway lane. The 1-m sections at both ends of the trafficked area (Stations 0–2 and 14–16 in Figure 1) serve as "turnaround zones" in which the test wheel decelerates and accelerates. Pavement performance was evaluated for the 6 m length between these turnaround zones (Station 2–14) in which the HVS wheel speed is constant.

### 2.4.3 Data Collection

Table 3 summarizes the data collection sequence for Section 543.

**Table 3 Data Collection Program**

| HVS Repetitions | Laser Profilometer | Multi-Depth Deflectometer | Road Surface Deflectometer | Crack Monitoring |
|---|---|---|---|---|
| 0 | X | 40 kN | 40 kN | |
| 12005 | X | 40 kN | 40 kN | |
| 28881 | X | 40 kN | 40 kN | |
| 46323 | X | 40 kN | 40 kN | |
| 58791 | X | 40 kN | 40 kN | |
| 89619 | X | 40 kN | 40 kN | |
| 124341 | X | 40 kN | 40 kN | |
| 159071 | X | 40 kN | 40 kN | |
| 197535 | X | 40 kN | 40 kN | |
| 236588 | X | 40 kN | 40 kN | |
| 285201 | X | 40 kN | 40 kN | |
| 331855 | X | 40 kN | 40 kN | |
| 370225 | X | 40 kN | 40 kN | |
| 406098 | X | 40 kN | 40 kN | |
| 457197 | X | 40 kN | 40 kN | |
| 496169 | X | 40 kN | 40 kN | |
| 568356 | X | 40, 80, 100 kN | 40, 80, 100 kN | |
| 638196 | X | 40, 100 kN | 40, 100 kN | |
| 694154 | X | 40, 100 kN | 40, 100 kN | |
| 779237 | X | 40, 100 kN | 40, 100 kN | |
| 856127 | X | 40, 100 kN | 40, 100 kN | |
| 888069 | | | | |
| 927069 | X | 40, 100 kN | 40, 100 kN | |
| 939343 | | 40, 100 kN | | X |
| 994171 | X | 40, 100 kN | 40, 100 kN | |
| 1057304 | X | 40, 100 kN | 40, 100 kN | X |
| 1114295 | X | 40, 100 kN | 40, 100 kN | X |
| 1197685 | X | 40, 100 kN | 40, 100 kN | X |

## 3.0 SUMMARY OF TEST DATA

This chapter provides a summary of the test data collected for during the four stages of testing. Test data include:

- Stage 1: temperature, moisture content, and FWD data
- Stage 2: temperature, moisture content, and FWD data
- Stage 3: temperature, moisture content, permanent deformation, elastic deflection, and crack progression data
- Stage 4: FWD and forensic study data.

### 3.1 Temperature and Moisture Condition Data

Temperature and water content data were gathered throughout the test program for Section 543. These data are summarized in the following sections.

#### 3.1.1 Temperature Data

This section includes a summary of air and pavement temperatures during FWD tests and HVS loading.

Air temperatures were automatically collected during FWD tests by sensors incorporated in the FWD equipment. Pavement temperatures were estimated from air temperatures using Bell's equation. Average air and pavement temperatures during FWD tests conducted during Stages 1, 2, and 4 are summarized in Table 4. Additional FWD data with temperature are presented in Section 3.6.

**Table 4 Air and Pavement Temperatures for Section 543**

| Stage of Testing | Equipment | Average Temperature (°C) | |
|---|---|---|---|
| | | Air | Pavement |
| 1 | FWD on-board sensor | 24 | 19 |
| 2 | FWD on-board sensor | 21 | 17 |
| 3 | HVS thermocouples | 18 | 20 |
| 4 | FWD on-board sensor | 15 | 14 |

Figure 4 shows average daily temperatures inside Building 280 at the University of California Berkeley Richmond Field Station, where the HVS was located, and average air temperatures inside the HVS temperature control box. The average daily temperatures were calculated from hourly temperatures recorded during testing. Average air temperatures monitored inside the temperature control box were uniform with minimal variations. The average air temperature inside the temperature control box during testing was 18.3ºC.

Average daily asphalt concrete temperatures for Section 543 are shown in Figure 5. These temperatures were recorded at various depths in the pavement: overlay, upper lift of the asphalt concrete, lower lift of the asphalt concrete, and ATPB layer. Generally, the asphalt concrete temperatures were fairly uniform and varied only slightly with air temperature inside the temperature control box. Average temperatures in the asphalt concrete layers were approximately 6 percent higher than the average air temperatures inside the control box with an overall average of about 19.5ºC.

### 3.1.2 Rainfall and Moisture Content Data

Figure 6 shows average monthly rainfall data collected at the National Weather Service weather station in Richmond, California. Figures 7 and 8 show average volumetric moisture contents for the aggregate base, subbase, and subgrade materials obtained using a hydro-probe test device. Depths of moisture content measurements are summarized in Table 5.

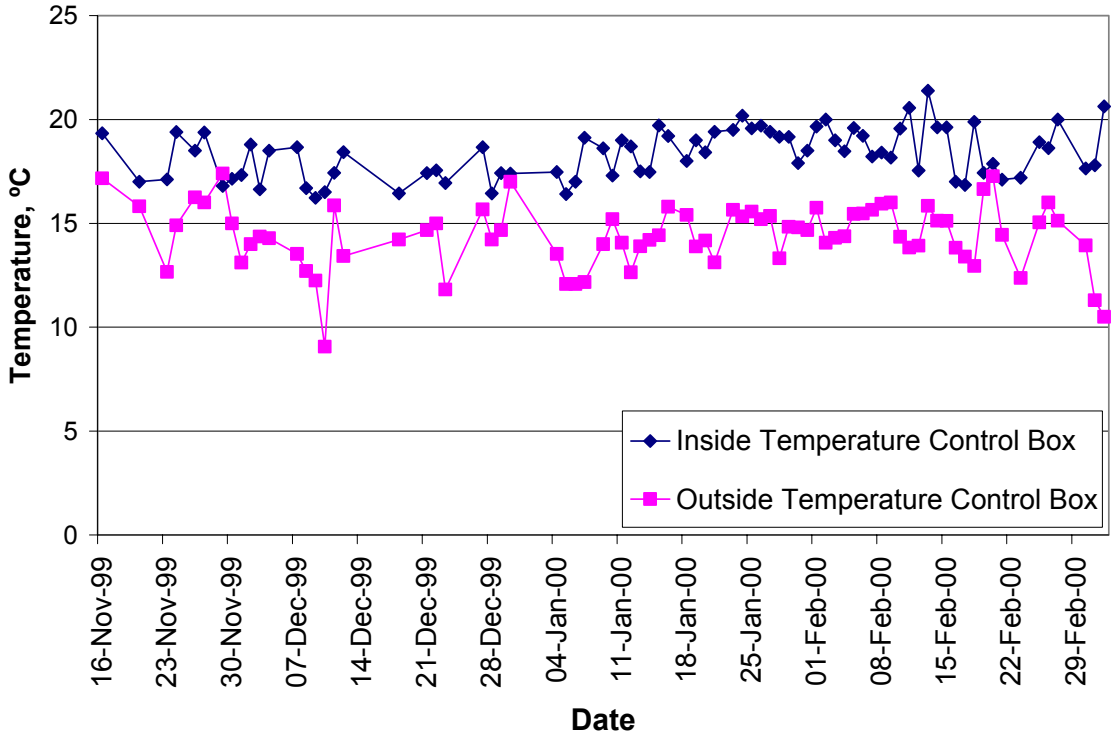


**Figure 4. Average air temperatures inside and outside HVS temperature control box, Section 543.**

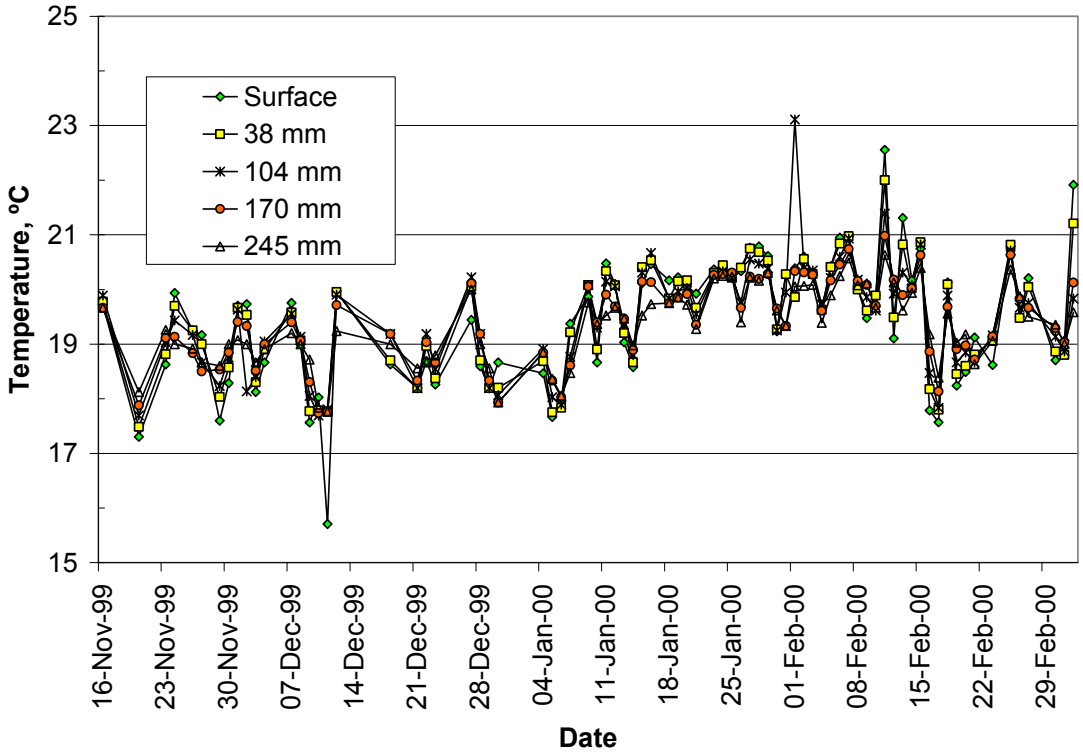


**Figure 5. Pavement temperatures at depth, Section 543.**

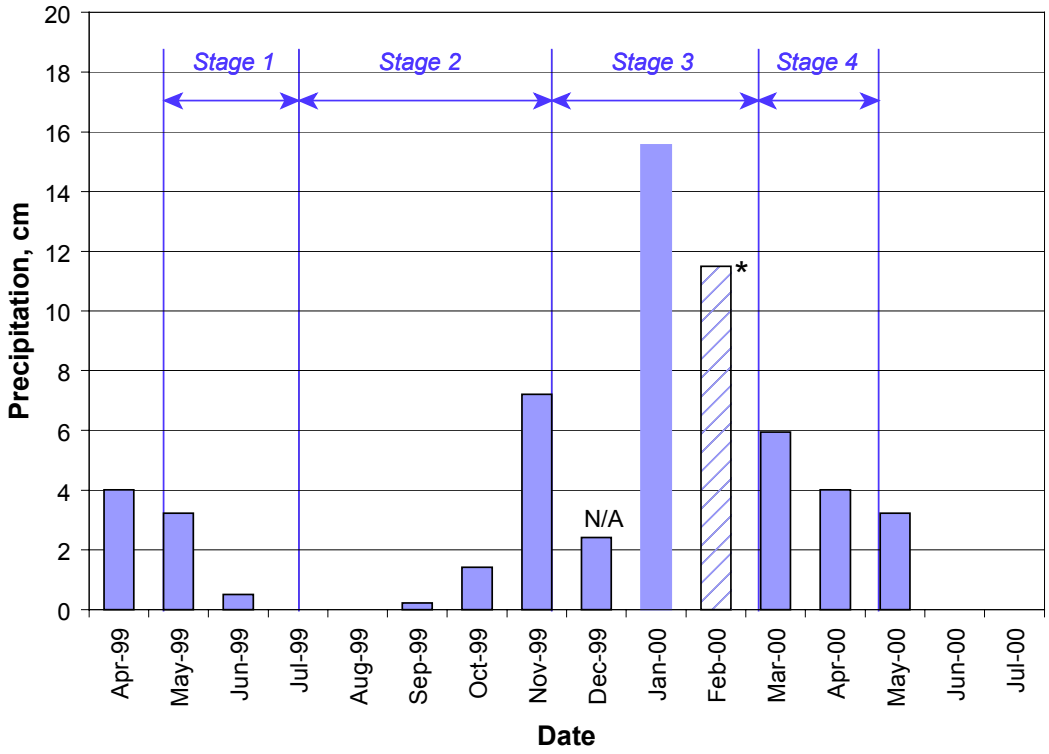


*Note: Data was not available for Richmond, California weather station for the month of February 2000. Data shown here for February 2000 is from nearby National Climate Data Center weather station in Berkeley, California.

**Figure 6. Average monthly rainfall during testing of Section 543.**

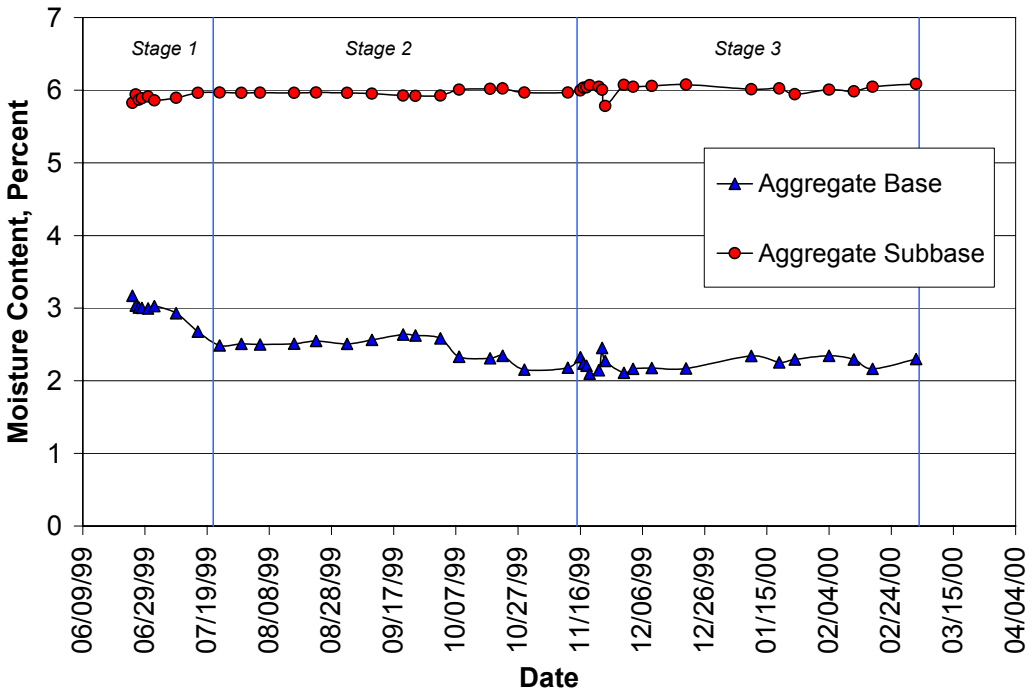


**Figure 7. Volumetric moisture content in aggregate base and subbase layers.**

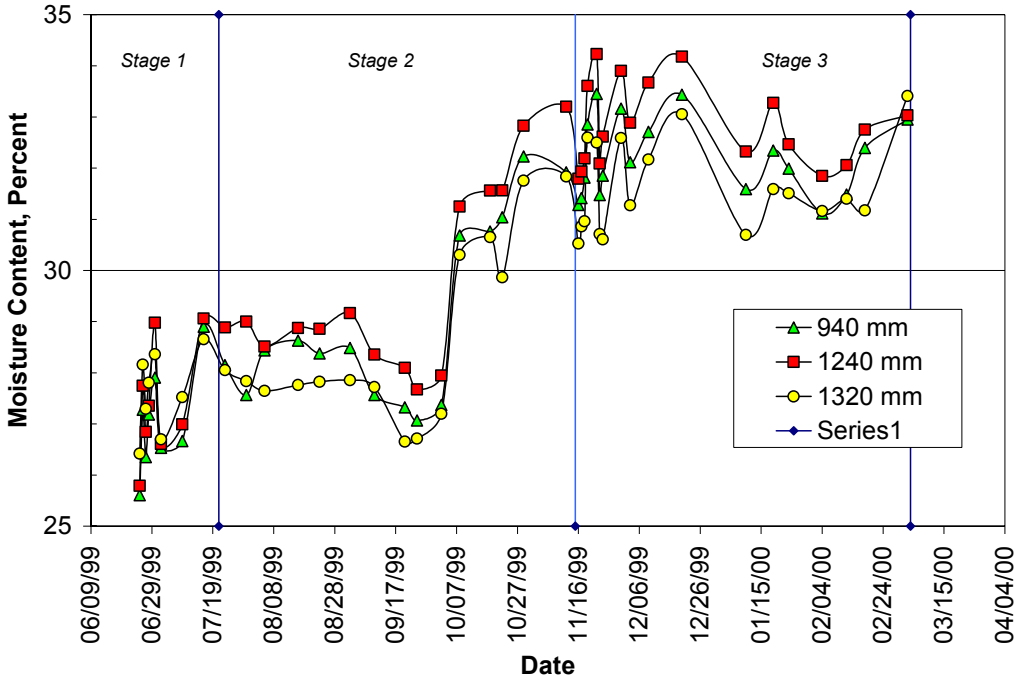


**Figure 8. Volumetric moisture content in the subgrade at various depths from the surface.**

**Table 5 Depths of Moisture Content Measurements**

| Unbound Layer | Depth from Surface, mm |
|---|---|
| Aggregate Base | 468 and 508 |
| Aggregate Subbase | 667 and 707 |
| Subgrade | 940, 1240, and 1320 |

Moisture contents of the base and subbase, Figure 7, were averaged across measurements taken at those layers. These data show that the moisture content of the aggregate base and subbase were not affected by the water that infiltrated from the surface through the infiltration holes. It is possible that the permeability of the aggregate base was sufficiently small to prevent water intrusion. Moisture content data for the subgrade, Figure 8, show variations that followed the precipitation trends. The subgrade soil at the test site was not isolated from the surrounding soil outside of Building 280, thus, being subjected to the same seasonal variations.

Figure 9 shows moisture contents from aggregate samples extracted from two boreholes drilled at the end of the test program. The two boreholes were located at Station 5 and 13.[1]

Volumetric moisture contents were estimated from gravimetric water contents using a bulk density in the aggregate base of 2.200 kg/m$^3$. This bulk density was obtained using the sand-cone method. These data indicate higher volumetric moisture contents for the sampled material than those obtained with the hydroprobe.

### 3.2 Permanent Deformation

Permanent deformation data were gathered using the laser profilometer and multi-depth deflectometers (MDDs). The following sections summarize these data.

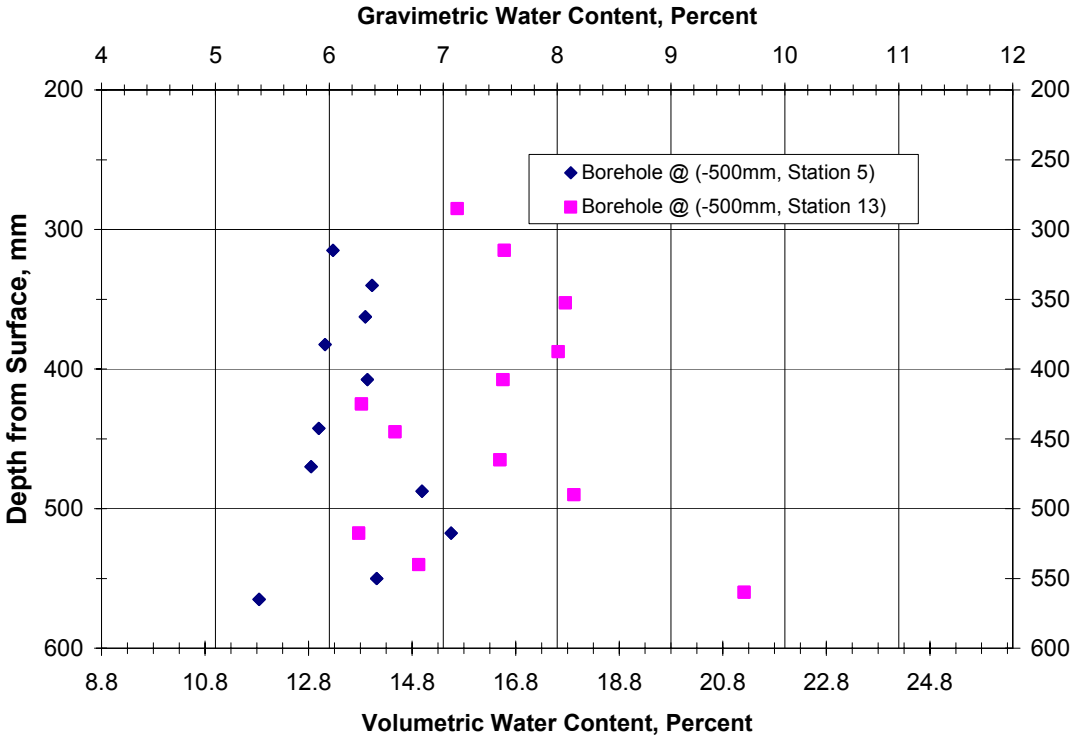


**Figure 9. Moisture contents from aggregate samples extracted during forensic study.**

[1] Figure 3.6 in Section 3.8, which discusses the forensic studies, shows locations of all of the boreholes placed in the test section. These two boreholes were located at a distance of ~500 mm, as shown in Figure 3.6.

### 3.2.1 Surface Rutting Measured with the Laser Profilometer

Figure 10 shows accumulated average maximum rut depth for Section 543. A rapid rate of permanent deformation is note under the 100-kN trafficking load compared to the 40-kN and 80-kN trafficking loads. Table 6 summarizes average rates of rutting for each of the three levels of traffic.

Figure 11 shows the rut depth distribution at the end of the 40-, 80-, and 100-kN trafficking loads. The rut distribution is fairly uniform throughout the section with greater rutting localized around Stations 3 and 13. The center of the HVS wheelpath is marked as 0 mm transverse distance.

**Table 6 Average Rate of Rutting at Three Traffic Loads**

| Trafficking Load | Rate of Rutting (mm/million load repetitions) |
|---|---|
| 40 kN | 3.8 |
| 80 kN | 7.7 |
| 100 kN | 30.0 |

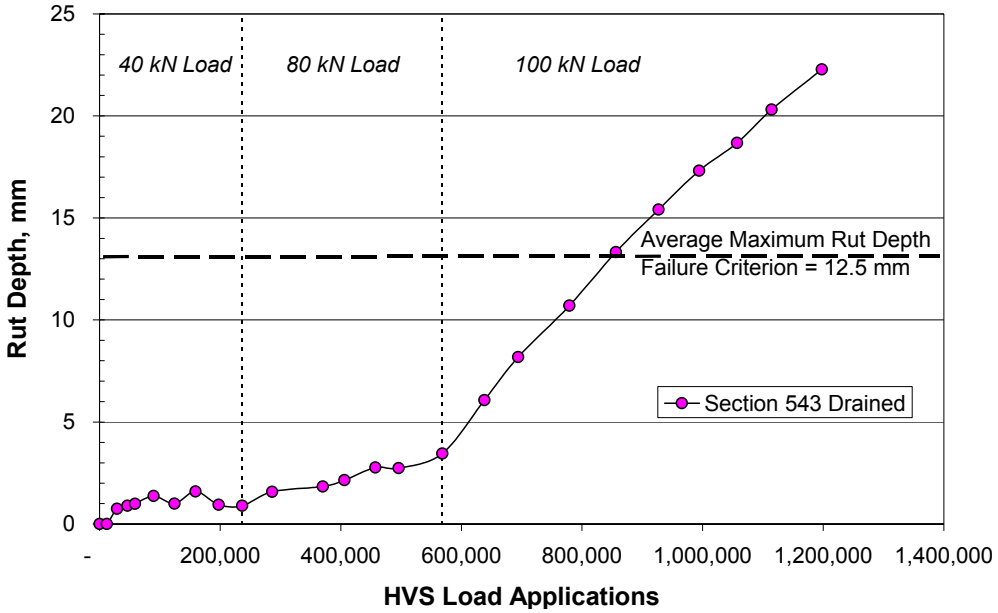


**Figure 10. Average maximum rut depth for Section 543.**

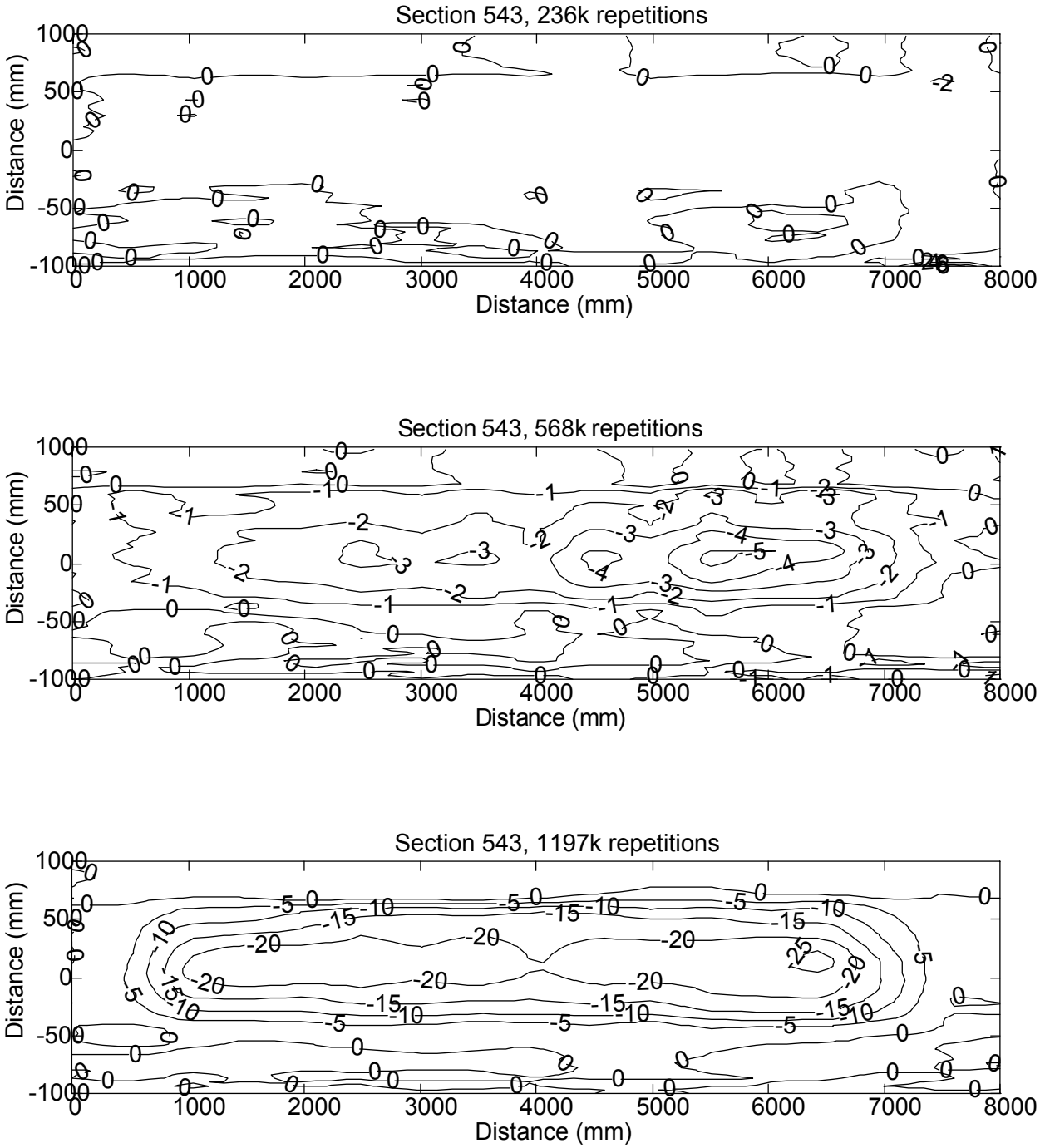


**Figure 11. Section 543 surface rut profiles at various stages of HVS trafficking.**

### 3.2.2 In-depth Permanent Deformation

Figure 12 shows the permanent deformation recorded at several layers in the pavement using the MDD (refer to Figure 1 for depths of MDDs in the pavement). The deformation data at the top of the subgrade are not show because the MDD installed at this location was not functioning during HVS trafficking.

The rapid increase in permanent deformation under the 100-kN load with load applications is evident for all the layers. The MDD sensor positioned at the ATPB and AB interface (250 mm depth) recorded the highest increase in permanent deformation among all layer interfaces. Cores obtained along the centerline of the test section indicate that the increase in permanent deformation under conditions of water infiltration and high loads at the ATPB and AB interface can be attributed to the following:

- stripping of the ATPB layer,
- intrusion of fines from the AB into the ATPB, and
- softening of the AB layer.

Figure 13 shows the permanent deformation attributed to each pavement layer with increase in HVS load applications. It can be seen from the figure that most of the rutting occurred in the upper layers (asphalt layers and granular base). The asphalt concrete layers and the ATPB significantly contributed to rutting during the trafficking of the 40-kN load. However, as the trafficking load increased, the contribution of the unbound granular material to the total rut depth increased significantly.

## 3.3 Comparisons of the Performance of Similar Test Sections with Dry Base Conditions

To provide some comparisons between the behavior of Section 543 and comparable sections tested earlier under dry conditions, the test results from Section 543 will be compared to

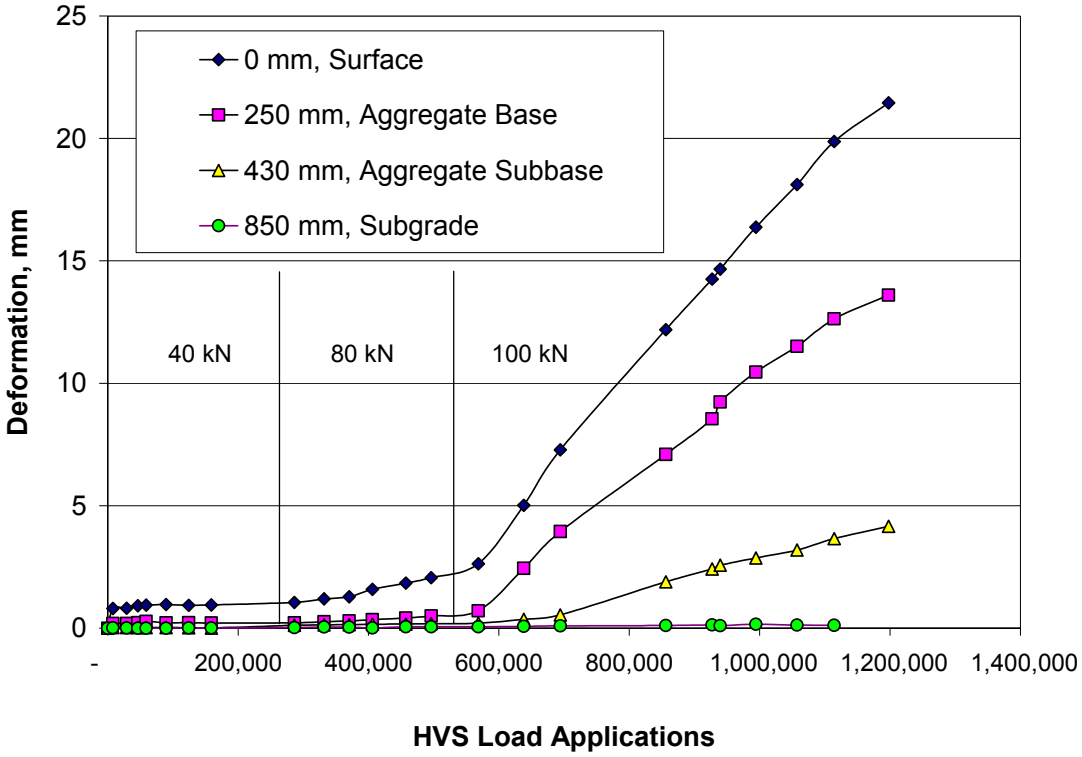


**Figure 12. In-depth permanent deformation in Section 543.**

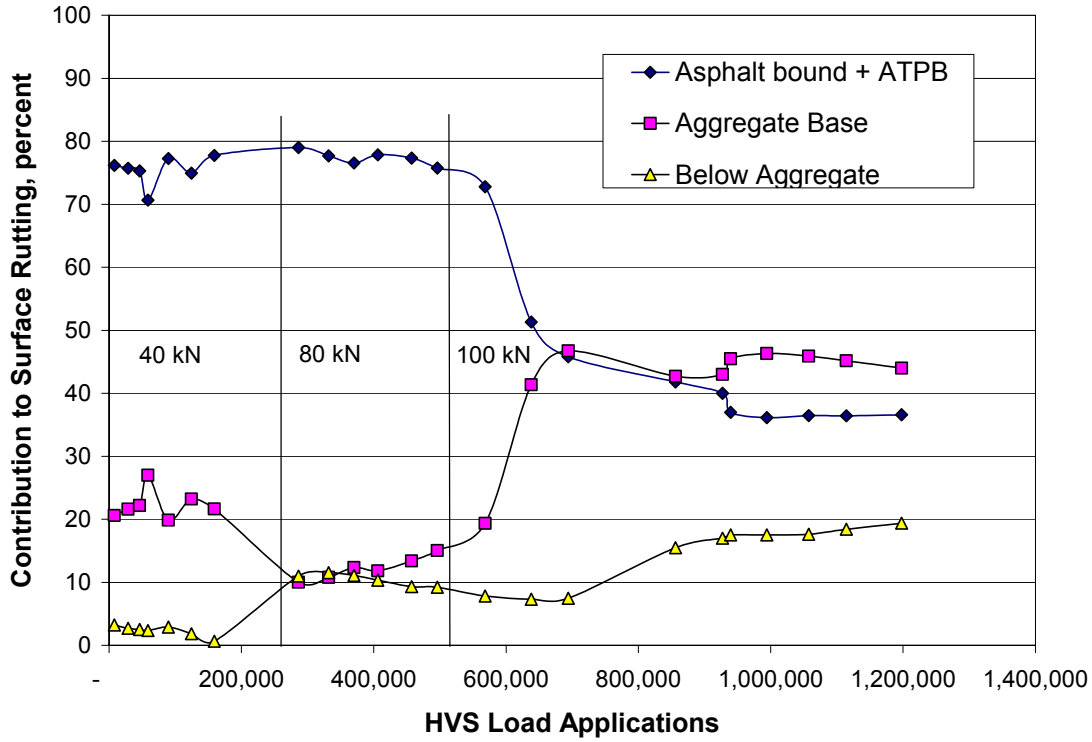


**Figure 13. Contribution of pavement layers to surface rutting in Section 543.**

the test results from the initial Goal 1 Test Sections 500 and 502 and Goal 3 Test Sections 514 and 515. The two Goal 1 sections were the original sections containing ATPB and tested in the dry condition. There was some difference in response of these two sections due to changes in subgrade water content. Sections 514 and 515 corresponded to Sections 500 and 502, which had been overlaid with layers of DGAC and ARHM-GG, respectively. Summaries of HVS loadings for the Goal 1 and Goal 3 test sections are included in Table 7.

**Table 7 HVS Traffic for Previous Sections Tested under Dry Conditions**

| **Section** | **Goal 1 Load Applications ($\times 10^3$)** | | | **Goal 3 Load Applications ($\times 10^3$)** | | |
|---|---|---|---|---|---|---|
| **(Goal 1/Goal 3)** | 40 kN | 80 kN | 100 kN | 40 kN | 80 kN | 100 kN |
| 500/514 | 150 | 50 | 2370 | 172 | 145 | 1350 |
| 502/515 | 150 | 50 | 2470 | 128 | 218 | 2065 |

Figure 14 shows in-depth permanent deformation data obtained with the MDDs for the Goal 1/Goal 3 HVS test sections. Locations of the MDDs are similar to those for Section 543, i.e., close to the surface, top of the aggregate base, top of the aggregate subbase, and top of the subgrade.

A comparison of Figure 12 with Figure 14 indicates a significant difference in rutting performance of the layers. Less surface rutting was observed in Sections 500 and 502 even though more than 4 million HVS load applications were applied. Is addition, the sections barely approach the surface rutting failure criterion of 12.5 mm after the two HVS programs. Rutting in the aggregate base layers and in the subgrade were less than 5 mm and 2 mm respectively after both HVS programs. In contrast, Section 543 reached the surface rutting failure criterion of 12.5 mm after about 850 thousand HVS load applications. At this level of rutting, about 8 mm of rutting occurred on top of the aggregate base. These results point to a significant difference in performance of the drained section in the dry state versus that in the wet condition.

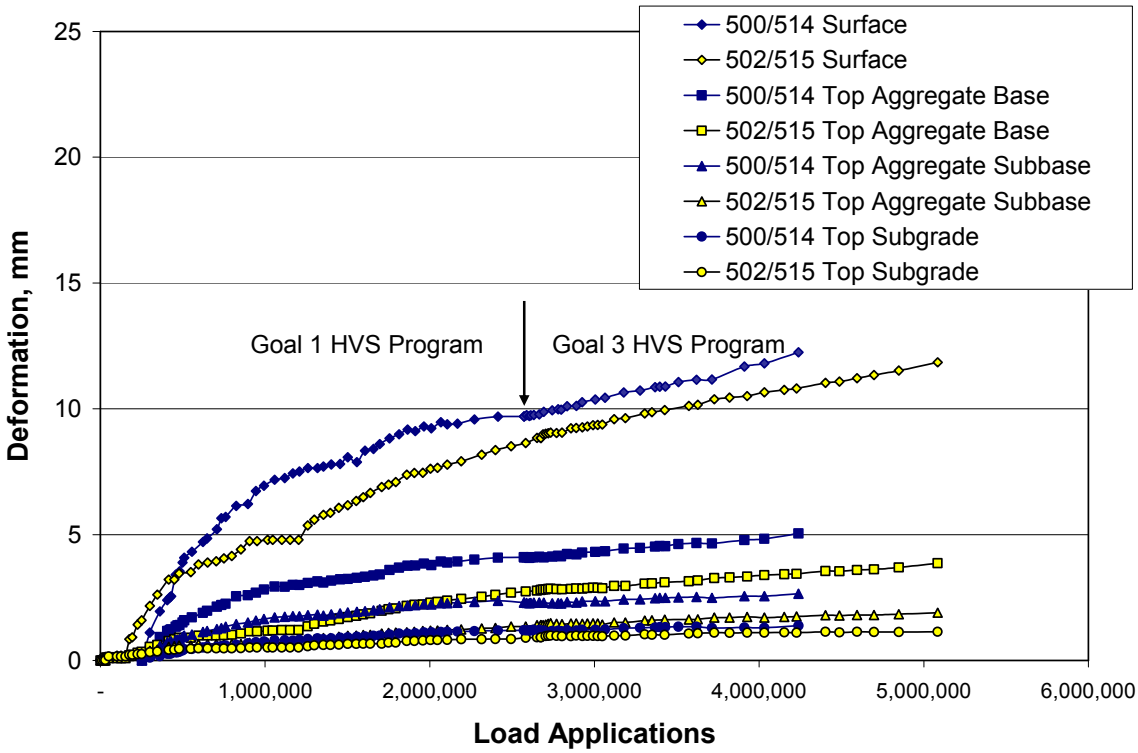


**Figure 14. In-depth permanent deformation from Goal 1/Goal 3 test sections.**

### 3.4 Elastic Deflections

Elastic deflections in the pavement sections were measured with the Road Surface Deflectometer (RSD) and MDDs. Surface and in-depth deflection data presented in the following sections represent peak values obtained from the deflection response of the pavement.

#### 3.4.1 Surface Elastic Deflection Data

Surface elastic deflections were monitored using the RSD along the section centerline at Stations 4, 6, 8, 10, and 12 under the 40-, 80-, and 100-kN test loads. Figure 15 shows average deflection data for the three test loads. Elastics deflections progressively increased under the 80-kN and 100-kN trafficking loads, with the highest rate of increase under the 100-kN trafficking

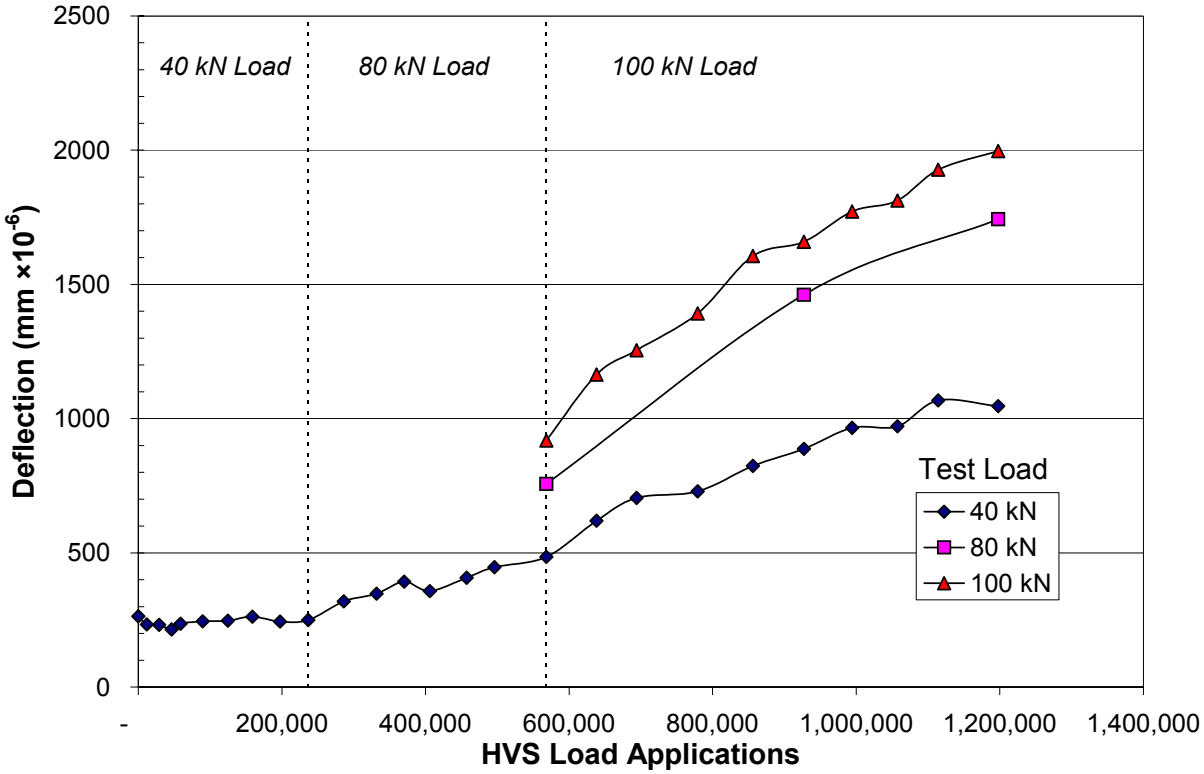


**Figure 15. RSD deflections for Section 543.**

load. No significant increase in elastic deflections was recorded during trafficking under the 40-kN load.

Figure 16 shows RSD deflections along Section 543 at the completion of HVS testing. The highest deflections were measured around Station6, while the lowest deflections were measured near Station 12.

### 3.4.2 In-depth Elastic Deflections

In-depth elastic deflection data under the 40-, 80-, and 100-kN test loads are presented in Figures 17–19. Response of the pavement layers under the 40-kN test load, Figure 17, remained relatively constant during trafficking at 40 kN. Under the trafficking at 80 and 100 kN, progressive increases in elastic deflections were recorded in all of the layers with the highest rate

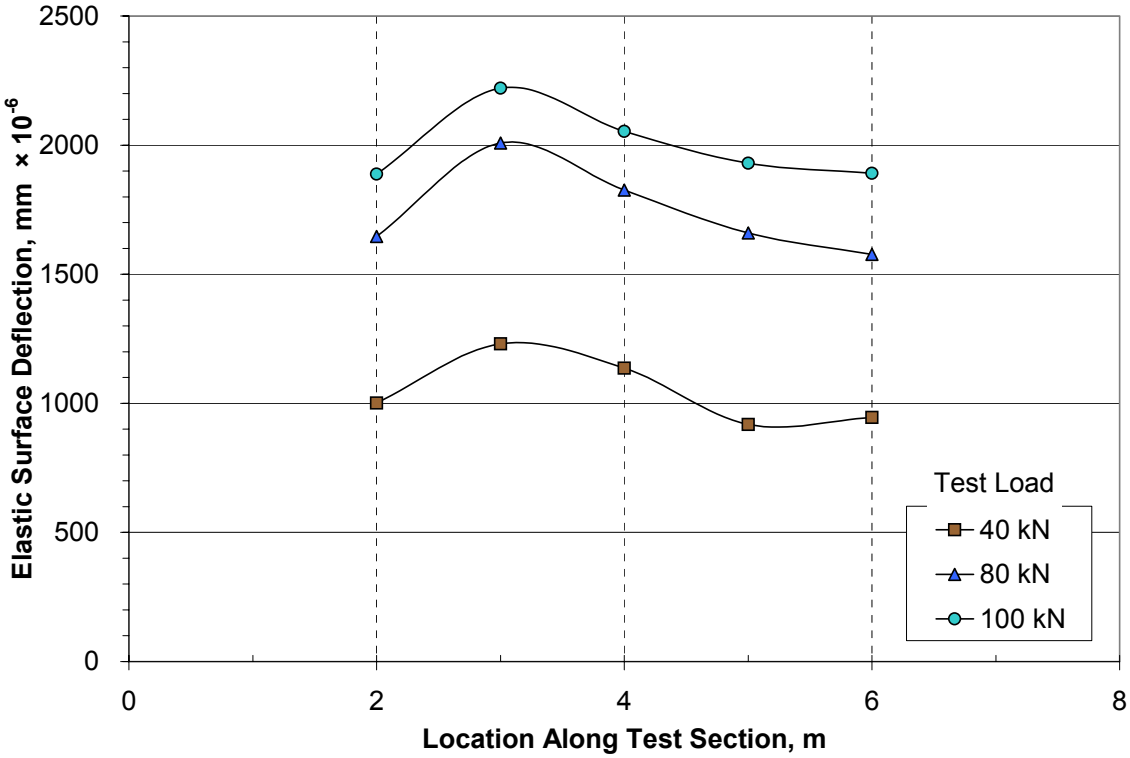


**Figure 16. RSD at the end of HVS trafficking.**

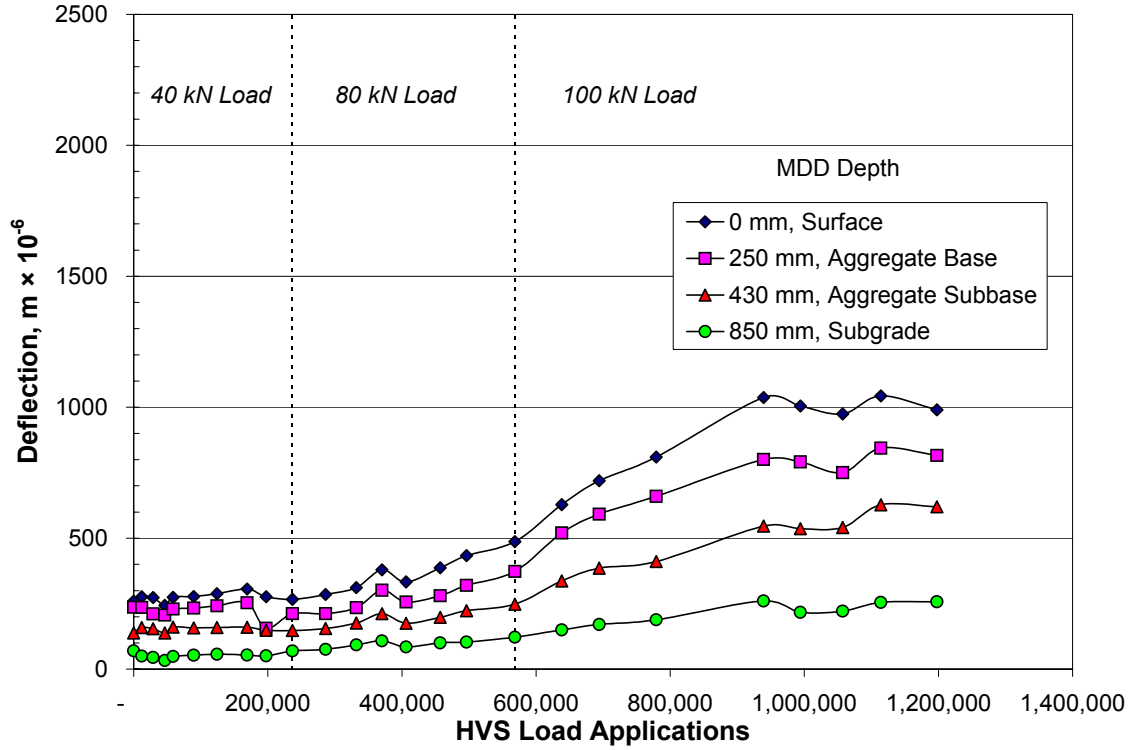


**Figure 17. In-depth elastic deflections under 40-kN test load, MDD 7.**

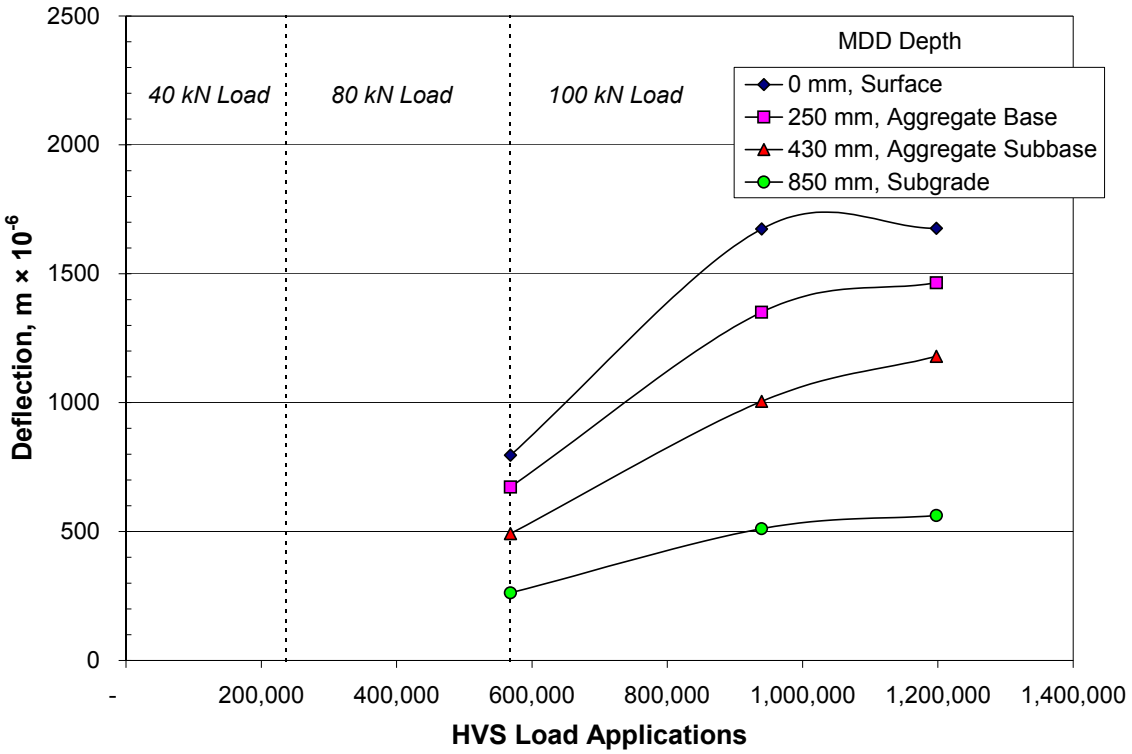


**Figure 18. In-depth elastic deflections under 80-kN test load, MDD 7.**

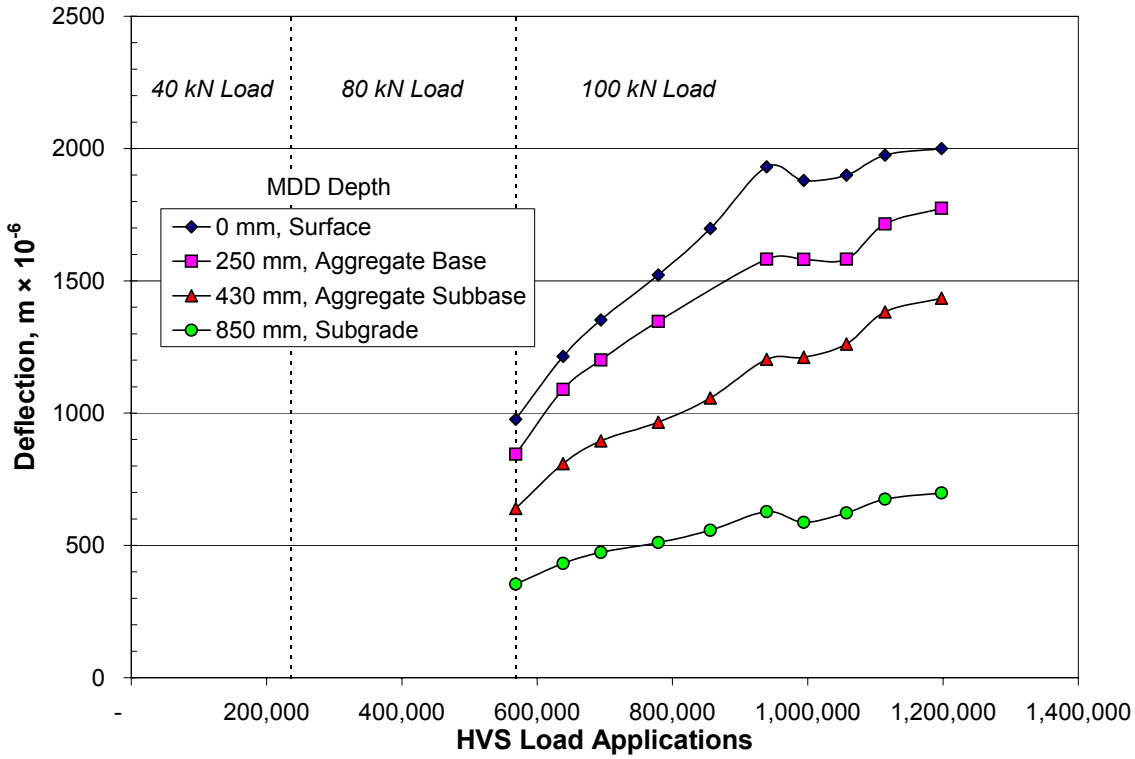


**Figure 19. In-depth elastic deflections under 100-kN test load, MDD 7.**

of increase observed with the 100-kN load. The data also show that the rate of increase of the elastic deflections leveled off at approximately 950,000 load applications when surface cracking appeared.

The percent contribution of each pavement layer to elastic surface deflection is presented in Figure 20 for the 40-kN test load. Table 8 summarizes the percent contribution of each pavement layer to surface deflections under each trafficking level under all test load levels. On average, 80 percent of the total surface deflection can be attributed to the unbound layers.

**Table 8 Percent Contribution of Pavement Layers to Surface Deflection**

| **Pavement Layer** | **Average Percent Contribution to Surface Deflection at Trafficking Load** | | |
|---|---|---|---|
| | **40 kN** | **80 kN** | **100 kN** |
| Asphalt Layers | 16 | 24 | 20 |
| Aggregate Base | 29 | 22 | 25 |
| Below Aggregate Base | 56 | 53 | 55 |

Figure 21 presents the deflection data as a profile of deflections with respect to pavement depth. The reduction in slope of the upper layers (asphalt bound and aggregate base) indicates a reduction in stiffness of these layers. Based on the performance data, the reduction in stiffness of these layers is due to fatigue cracking in the asphalt bound layers, stripping in the ATPB layer, and softening of the aggregate base due to high moisture content in the aggregate base layer, and high trafficking load levels.

Figure 22 presents elastic deflections as a function of the HVS load. These results illustrate the non-linear response of the layers beneath the 250-mm pavement depth (all unbound layers). The thick line in the figure delineates a linear elastic response. The importance of properly characterizing the pavement materials is demonstrated by the results. In most mechanistic-based analysis tools, to attain reasonable solutions, pavements are analyzed using linear elastic theory, i.e., all layers are assumed to exhibit linear elastic response. For those

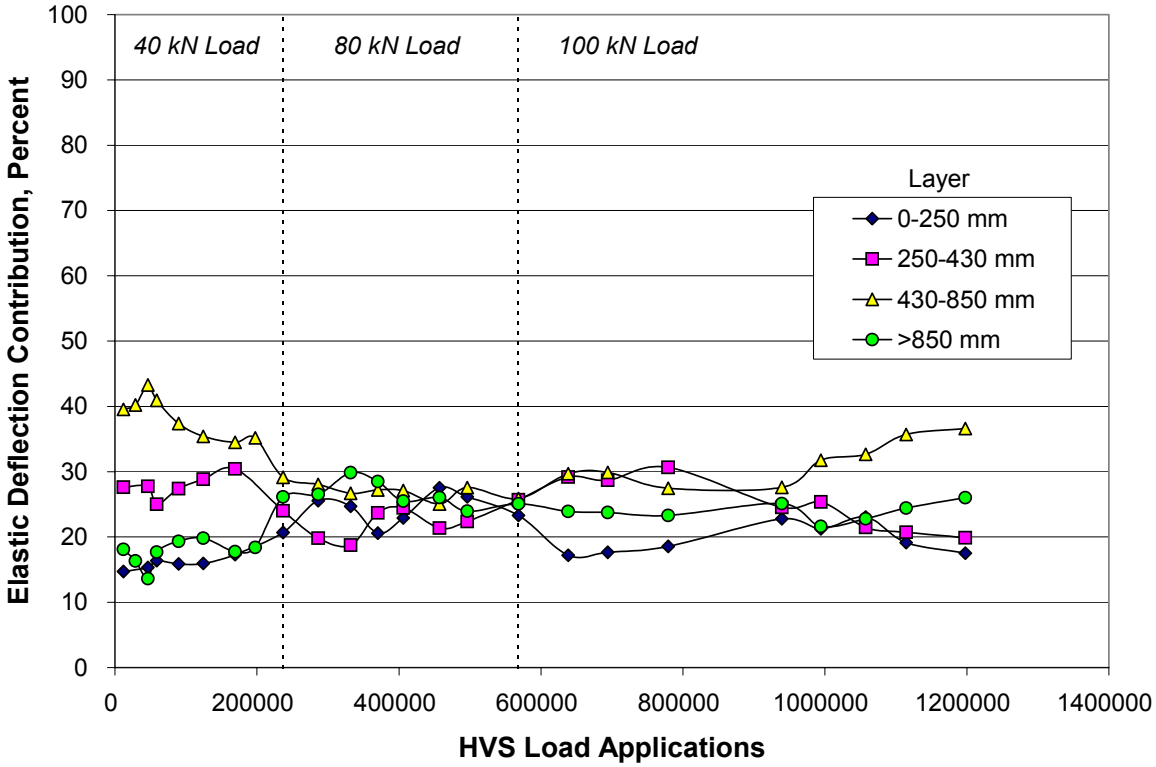


**Figure 20. Contribution of pavement layers to surface elastic deflection based on 40-kN load, MDD 7.**

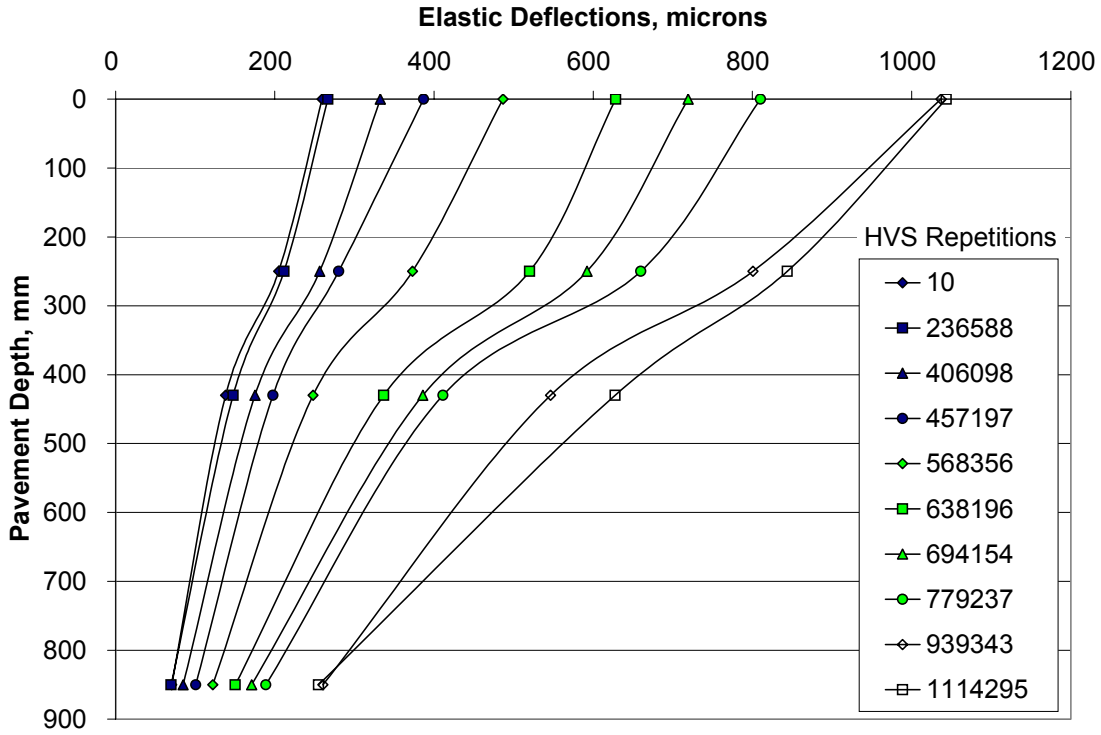


**Figure 21. Profile of elastic deflections with depth.**

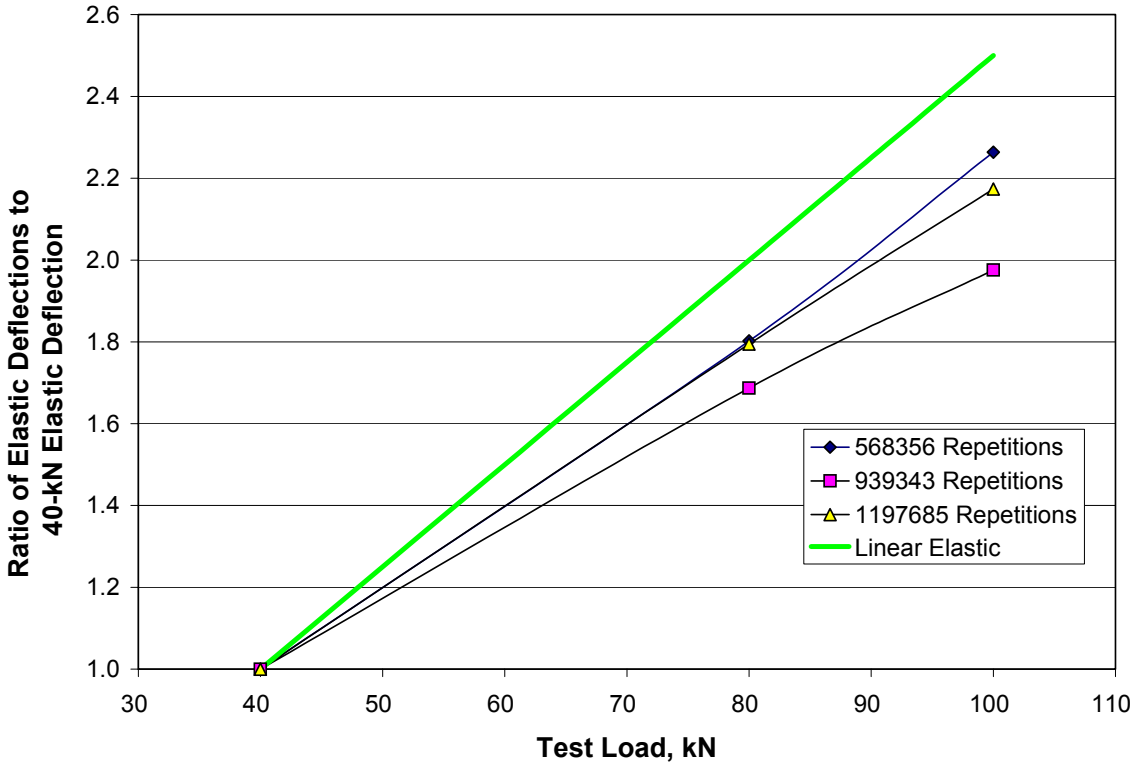


**Figure 22. Elastic deflections versus test load level at pavement depth of 250 mm, MDD 7.**

situations in which materials exhibit non-linear characteristics, the prediction of pavement responses (stresses, strains, and deflections) is not correct. In turn, where these results are used to estimate fatigue cracking, rutting, etc., predictions of pavement performance may be in error.

### 3.4.3 Back-calculated Moduli from In-depth Elastic Deflections

Moduli of the pavement layers were calculated from the in-depth elastic deflection basins measured with the MDDs. Deflections were calculated using the Odemark-Boussinesq method for a four layer system (asphalt bound layers, aggregate base layer, aggregate subbase, and subgrade) and assuming a non-linear response of the subgrade at the positions where in-depth deflections were measured with the MDDs (see Figure 2). Differences between measured and calculated deflections were minimized by changing the moduli of the layers.(*7*)

Figure 23 summarizes the back-calculated moduli from the MDD data obtained for the 100-kN trafficking load. Back-calculated moduli for the 40- and 80-kN loads yielded what appeared to be specious results and are not presented here.

Decrease in the modulus of the asphalt bound layer (including the ATPB) with HVS load applications is presented in Figure 23. This reduction is due to fatigue cracking, as shown in Figure 24, and by the deterioration of the ATPB due to stripping. A comparison of the moduli of the asphalt bound layer (including the ATPB) back-calculated from MDD deflection with those back-calculated from FWD deflections (see Section 3.6) indicates lower values than those back-calculated from the MDDs. This difference is due at least in part, to the slower rate of loading at which the tests were conducted. MDD deflections were measured under a slow moving wheel load while FWD deflections were measured at a time of loading simulating a velocity of more than 70 kph. Since the asphalt concrete modulus is dependent on time of loading, one would expect a higher value at a shorter time of loading. Back-calculated moduli of the unbound aggregate base are lower than those for the aggregate subbase and similar to the subgrade moduli for the 100-kN load. This low modulus in the aggregate base likely was produced by an increase in moisture content due to water infiltrating the base from the saturated ATPB. Comparison of moduli determined from MDD deflections and those from the FWD at the end of HVS testing suggests fair agreement among the two approaches. Back-calculated moduli of the aggregate base and subbase (average of these two) from the MDDs are 14 percent lower than those back-calculated from the FWD for the combined aggregate base and subbase. Back-calculated moduli of the subgrade from MDDs were 40 percent lower than those from the FWD measurements. Differences in moduli among the two approaches may result from differences in velocity, load level, and wheel configuration at which the deflections were measured in the two tests. Change

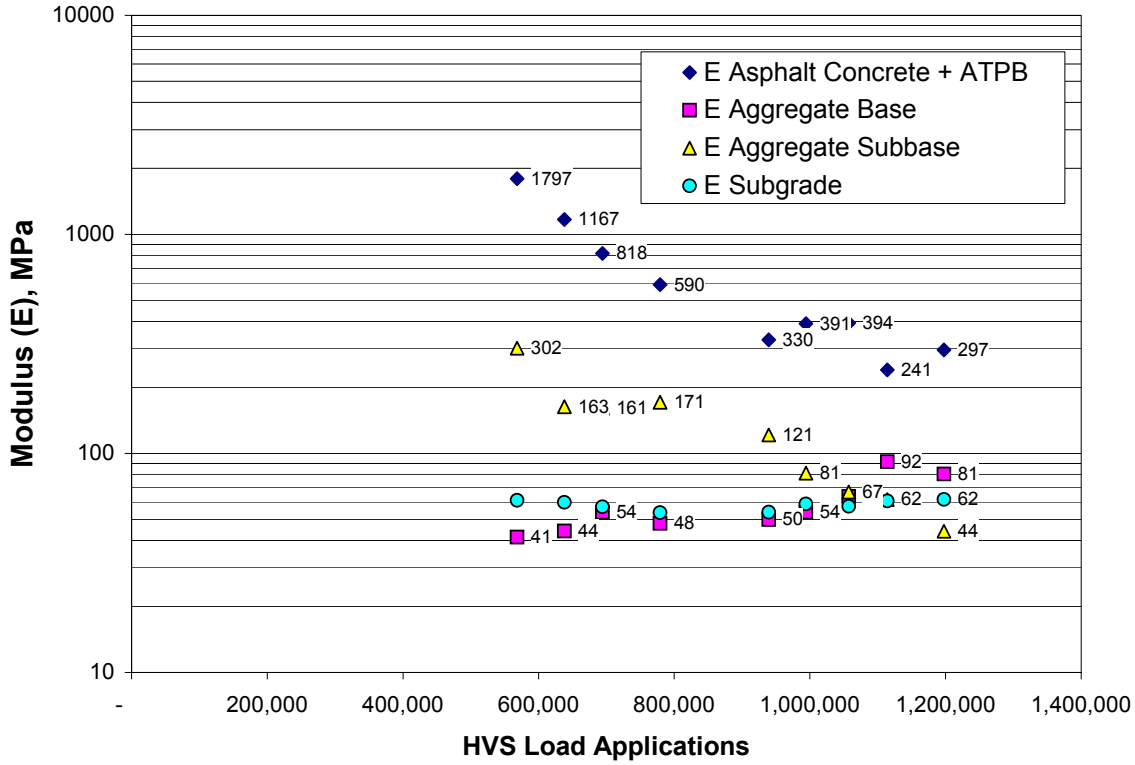


**Figure 23. Summary of back-calculated moduli from in-depth deflections.**

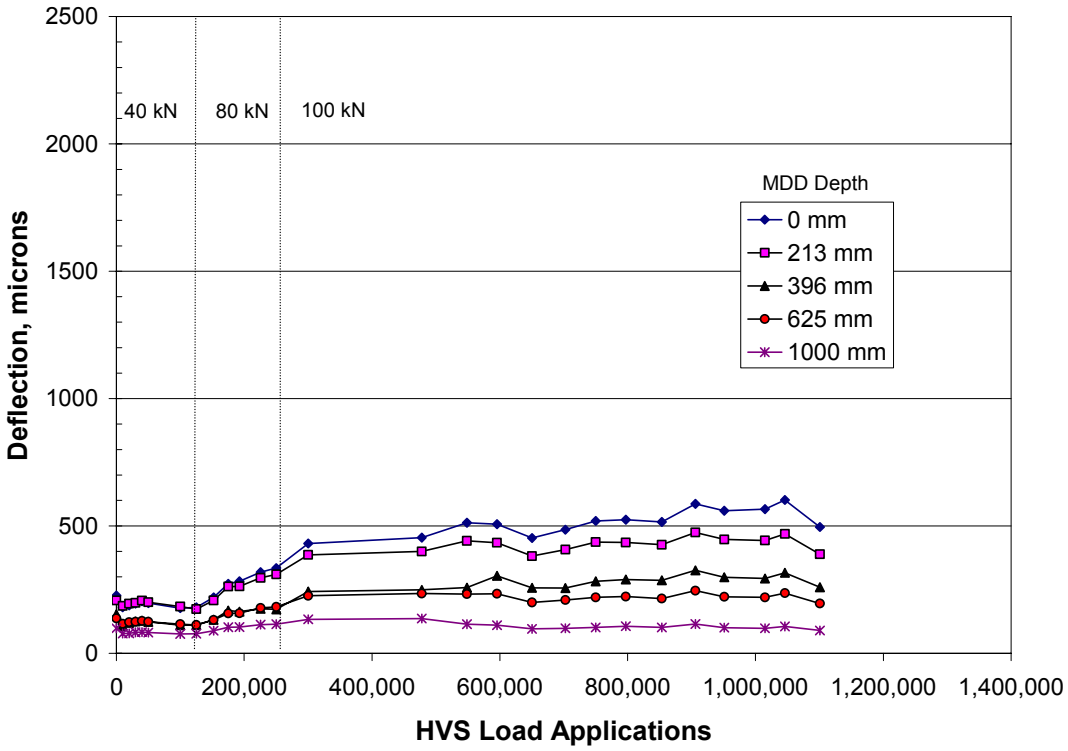


**Figure 24. In-depth elastic deflections for Section 502 (tested under dry conditions).**

in the moduli of the asphalt concrete resulting from time of loading differences would change the state of stresses in the unbound layers, which in turn affects the moduli of the unbound layers. The HVS 100-kN dual wheel load versus that used in the FWD test (20 to 60 kN on a circular plate), could also contribute to the differences.

### 3.4.4 Comparison with Previous Section Tested under Dry Conditions

Pavement Section 502 is similar to Section 543 and was previously tested under the HVS. Differences between Section 502 and Section 543 and the traffic loading conditions for Section 502 are discussed in Section 3.2.3. In-depth MDD elastic deflections for the 40-kN test load are presented in Figure 24. Elastic deflections at the beginning of the test were similar for both sections, indicating similar responses under intact conditions, as shown in Figure 24. Significant differences were observed under the 100-kN trafficking load. Elastic surface deflections level off at about 500 microns for Section 502 and about 1000 microns for Section 543. The increase in deflection in Section 543 indicates damage in the pavement structure and can be attributed to failure of the ATPB layer.

## 3.5 Surface Cracking

Figures 25a, b, and c, respectively, show cracks detected during HVS trafficking after about 951,000, 1.08 M, and 1.18 M load applications. The observed cracks were predominantly transverse hairline cracks and were sometimes difficult to detect visually. The typical widest crack widths were approximately 0.2 mm. These hairline cracks did not spall or increase significantly in width during HVS trafficking. Lack of crack deterioration is attributed to minimal amounts of dust (mineral particles) on the pavement surface. The HVS temperature

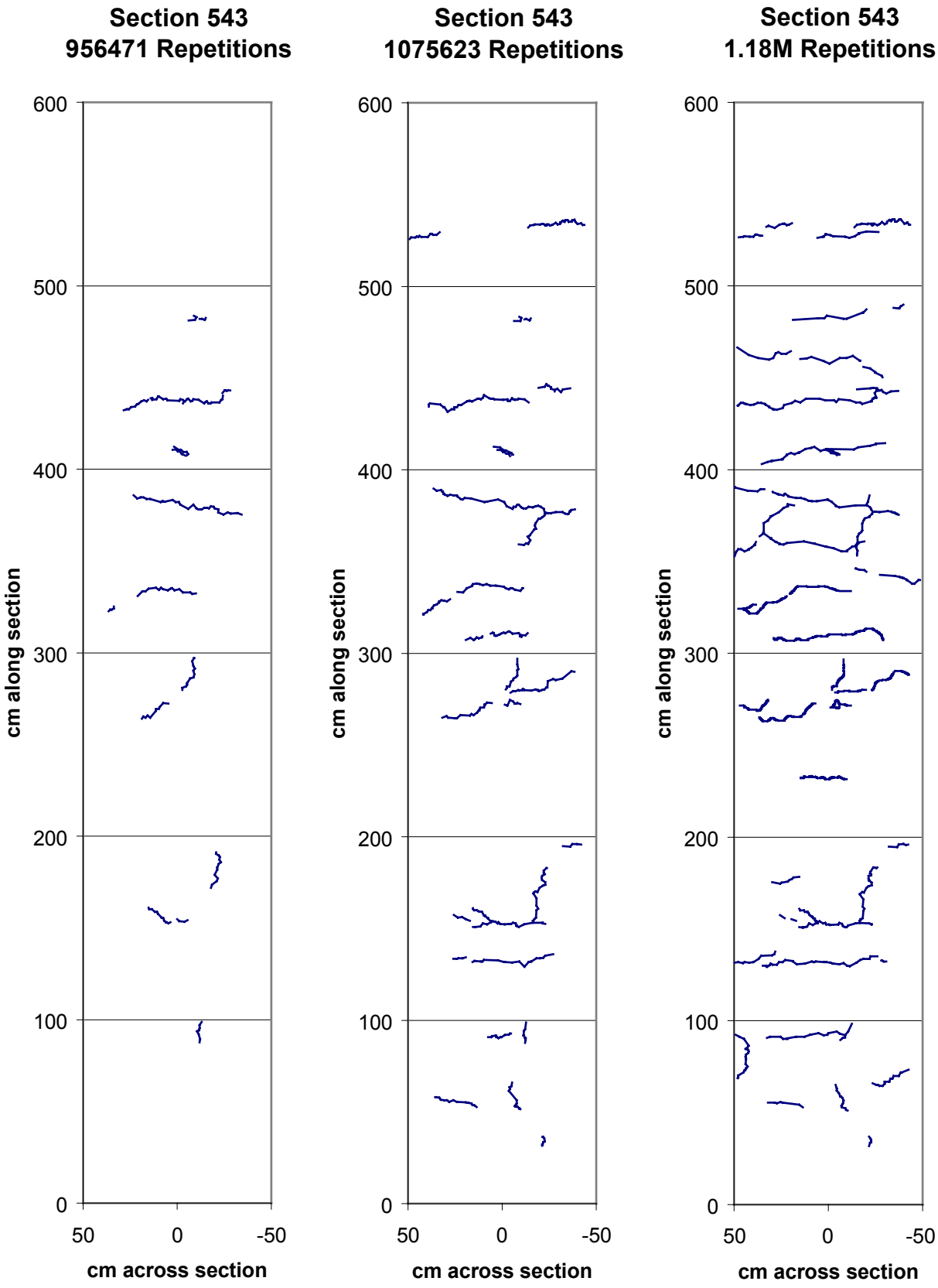


**Figure 25. Surface crack schematics for Section 543.**

control box, which limited daily expansion and contraction of the asphalt pavement, also likely mitigated crack deterioration.

Inspection of the surface during HVS testing revealed deposits of fine silt accumulated on the pavement surface along some of the cracks. The fine silt was periodically removed, but reappeared after some trafficking. The fine silt was likely pumped from the aggregate base through the cracks in the asphalt concrete layers to the surface by the rapid dissipation of water pressure in the ATPB under the traffic loading of the HVS.

Figure 26 shows the extent of surface cracking along the test section at the completion of HVS trafficking. More cracking was recorded between Stations 8 and 14 (400–700 cm) than between Stations 2 and 8 (100–400 cm). These results are compatible with the deflections measured with the FWD, which indicate higher FWD deflections where higher crack density was measured.

Figure 27 shows the increase of crack density with HVS trafficking. A rapid increase in crack density is observed after about 1,000,000 HVS load applications. These surface cracks appeared and rapidly increased under trafficking at the 100-kN load. Referring again to Figures 16–18, it will be observed that after 1,000,000 HVS load applications, the elastic deflections reached maximum values and remained at those levels for the duration of HVS trafficking.

### 3.6 FWD Test Results

FWD tests were conducted at intervals during HVS loading to assess changes in stiffness of the various pavement layers. This section summarizes the results of deflection measurements and moduli determined by back-calculation using the measured deflections.

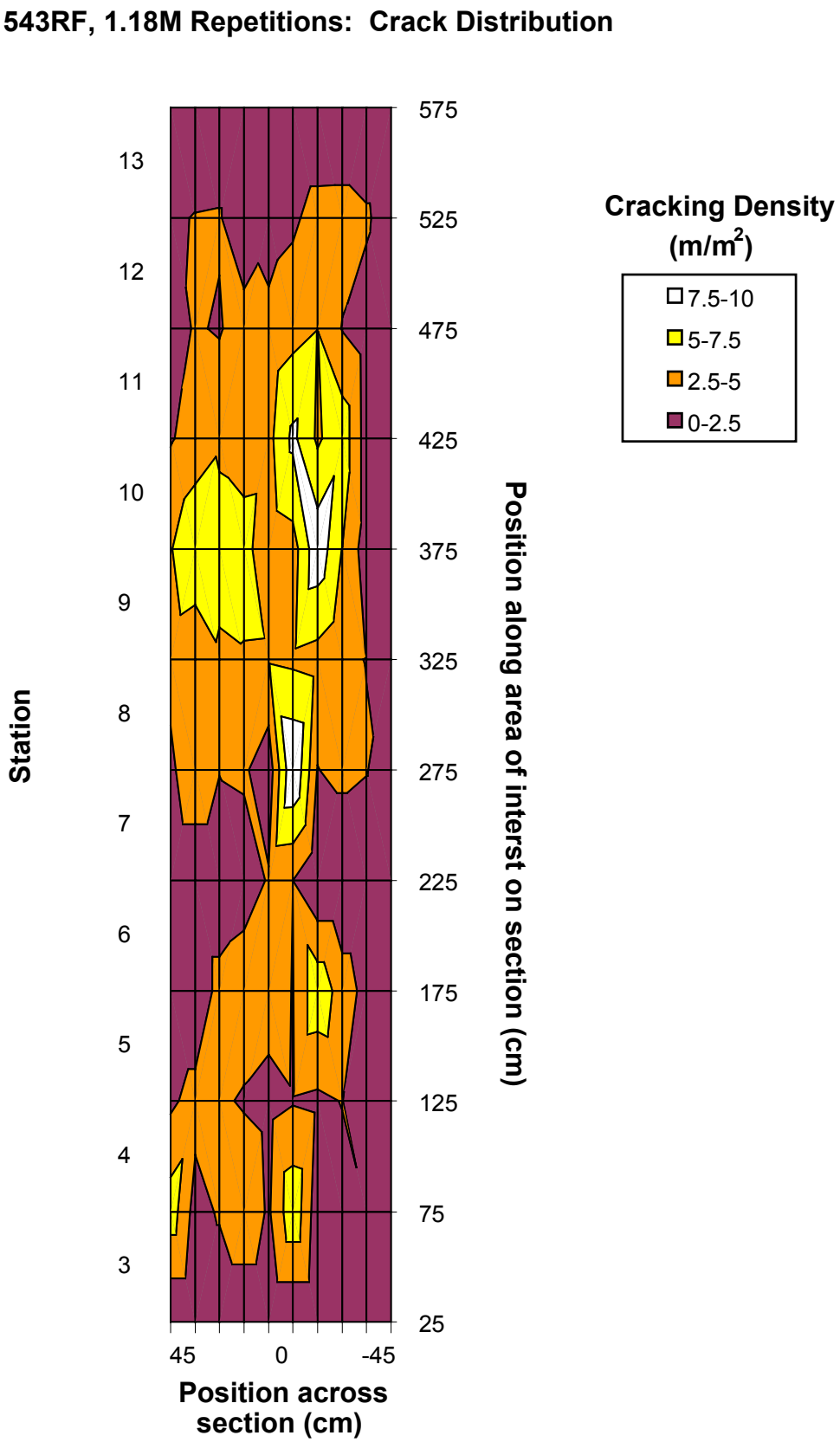


**Figure 26. Density of cracking on Section 543 after completion of HVS trafficking.**

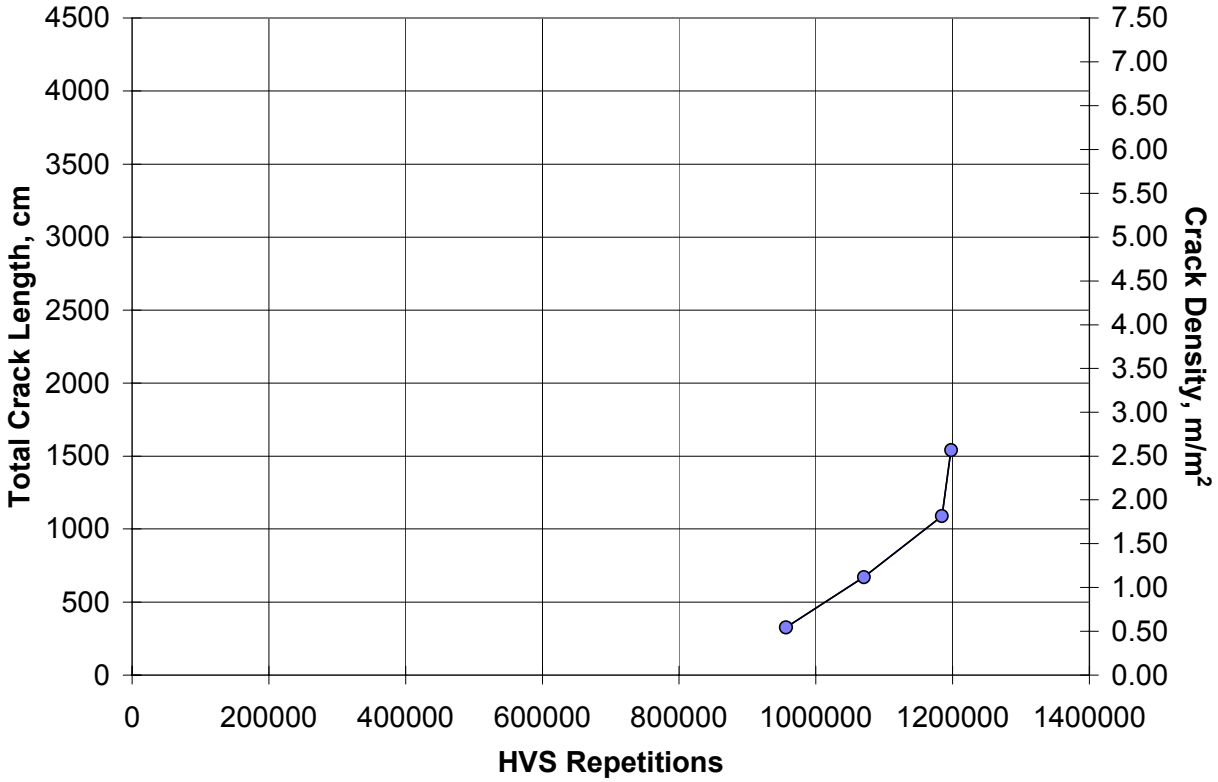


**Figure 27. Progression of crack density on Section 543.**

3.6.1 Deflections

Figure 28 summarizes elastic deflections measured under the FWD load plate (D1) normalized to a 40-kN load for the Stages 1, 2, and 4, as described earlier. As shown in Figure 28, D1 deflections showed no significant change before and during the water infiltration stages (Stages 1 and 2). However, a significant increase in elastic deflections was observed after the completion of HVS trafficking and during the forensic study (Stage 4). Table 9 summarizes these results for each period of testing. In general, elastic deflections after HVS trafficking were about 3.9 times higher than those before HVS trafficking.

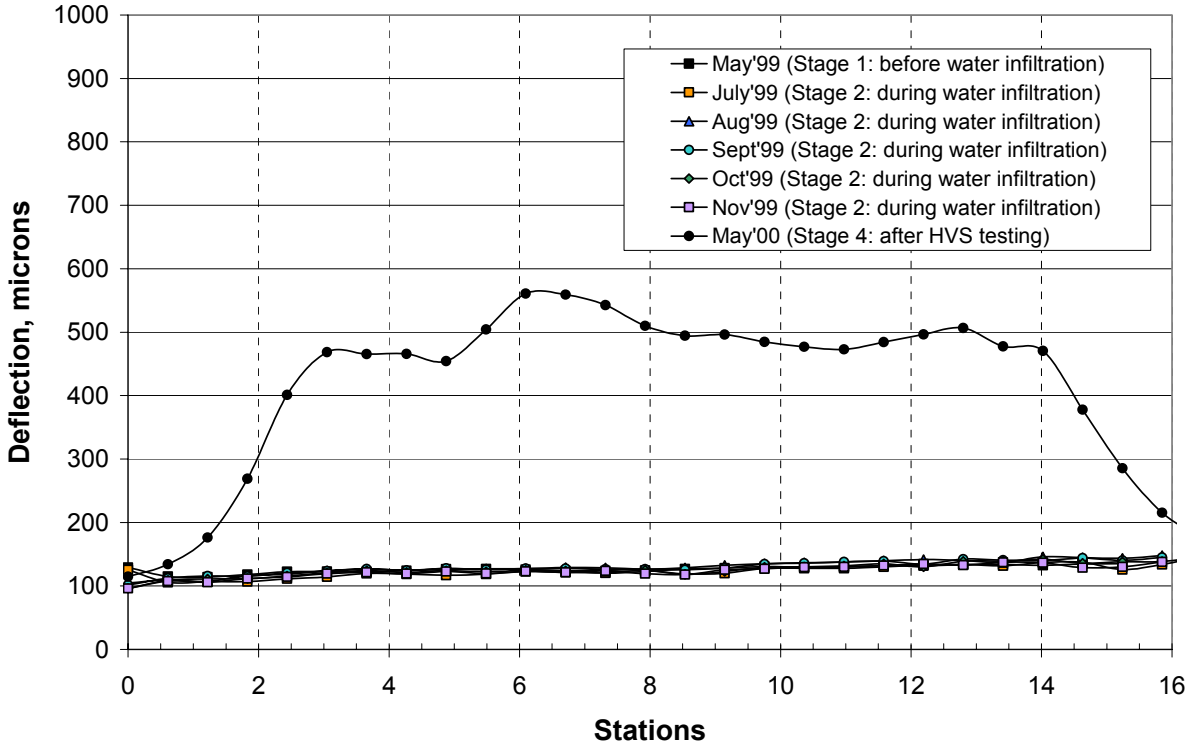


**Figure 28. Summary of FWD elastic deflections.**

**Table 9 D1 Normalized Deflections for Section 543**

| Stage of Testing | Date | Average Deflections (microns) | Standard Deviation (microns) | Average Temperature (ºC) |
|---|---|---|---|---|
| **1** | May 1999 | 127 | 6 | 24.0 |
| **2** | July 1999 | 124 | 10 | 18.6 |
| | August 1999 | 130 | 12 | 21.0 |
| | September 1999 | 129 | 11 | 21.4 |
| | October 1999 | 126 | 11 | 23.0 |
| | November 1999 | 123 | 10 | 21.0 |
| **4** | May 2000 | 490 | 37 | 18.0 |

3.6.2 Back-calculated Moduli from FWD Deflections

Moduli were back-calculated from FWD deflections obtained from three target loads (20, 40, and 60 kN) for a three layer system consisting of asphalt concrete (AC), aggregate base (AB), and subgrade (SG). A three layer system was selected for simplicity. Back-calculated

moduli were determined using the program ELMOD 4.5 (Odemark-Boussinesq method assuming a stress dependent subgrade modulus). For Section 543, back-calculations were conducted for two cases to consider the ATPB layer since this layer typically has moduli values between those of the asphalt bound layers and the aggregate base. In one case, the ATPB layer was included as part of the asphalt bound layers and in the other case as part of the aggregate base. Table 10 summarizes the layers and thicknesses for the two cases considered.

**Table 10 Summary of Layers and Thicknesses Considered for Back-calculation**

| Case 1 | | Case 2 | |
|---|---|---|---|
| **Layer** | **Thickness, mm** | **Layer** | **Thickness, mm** |
| AC = Asphalt Bound Layers + ATPB | 247 | AC = Asphalt Bound Layers | 178 |
| AB = Aggregate Base + Aggregate Subbase | 268 | AB = Aggregate Base + Aggregate Subbase +ATPB | 437 |
| SG = Subgrade | infinite | SG = Subgrade | infinite |

Results of the back-calculation process are presented in Figures 29 through 32. Results are presented for the three load levels and the two cases considered. Also presented in the figures are results of the back-calculation process using the MDD deflections (Stage 3) for the 100-kN dual wheel load.

Figure 29 shows the moduli of the asphalt concrete layers with and without the ATPB layer. Moduli of the asphalt bound layers were higher than the moduli of the asphalt bound layers including the ATPB for Stages 1 and 2. This indicates that the modulus of the ATPB is significantly lower than that of the asphalt bound layers. Figure 30 shows a reverse effect for the aggregate base when the ATPB is considered as part of this layer. The modulus of the aggregate base and ATPB were considerably higher than the modulus of the aggregate base without the ATPB, indicating that the modulus of the ATPB is higher than that of the aggregate base.

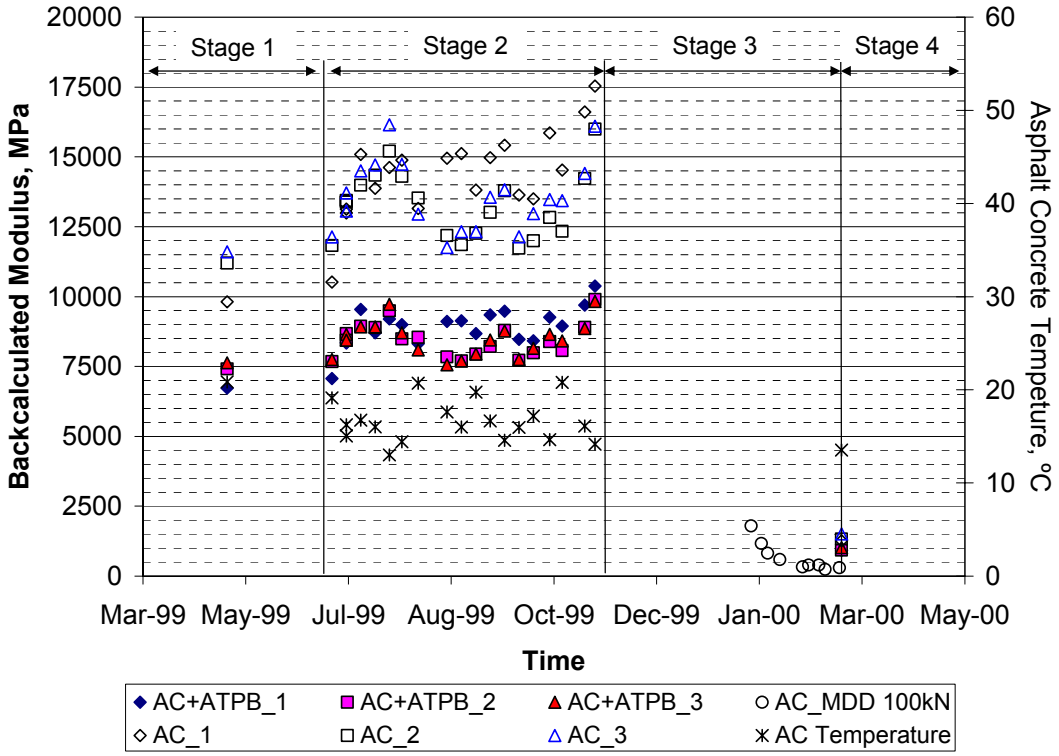


**Figure 29. Results of back-calculation, asphalt concrete layer with and without ATPB layer.**

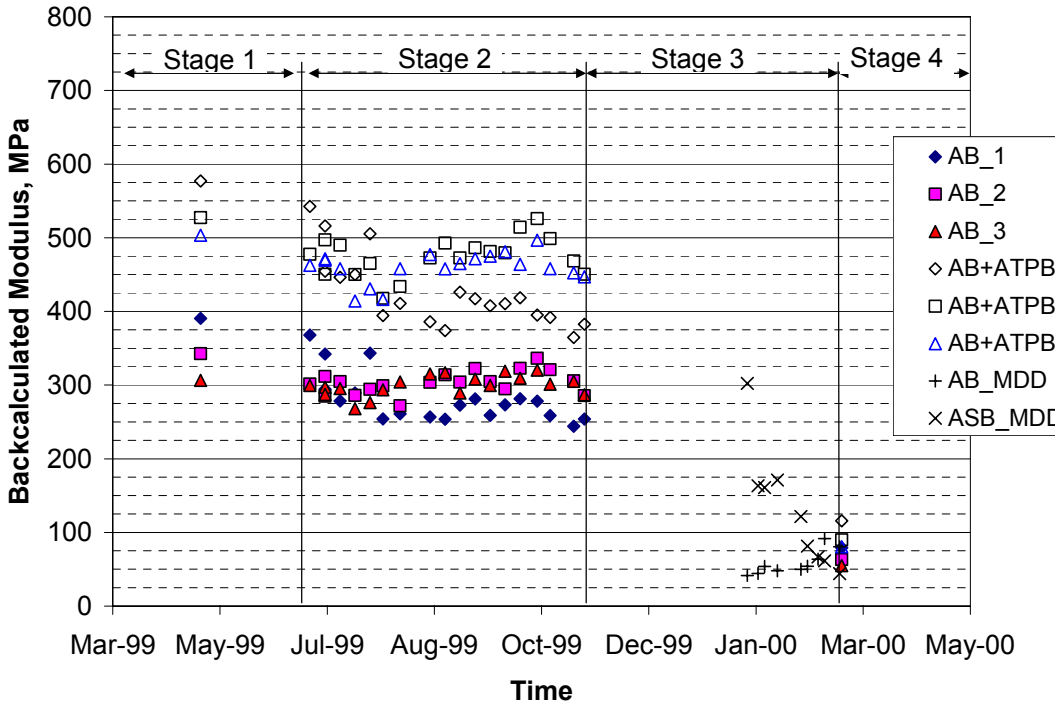


**Figure 30. Results of back-calculation, aggregate base layer.**

Using Odemark's method of equivalent thickness, it is possible to estimate moduli of the ATPB based on the results of the two cases considered. Figure 31 shows the results of this approach. ATPB moduli for Stages 1 and 2 are within the same range as those obtained from previous laboratory results. Figure 32 shows no significant difference in the modulus of the SG layer for the two cases considered.

Relative to performance of the section, Figures 29 through 31 show the significant deterioration of the bound layers and the aggregate base after HVS testing. Moduli of the asphalt concrete layers were determined to be less than 1500 MPa at the conclusion of HVS testing. Deterioration of the asphalt bound layers resulted from fatigue cracking as evidenced by the surface cracks recorded during testing. Extracted cored indicated that cracks started from the bottom lift of the asphalt concrete.

The rapid increase in surface cracking is likely the result of the significant reduction in the stiffness of the ATPB and aggregate base, resulting in increased bending strains at the underside of the asphalt concrete layers. Figure 31 demonstrates deterioration of the ATPB produced by HVS trafficking. Estimated moduli of the ATPB after HVS trafficking were between 200 and 400, a significant decrease from the initial measured moduli. As stated in Section 3.2.2, the significant reduction in the stiffness of the ATPB was due to stripping resulting from loading and the intrusion of fines from the aggregate base.

Damage in this aggregate base resulted from an increase in the moisture content and increase in stress level due to the stiffness reduction in the ATPB layer (see Figure 30).

Figure 32 shows that the modulus of the subgrade experienced a significant reduction (approximately 40%) after HVS testing. This reduction in modulus is the result of an increase in the stress levels at the surface of the subgrade resulting from stiffness reductions of the upper

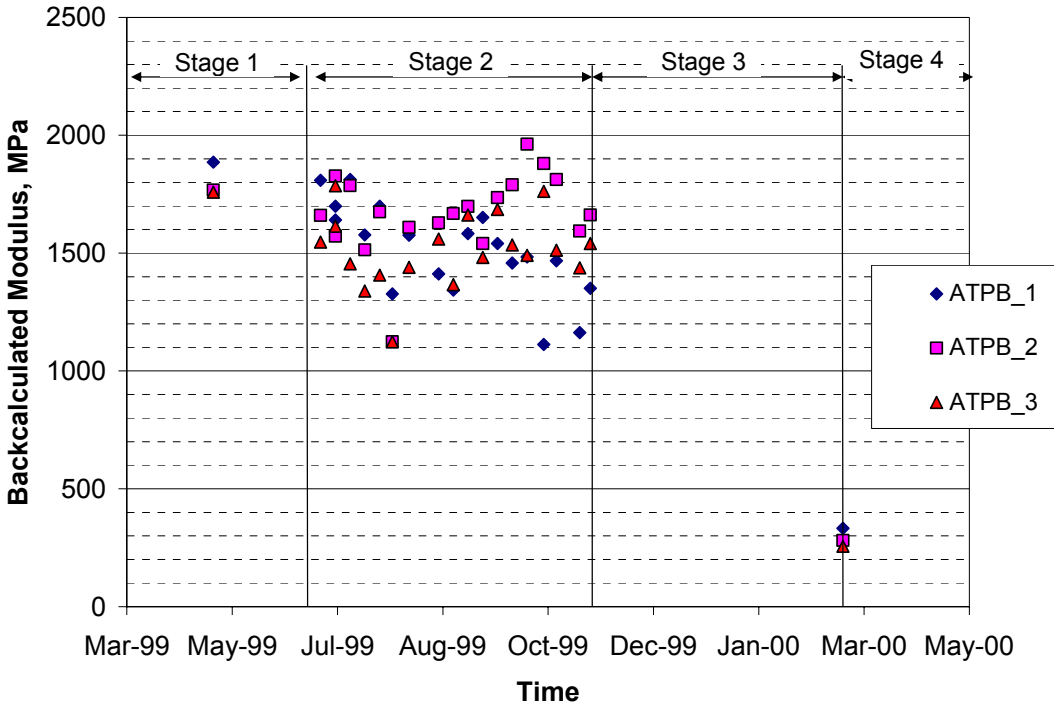


**Figure 31. Results of back-calculation, ATPB layer.**

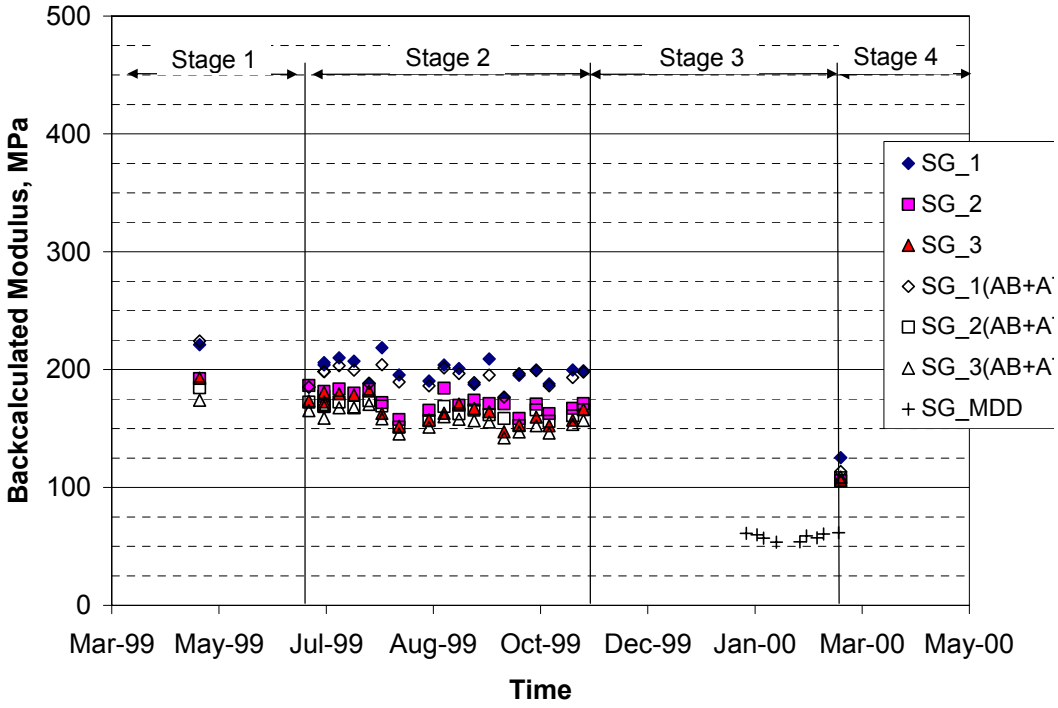


**Figure 32. Results of back-calculation, subgrade.**

layers. Figure 33 includes average values for the layer moduli obtained from back-calculation for the four stages of testing.

### 3.7 Ground Penetrating Radar (GPR) Surveys

GPR was conducted to estimate changes in the thickness of the asphalt concrete and ATPB layers. Figure 34 shows the variation in thickness of the asphalt concrete and ATPB layer during HVS trafficking. As shown in the figure, the GPR results indicate an average thickness of the bound layers (asphalt rubber, asphalt concrete, and ATPB layers) of 253 mm. The GPR estimate of the bound layer thickness is reasonable when compared with the as-built layer thickness of 240 mm directly observed in the test pit. The GPR estimated an average reduction in thickness for the bound layers across the whole trafficked section of about 25 mm at the end of HVS trafficking, which is somewhat high compared to maximum surface rut depths measured with the profilometer of approximately 23 mm.

Figure 35 shows the reduction of bound layer thickness across the section. In this figure, the GPR data contours follow trends obtained using the profilometer. However, the GPR surveys overestimate the reduction in layer thickness. According to the GPR surveys, the thickness reductions were about twice the magnitude of those measured with the profilometer. Based on the forensic activities, reduction in bound layer thickness was mostly due to the change in characteristics of the ATPB layer in the trafficked areas. This overestimation by the GPR surveys may be due to the contamination of the ATPB with fine material from the aggregate base, which produces about the same GPR image as the aggregate base.

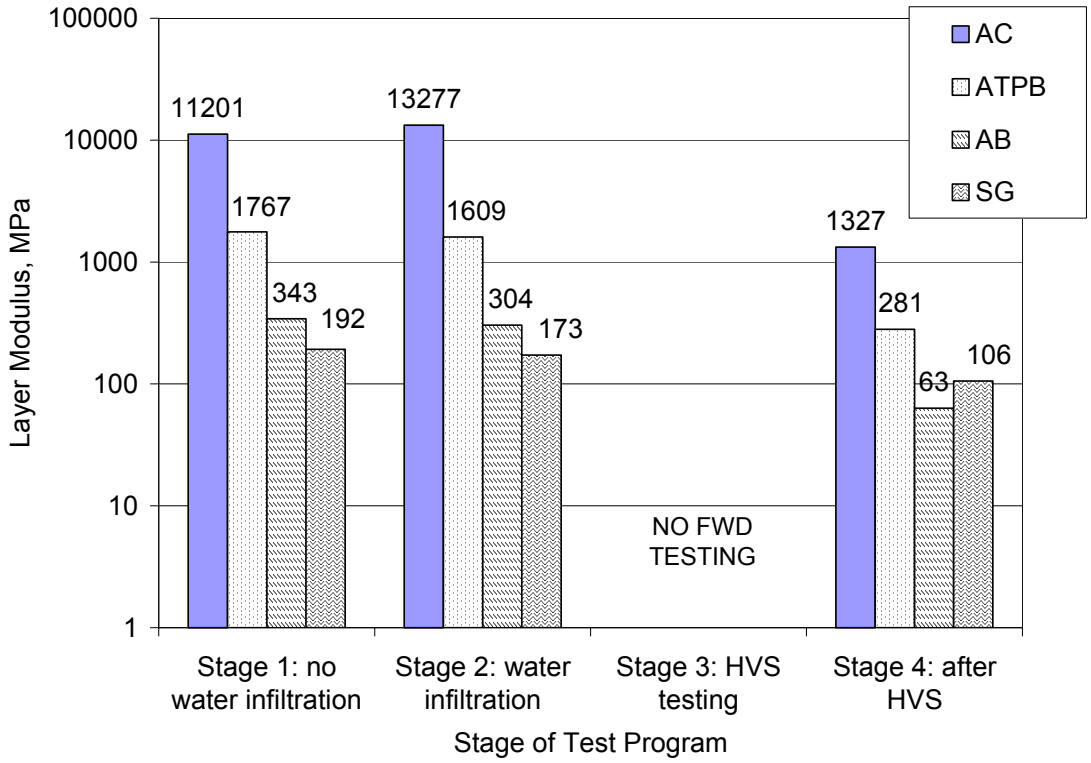


**Figure 33. Average values of layer moduli obtained from back-calculation for the four stages of testing.**

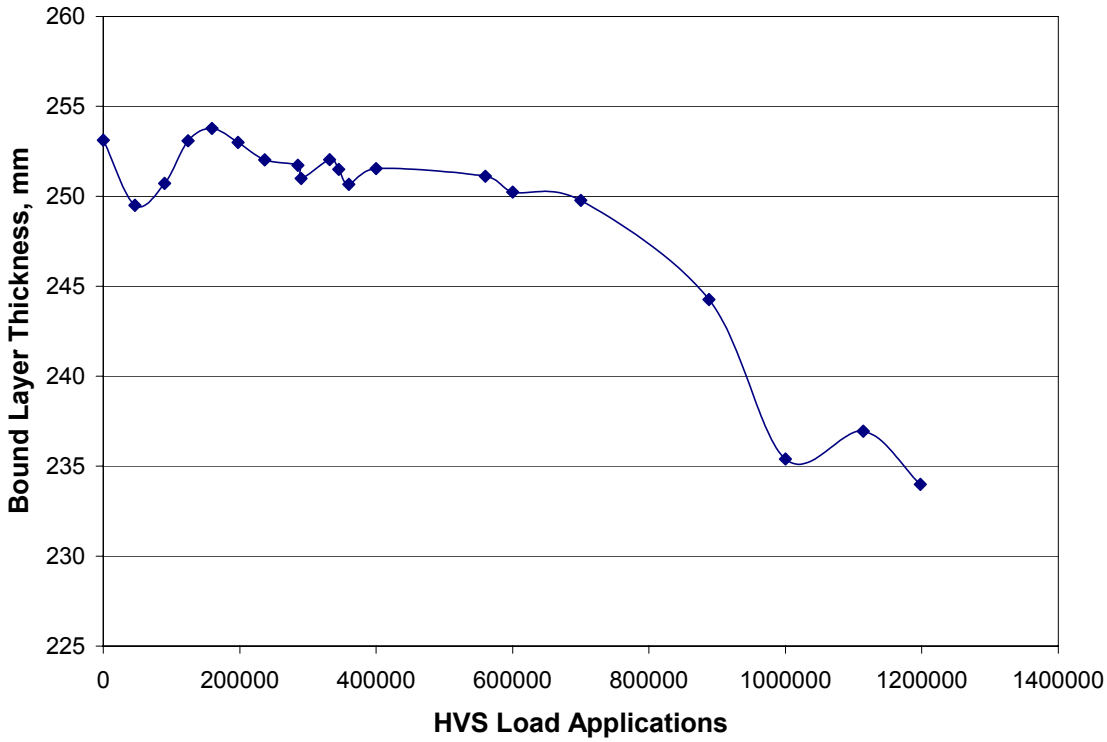


**Figure 34. Variation in bound pavement layers as measured with Ground Penetrating Radar (GPR).**

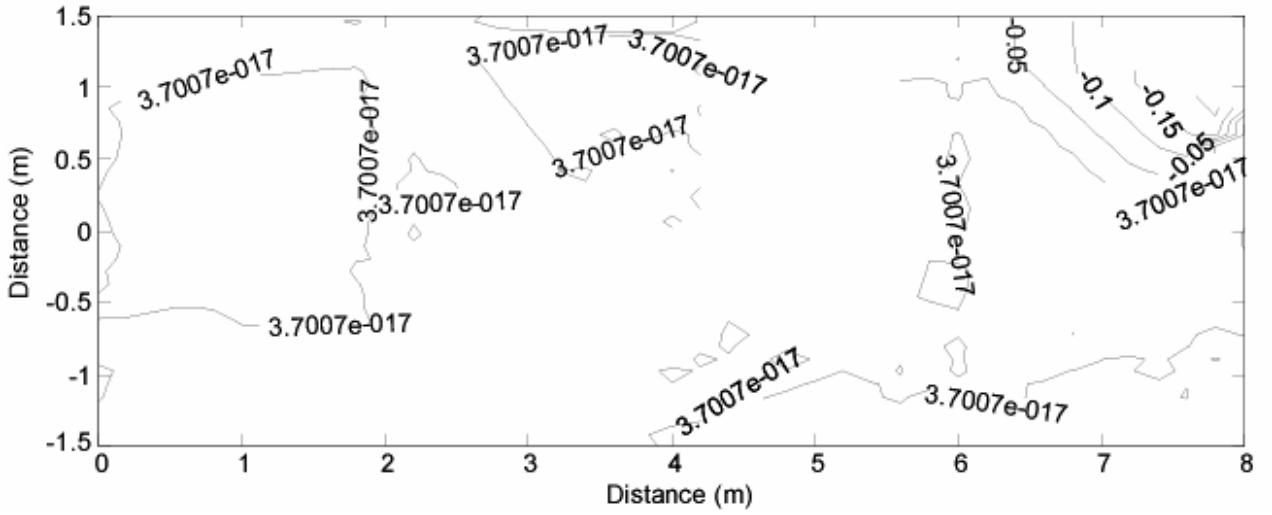


217k HVS load applications

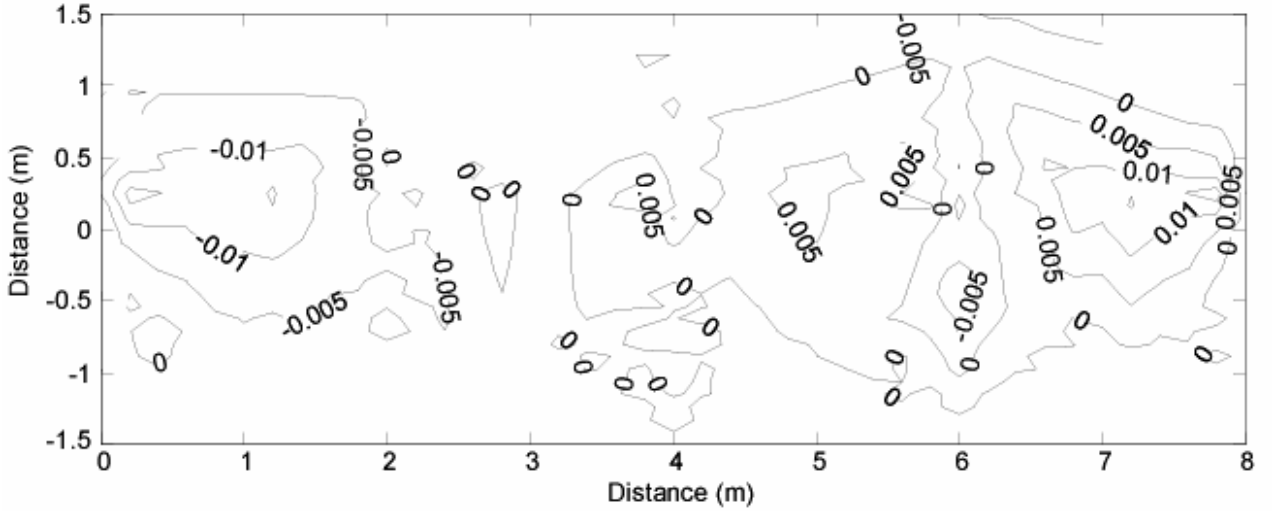


514k HVS load applications

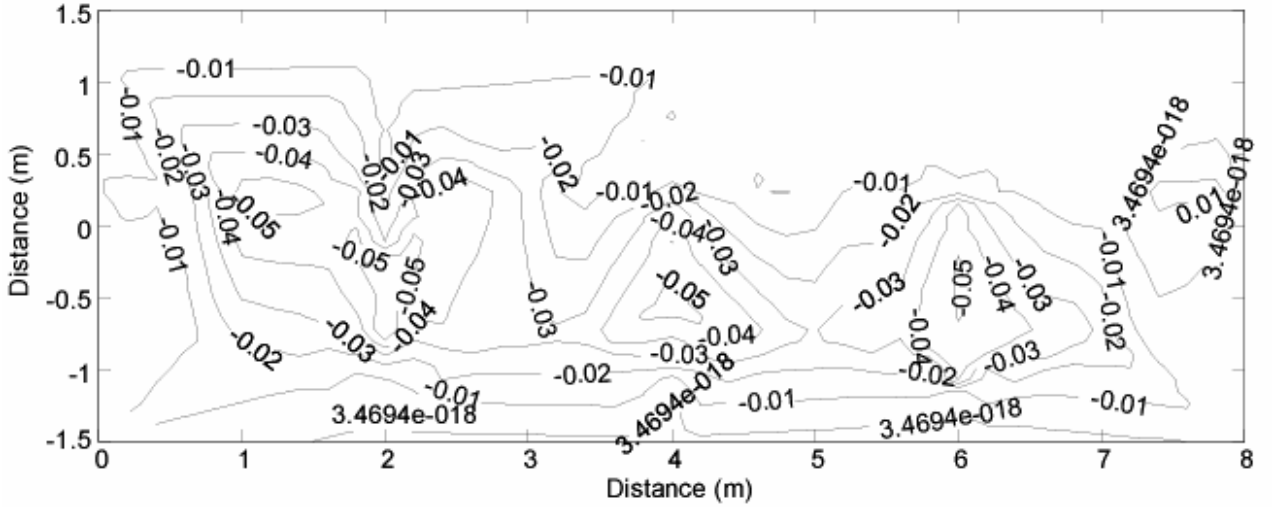


1,197k HVS load applications

**Figure 35. Reduction in bound layer thickness across Section 543 as measured with GPR.**

## 3.8 Forensic Activities

Forensic activities included core extraction, dynamic cone penetrometer testing, and trenching of the test section for direct observation of and data collection from the pavement structure. The locations of forensic activities on Section 543 are shown in Figure 36.

### 3.8.1 Extracted Cores

Figures 37 and 38 show two extracted cores from Station 13. One core is from the centerline of the trafficked area (Figures 37a and 37b) and the other is from about 1.4 m from the centerline outside the trafficked area (Figure 36). Figure 37 shows the significant deterioration of the asphalt concrete at the lift interfaces. This deterioration is likely due to lack of bonding between the asphalt layers, which allowed for bending and movement along the interfaces. During construction, a tack coat was applied between the AC and the asphalt rubber (ARHM-

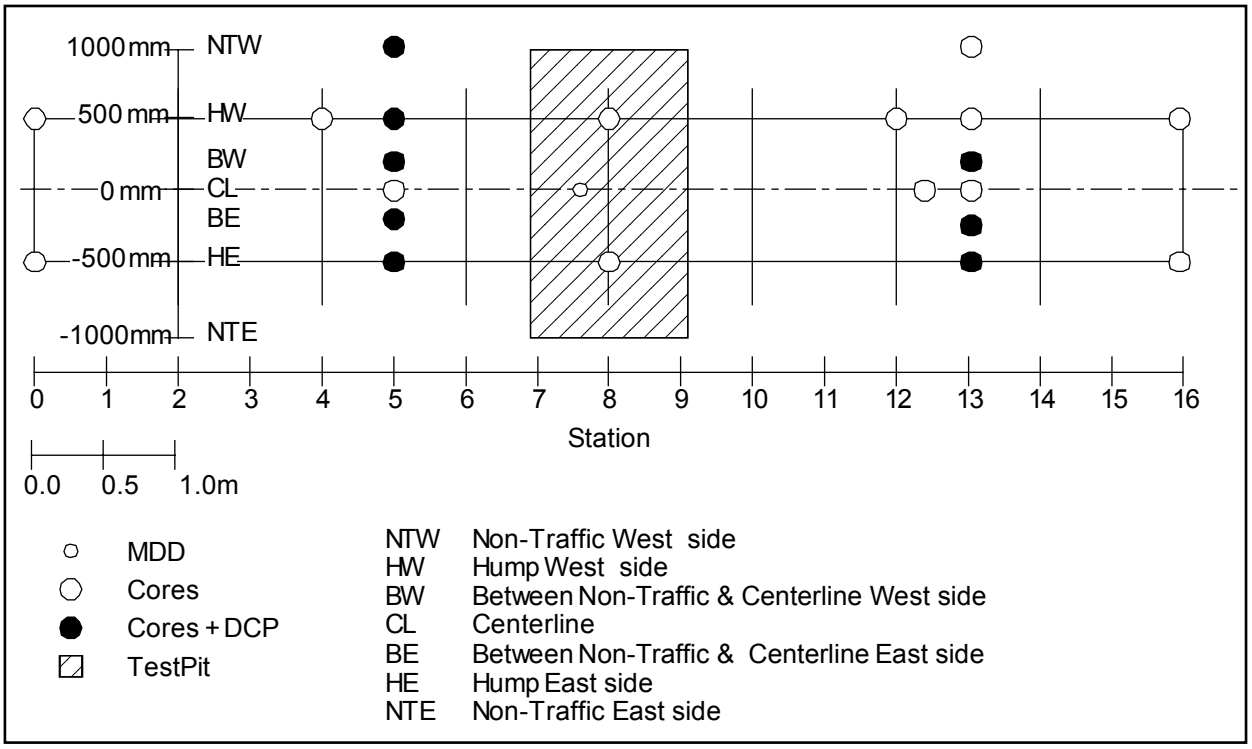


**Figure 36. Locations of forensic activities on Section 543.**


**a. Asphalt Layers** **b. Asphalt Treated Permeable Base**

**Figure 37. Core extracted from centerline at Station 13, Section 543.**

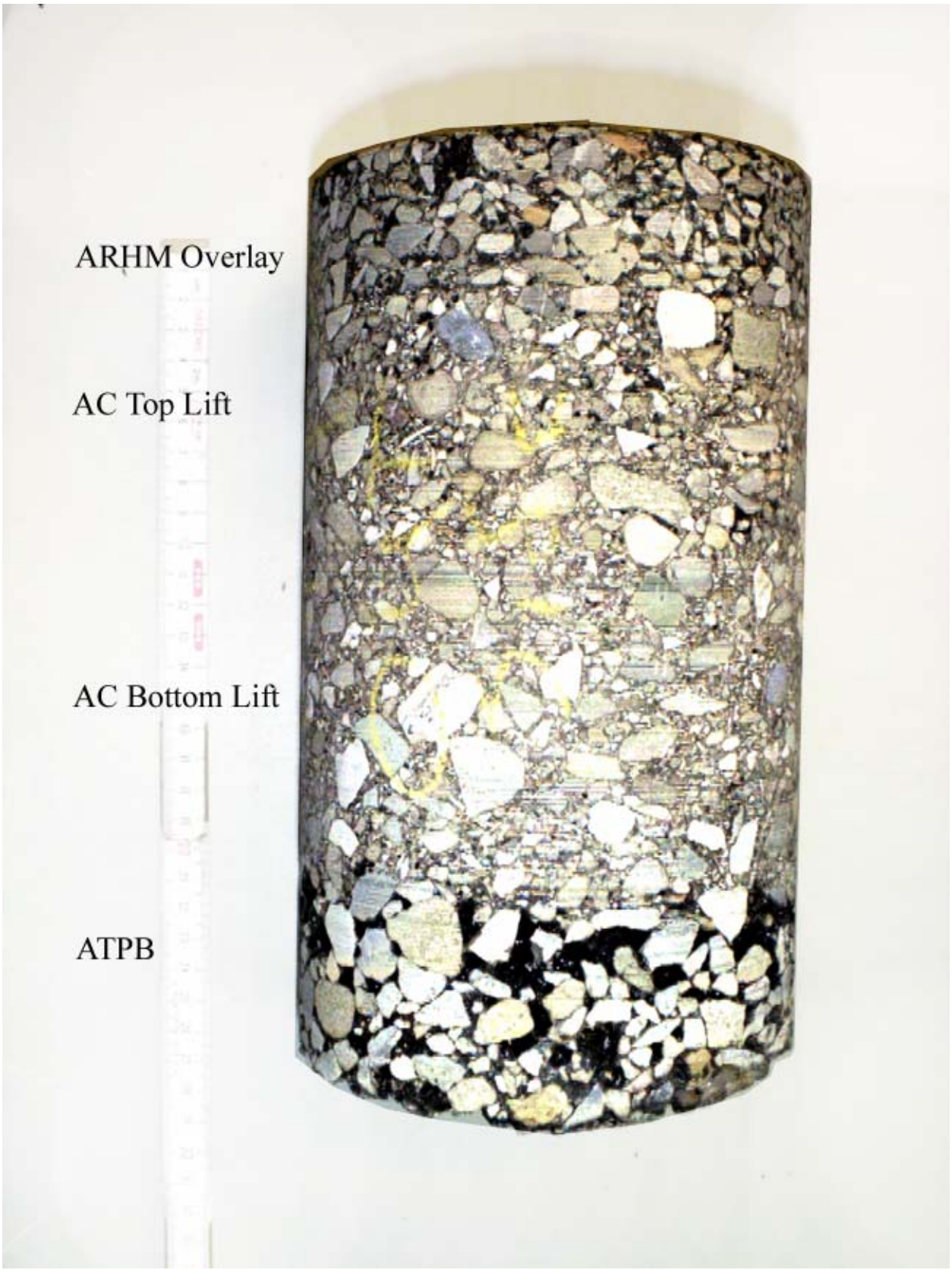


**Figure 38. Core extracted from outside the trafficked area at Station 13, Section 543.**

GG) layers. A tack coat was not applied between the top and bottom AC lifts. The extracted core showed no bonding between the layers. In addition, the ATPB could not be extracted as a solid cohesive mass because the asphalt binder was completely stripped from the aggregate (see Figure 37-b).

Figure 38 shows a core extracted from outside the trafficked area. Bonding was evident through the layers with the ATPB layer still intact and attached, demonstrating that the ATPB did not show any stripping in the non-trafficked areas.

Stripping in the ATPB resulted from traffic loading. The loading likely created high pore water pressure in the ATPB since it was essentially in an undrained condition. The high pressure resulted in infiltration of water into the binder and a reduction in its cohesion (stiffness). It also probably caused water vapor to permeate the interfaces between the asphalt and aggregate. This contributed to debonding and eventual stripping of the asphalt from the aggregate.

Figure 39 shows a major crack through the asphalt concrete layer. From earlier tests, cracking was observed to have started at the bottom of the top layer of the asphalt concrete, although in the sections which had been overlaid with either DGAC or ARHM-GG (RAC-G), cracking eventually extended throughout the existing and overlay pavement layers.

Because of the reduced stiffness of the ATPB in the wet condition, it is hypothesized that cracking started at the bottom of the DGAC and propagated to the pavement surface.

Figure 40 shows the significant contamination of the ATPB near its interface with the aggregate base with fine silt material. It should be noted that the aggregate base had been primed prior to the placing of the ATPB. The results of this test suggest that it would be desirable to place a filter fabric on top of the untreated base prior to placing the ATPB to preclude upward migration of fines when the drainage system is not effective.

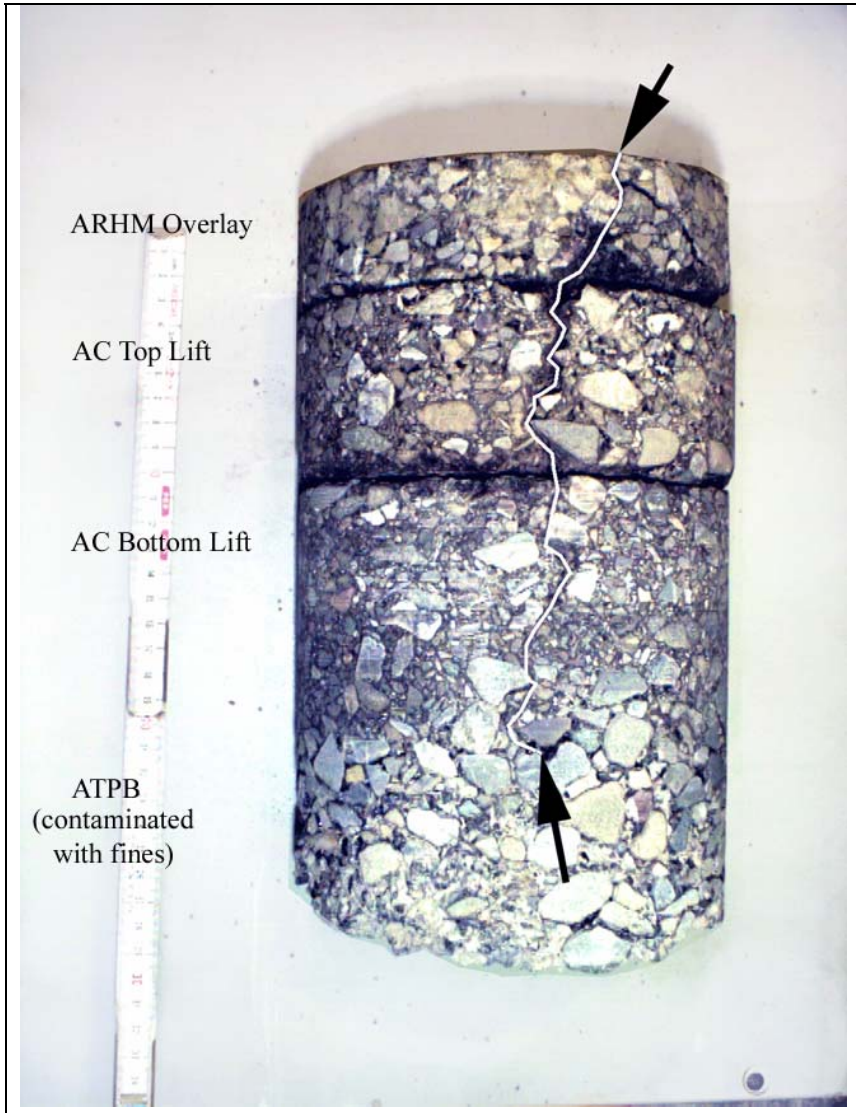


**Figure 39a. Front view.**

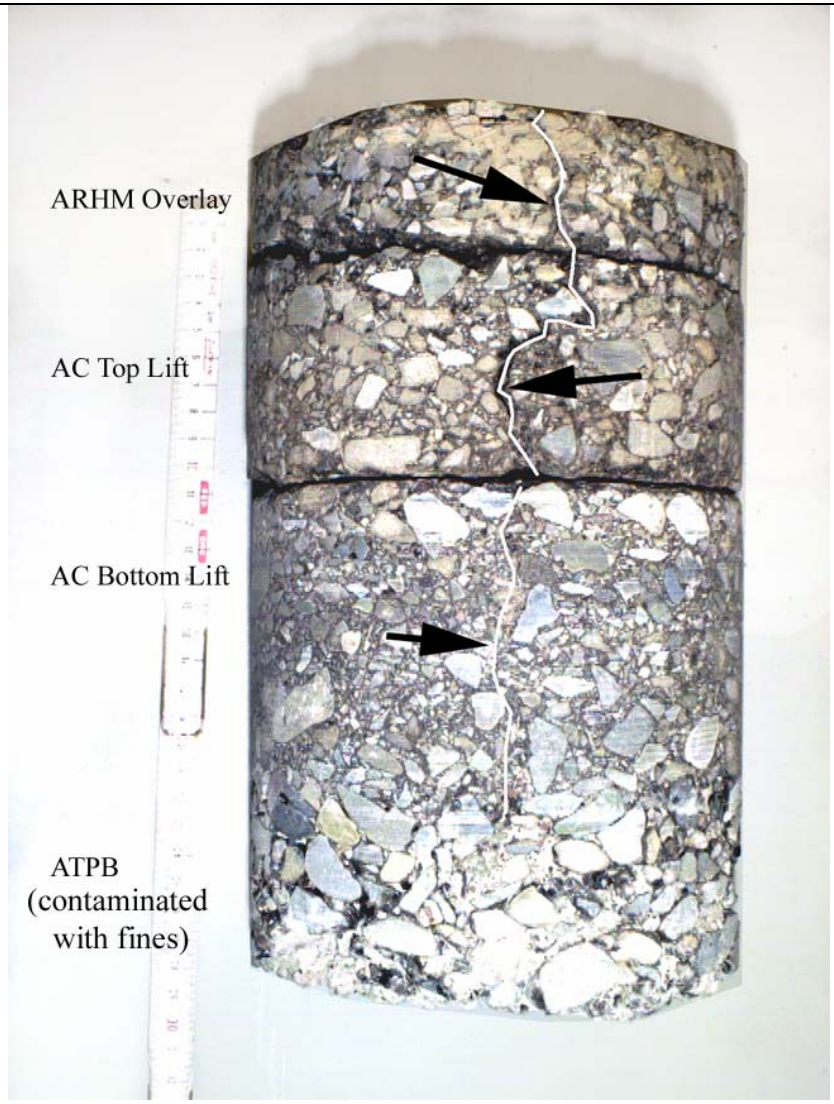


**Figure 39b. Opposite view.**

**Figure 39. Core extracted from centerline at Station 9, Section 543.**

Note: Sample is a slab shown upside-down (ATPB at top of image).

**Figure 40a. Fines-clogged ATPB slab from Section 543.**

Note: Sample is shown upside-down (ATPB at top of image).

**Figure 40b. ATPB slab from another HVS test section demonstrating appearance of ATPB without fines infiltration.**

**Figure 40. ATPB with and without fines infiltration.**

### 3.8.2 Percolation Tests

Field percolation tests were conducted to measure the permeability of the ATPB and the aggregate base layers at various HVS test locations. Figure 41 shows the location selected for the field percolation tests. Table 11 summarizes the conditions in which the sections were tested under the HVS.

**Table 11 Description of Test Sections Used for Percolation Tests**

| Section | ATPB | Base Condition | Traffic Load, kN | Asphalt Concrete Temperature (ºC) | Test Program Reference |
|---|---|---|---|---|---|
| 505 | Yes | No water infiltration | 40 | 50 | 9 |
| 512 | Yes | No water infiltration | 40 | 50 | 9 |
| 518 | No | No Water infiltration | 40,80, 100 | 20 | 10 |
| 543 | Yes | Water infiltration | 40,80,100 | 20 | |

Percolation test locations were classified based on the level of compaction added to the ATPB and aggregate base due to trafficking. The following levels of compaction in the sublayers (ATPB and aggregate base) were established:

- Level 1: No compaction in the sublayers due to HVS traffic. Percolation tests were conducted outside of trafficked sections.
- Level 2: Compaction in the sublayers due to light HVS traffic. Percolation tests were conducted on sections trafficked under a 40-kN load (Sections 505 and 512).
- Level 3: Compaction in the sublayers due to heavy HVS traffic. Percolation tests were conducted on sections trafficked under 40-, 80-, and 100-kN loads (Sections 518 and 543).

Cores (150 mm) were extracted from the AC and ATPB layers in the trafficked and untrafficked areas of the test section, as indicated in Figure 1. Because of the coring method, the holes were approximately 160 mm in diameter. The AB was excavated by hand approximately

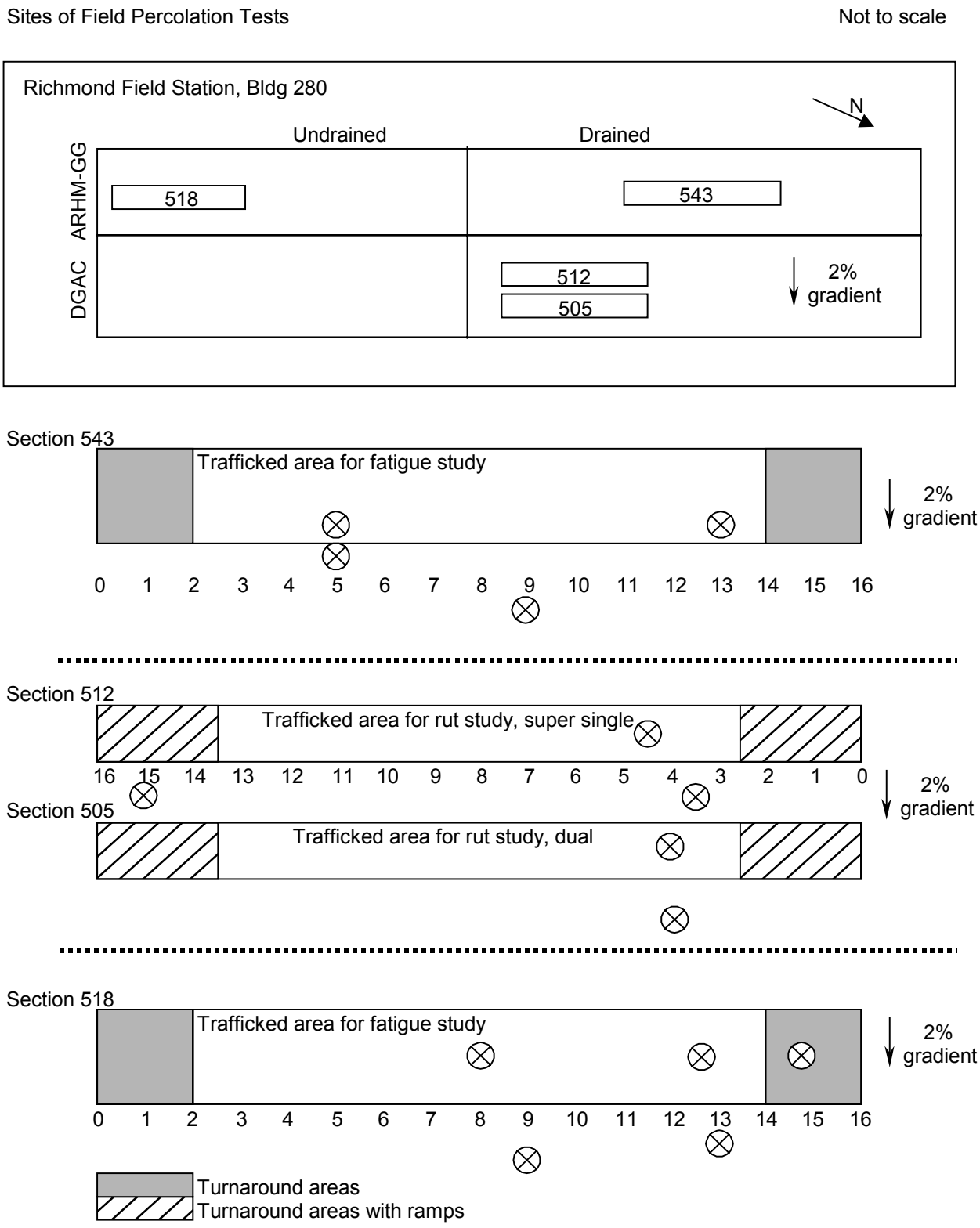


**Figure 41. Sites of field percolation tests.**

150 mm below the ATPB or AC, so that the bottom of the hole is approximately 50 mm above the ASB. The holes were filled with water to the base of the ATPB or top of the AC, and allowed to percolate through the AB for 24 hours. This delay period allowed the AB to saturate. After 24 hours, the water level was increased to the top of the AB and testing began. Care was taken to ensure the water level was below the top of the AB during testing, thereby preventing water from running between layer interfaces. The monitoring plan was scheduled to record the water level at 30 minute intervals for the first 4 to 6 hours and every hour thereafter. The percolation rate was calculated as the drop in head per hour.

Figures 42 and 43 summarize the percolation rates for the aggregate base and ATPB layers at the designated level of compaction. Figure 42 shows a contrast between aggregate base beneath ATPB and without ATPB. The lines in Figure 42 show tendencies of the data using a linear regression model. The contrast is probably due to the ATPB providing less intense stresses on top of the aggregate base that would otherwise further compact the aggregate base layer, both during construction and later during trafficking.

Figure 43 shows the dramatic difference between the high permeability of the ATPB when this layer is intact and the permeability of the ATPB under the trafficked area of Section 543 (Test 543-5a). The permeability of the intact ATPB is about 1 cm/sec. The permeability of the ATPB at the trafficked area in Section 543 was reduced about three orders of magnitude by the fine material that infiltrated the ATPB layer from the aggregate base. This infiltration of fines into the ATPB only occurred under the saturated base condition and when the section was subjected to heavy loading from the HVS. Results from this are discussed earlier in this report.

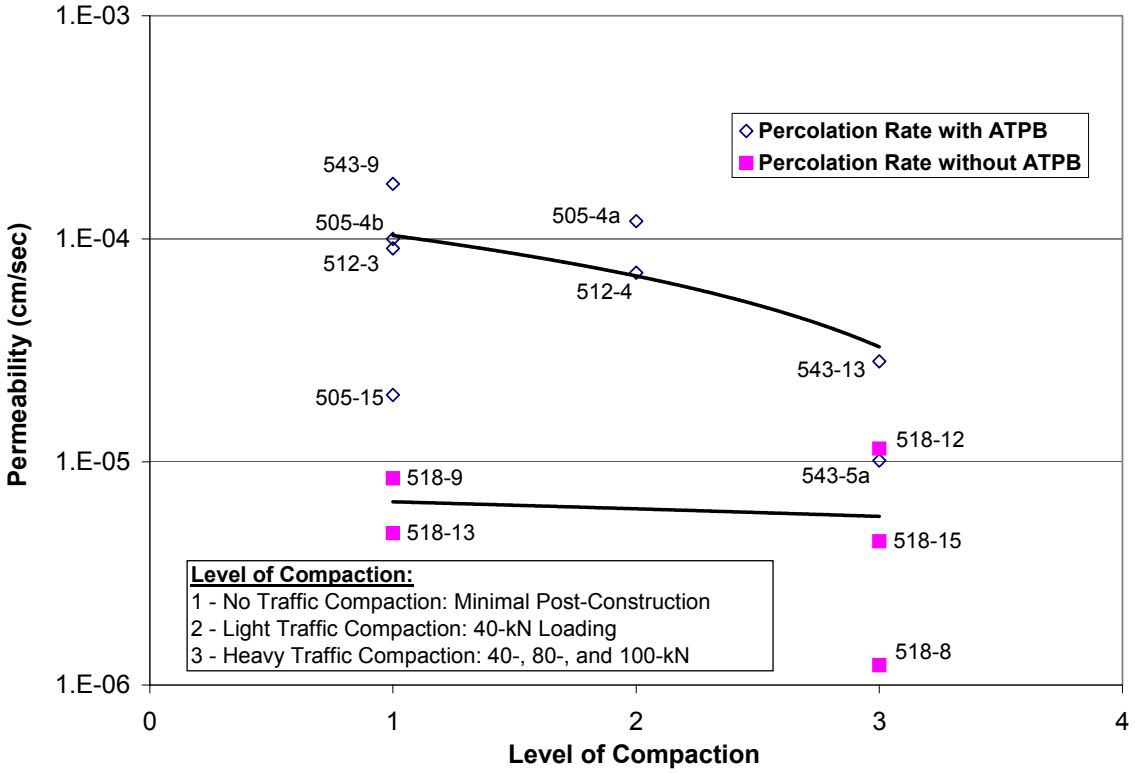


**Figure 42. Percolation tests on aggregate base.**

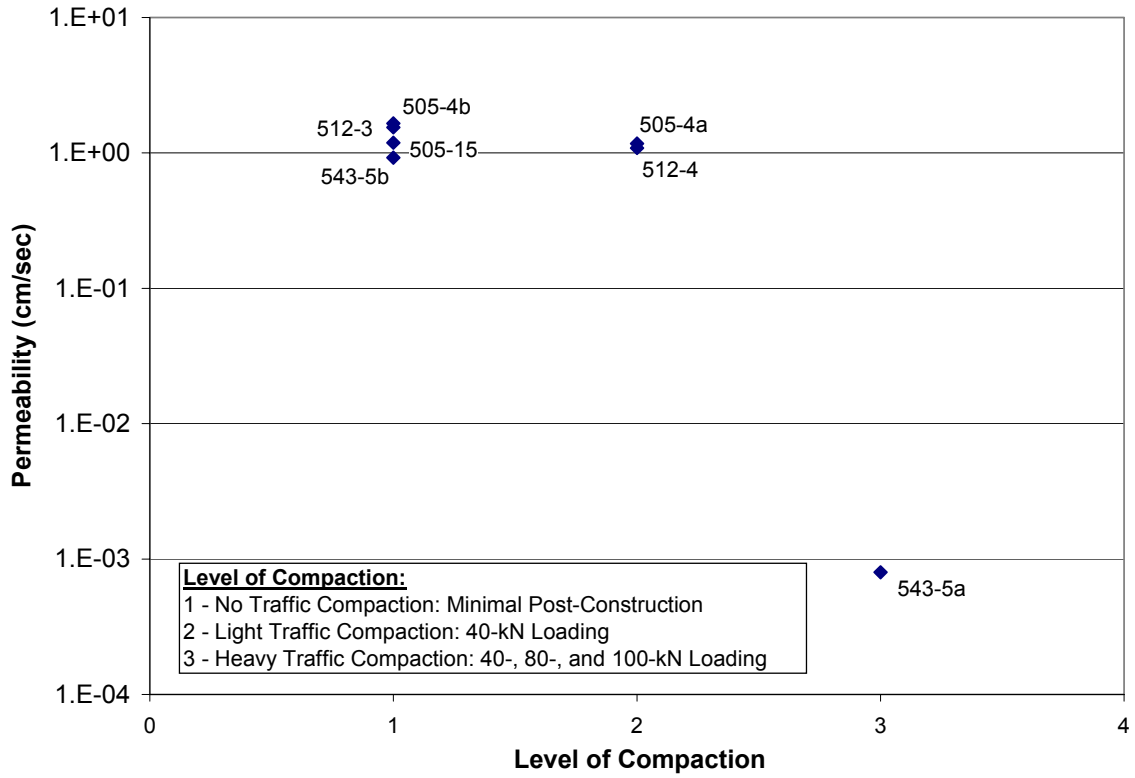


**Figure 43. Percolation tests on ATPB.**

### 3.8.3 Air-Void Content

Figure 44 summarizes air-void content data for all the bound layers after the completion of HVS trafficking. Lower air-void contents were observed within the trafficked area compared to outside the trafficked area for the ARHM-GG wearing course and the ATPB layer, with the lowest air-void contents measured along the traffic centerline. A significant reduction in air-void content (from 11–13 percent to about 9 percent) was observed for the ARHM-GG overlay as a result of HVS trafficking. The high air-void contents observed in the ARHM-GG were anticipated and reported in References (*8*) and (*9*). Figure 44 also shows the significant reduction in air-void content in the ATPB layer. Air-void content of the ATPB may have been affected by the fine silt contamination (Section 3.6.1). Small reductions in air-void content were observed in the other asphalt concrete layers. Variations are attributed to construction variability.

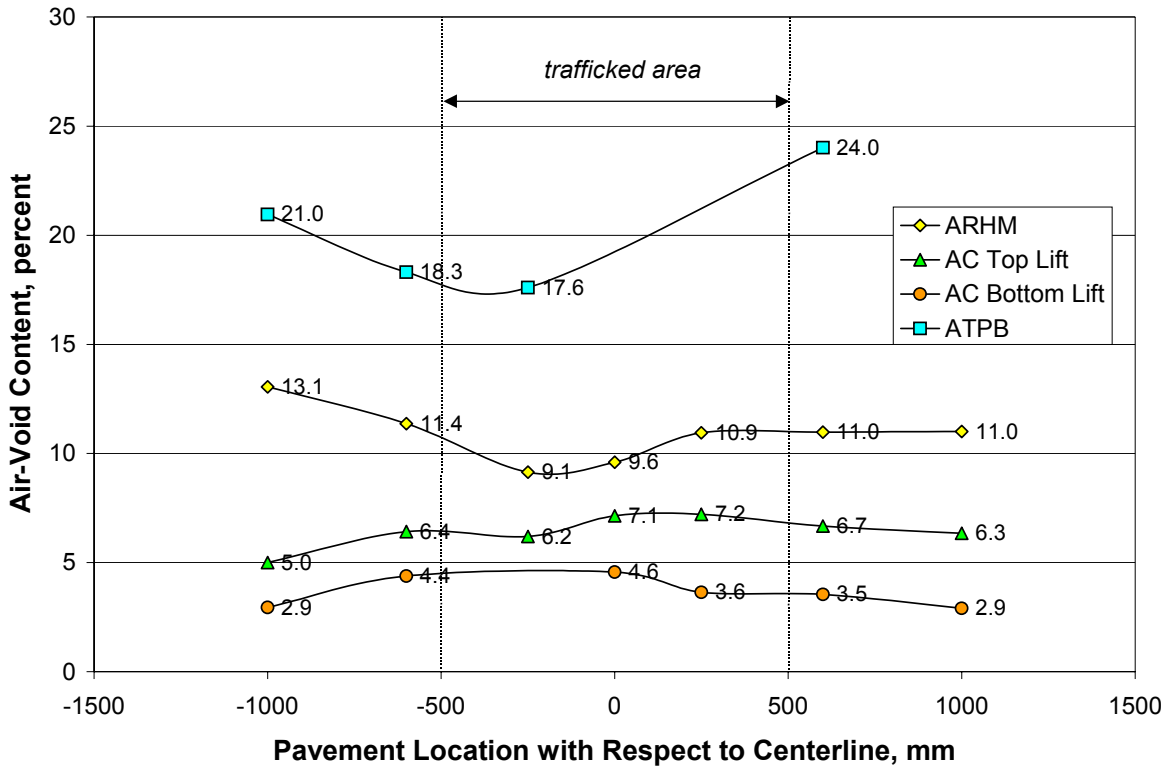


**Figure 44. Average air-void contents across Section 543 after HVS trafficking.**

Table 12 summarizes air-void contents in the bound layers in three distinct regions of the test section: 1) trafficked area, which is the zone within the width of the HVS wheelpath excluding the turnaround zones; 2) "hump areas," which are the zones of uplifted material at the edges of the trafficked area; and 3) non-trafficked areas, which are located outside of the HVS wheelpath and beyond the hump areas.

**Table 12 Summary of Air-Void Contents for Section 543**

| Asphalt Layers | Average Air-Void Content in Region, percent | | |
|---|---|---|---|
| | **Trafficked Area** | **"Hump Areas"** | **Non-Trafficked Areas** |
| ARHM Overlay | 9.1 | 11.0 | 13.1 |
| Asphalt Concrete, Top Lift | 6.2 | 6.7 | 6.3 |
| Asphalt Concrete, Bottom Lift | 4.4 | 3.6 | 2.9 |
| ATPB | 17.6 | 19.2 | 21.0 |

### 3.8.4 Dynamic Cone Penetrometer (DCP) Data

Figures 45–47 summarize the results of Dynamic Cone Penetrometer (DCP) tests for Section 543 performed inside and outside the trafficked area. Measurements were obtained within a distance of ±1 m from the centerline. These figures show the amount of penetration versus the number of blows applied. The slopes of these curves are proportional to the strengths of the various pavement materials. A steeper slope (more rapid cone penetration) indicates a layer with lower strength while a more gradual slope (lower penetration rate) indicates a stronger material.

Table 13 summarizes DCP data for the aggregate base, aggregate subbase, and subgrade after HVS trafficking. The data indicate that the aggregate subbase is slightly stronger than the aggregate base.

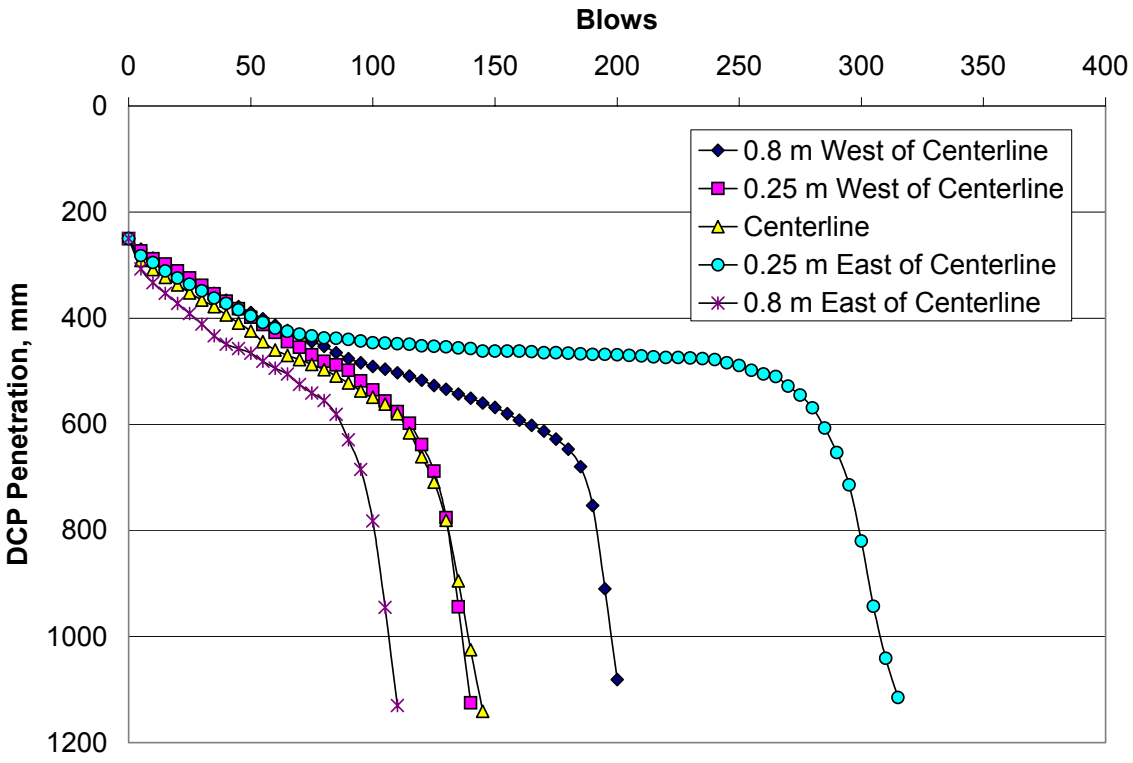


**Figure 45. Dynamic Cone Penetrometer (DCP) tests at Station 5, Section 543.**

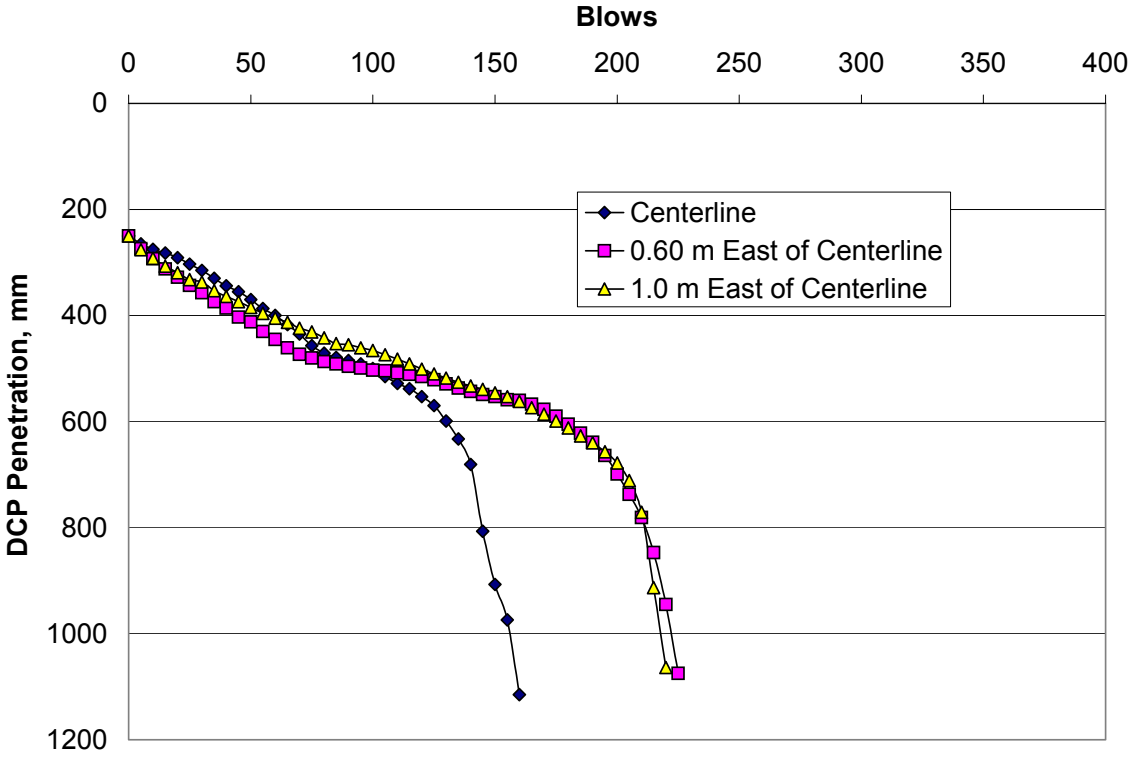


**Figure 46. Dynamic Cone Penetrometer (DCP) tests at Station 13, Section 543.**

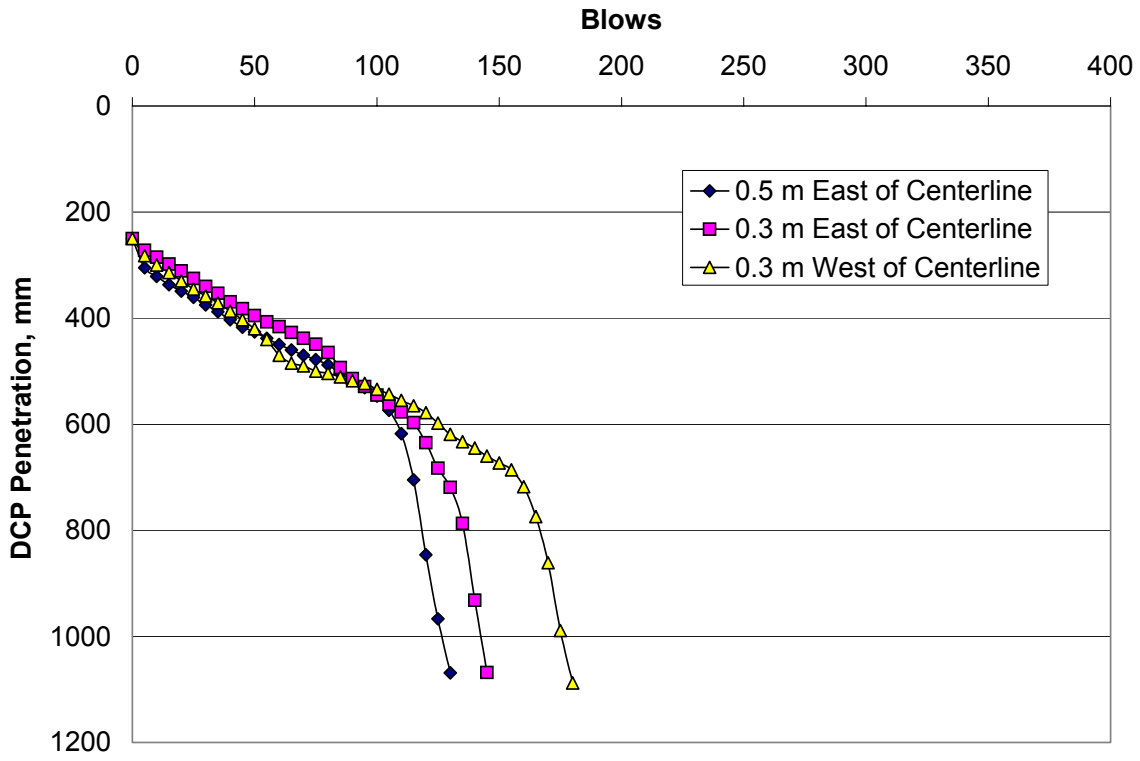


**Figure 47. Dynamic Cone Penetrometer (DCP) tests in trench, Section 543.**

**Table 13 Summary of DCP Penetration Rates, Section 543.**

| DCP Test Location | | Penetration Rate (mm/blow) | | |
|---|---|---|---|---|
| | | Aggregate Base | Aggregate Subbase | Subgrade |
| Station 5 | 0.8 m W of Centerline | 2.5 | 1.6 | 22.0 |
| | 0.25 m W of Centerline | 2.8 | 1.6 | 24.6 |
| | Centerline | 2.9 | 2.4 | 19.8 |
| | 0.25 m E of Centerline | 2.3 | 0.4 | 24.6 |
| | 0.8 m E of Centerline | 4.1 | 3.0 | 25.2 |
| Station 13 | Centerline | 2.6 | 2.6 | 20.7 |
| | 0.60 m E of Centerline | 3.0 | 1.2 | 19.6 |
| | 1.0 m E of Centerline | 2.2 | 1.7 | 29.3 |
| In Trench between Stations 7 & 9 | 0.3 m W of Centerline | 3.0 | 1.8 | 19.1 |
| | 0.3 m E of Centerline | 2.7 | 3.6 | 17.0 |
| | 0.5 m E of Centerline | 2.7 | 2.7 | 23.3 |
| | *Average* | *2.8* | *2.1* | *22.3* |
| | *Standard Deviation* | *0.5* | *0.9* | *3.5* |

### 3.8.5 Trench Data

After the completion of HVS trafficking, a transverse trench was excavated from Station 7 to Station 9 (see Figure 36) in order to enable direct observation of the pavement layers. Measurements from the trench were used to estimate thickness and rutting in the pavement layers. Figures 48 and 49 show profile data at the interface of each layer at the completion of HVS trafficking. During the data collection process, it was difficult to establish the boundary between the ATPB and the aggregate base due to the intrusion of fines from the aggregate base into the ATPB. The profiles show that the subbase thickness varied considerably across Section 543. Differences in subbase thickness were anticipated and reported in previous CAL/APT reports.(*8, 10–12*)

Figure 50 summarizes layer thickness inside and outside the trafficked area for the south and north faces in the open pit. Layer thicknesses are average thicknesses across the transverse distance at 500-mm intervals based on the transverse coordinate system shown in Figure 36.

The data indicate uniform thicknesses across the asphalt rubber and the two asphalt concrete lifts. No significant difference in layer thickness was measured between centerline thickness and thickness away from centerline. Therefore, significant rutting did not occur in these layers. Standard deviations for the thicknesses of the asphalt rubber, asphalt concrete top lift, and asphalt concrete bottom lift were 2, 3, and 4 mm, respectively.

Larger variability was found for the ATPB and aggregate base and subbase layers. Data from outside the trafficked area (between –1000 and –500 and between 500 and 1000) indicate thickness variability of the ATPB during construction. On average, the difference between the two non-trafficked areas was between 12 to 17 mm. Standard deviation for the ATPB layer across the two faces was 8 mm. Centerline thicknesses for the ATPB are thinner than the thicknesses across the non-trafficked area between –1000 to –500 and thicker than the

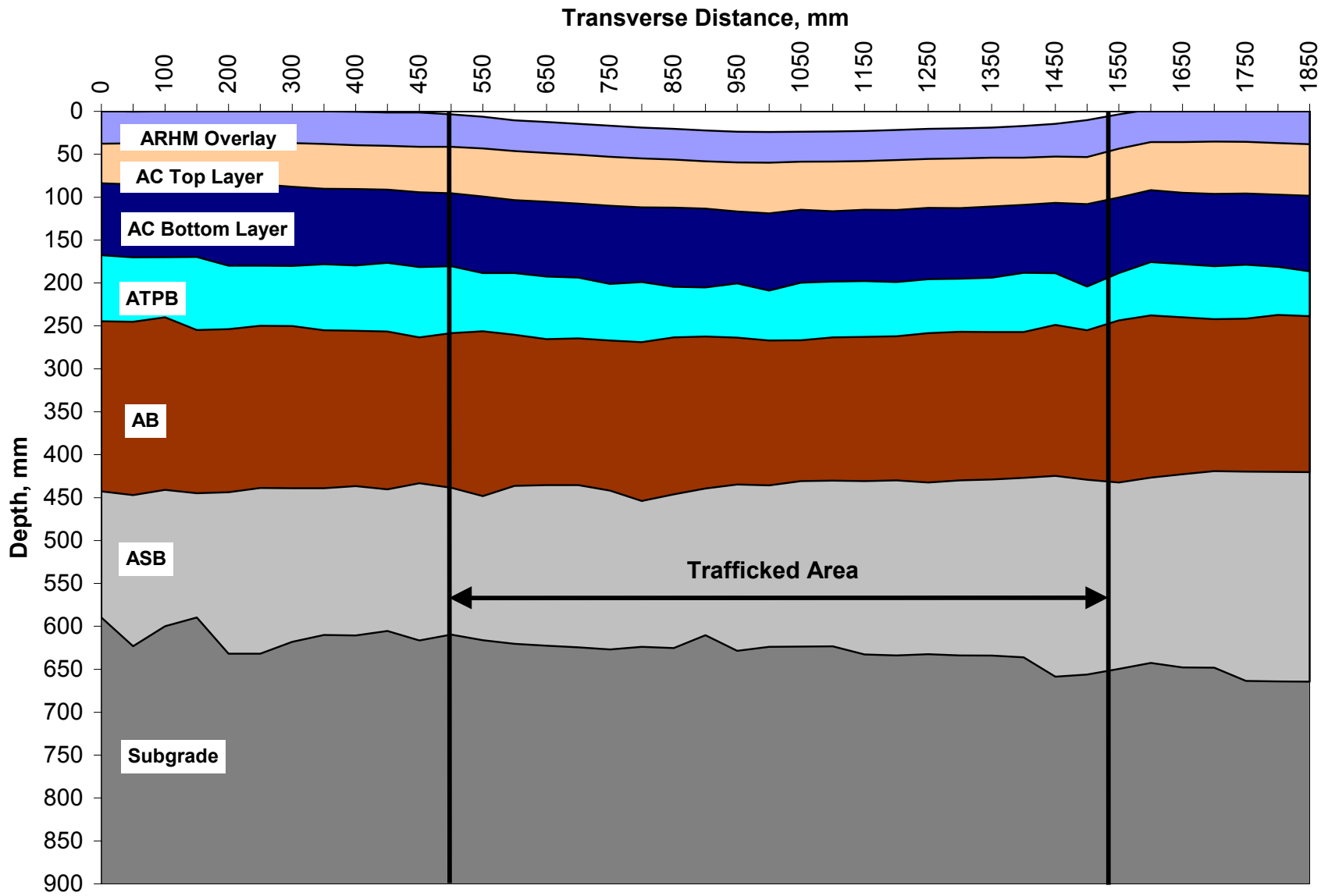


**Figure 48. Layer profiles measured in trench, south face of trench at Station 7, Section 543.**

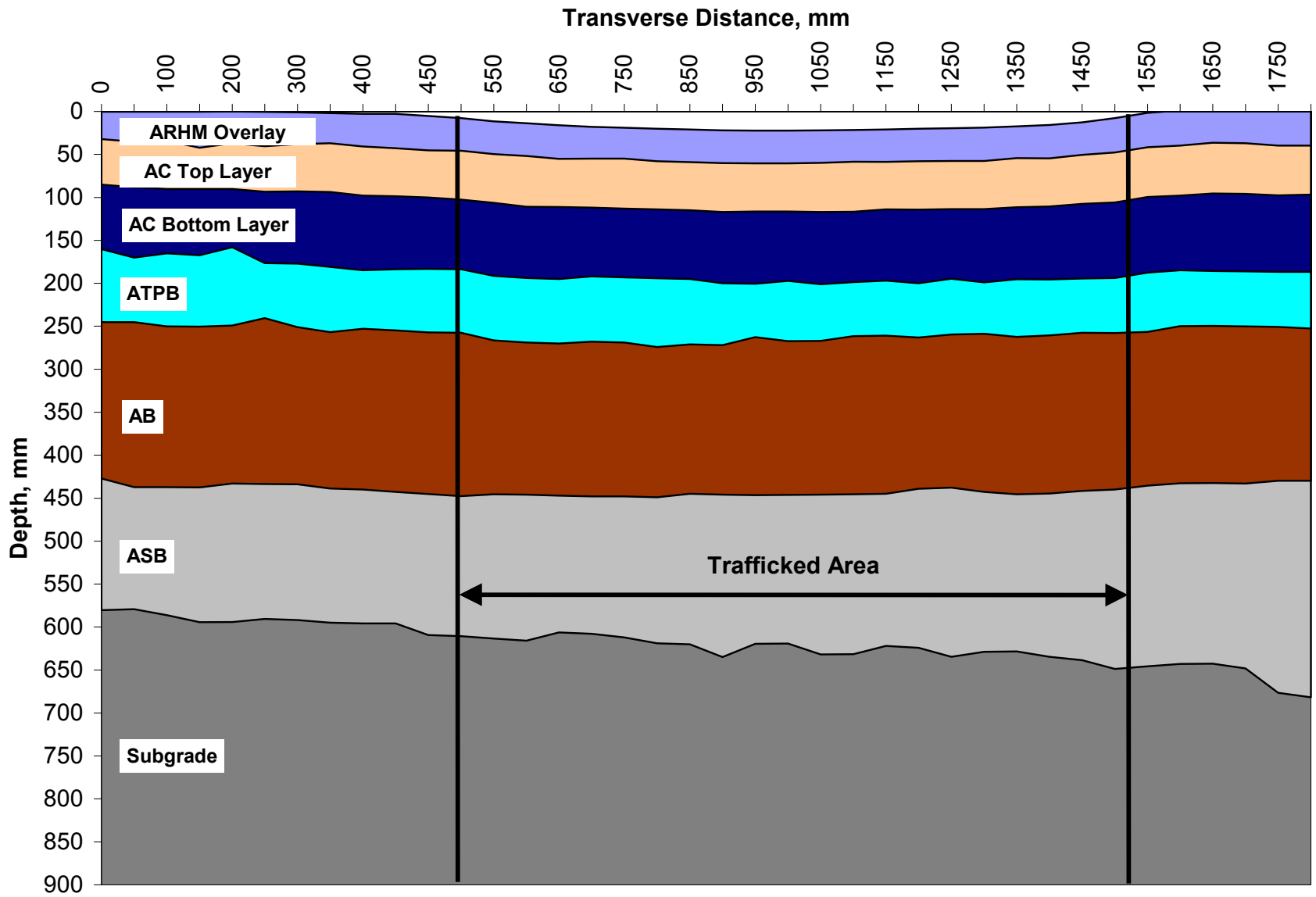


**Figure 49. Layer profiles measured in trench, north face of trench at Station 9, Section 543.**

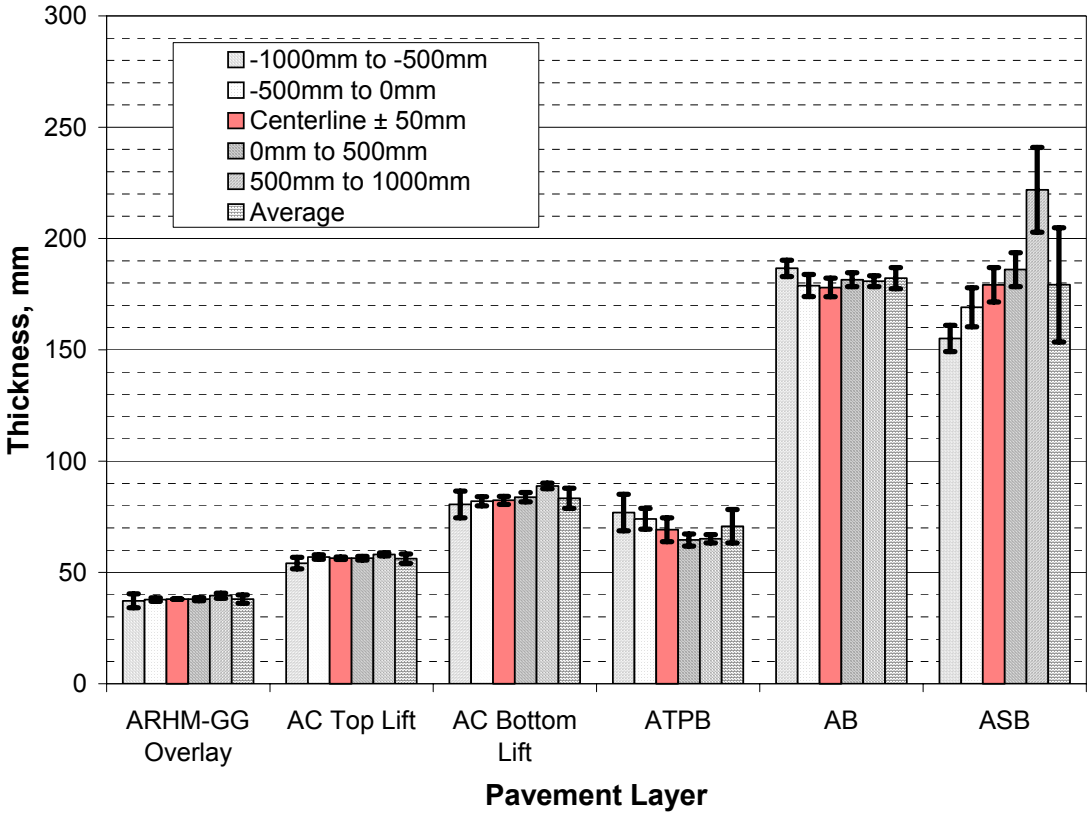


**Figure 50. Summary of layer thicknesses across transverse distance of trench.**

thicknesses across the non-trafficked area between 500 to 1000 mm. Therefore, no clear conclusion can be drawn regarding rutting in this layer based on the data from the test pit. However, the reduced thickness of the ATPB and the amount of fine intrusion from the aggregate base along the centerline of the section ±100 mm suggest deformations in the ATPB and aggregate base layers at the interface.

Thickness measurements for the aggregate base obtained at the centerline are lower than those obtained outside the trafficked areas. Differences were 6 and 13 mm for the north face and south face, respectively. Standard deviation for the aggregate base layer across the two faces was 8 mm. The data also show the thickness variation of the aggregate subbase across the transverse distance of the section. The standard deviation for the aggregate subbase thickness was 27 mm.

Based on the average thickness measurements obtained for the pavement layers, rutting occurred primarily in the area near the interface of the ATPB and the aggregate base. However, due to rough interfaces between the ATPB and aggregate base, between the aggregate base and the aggregate subbase, and between the aggregate subbase and the subgrade, accurate estimates of the thicknesses of the ATPB, aggregate base, and aggregate subbase and rutting estimates in each of these layers were difficult to determine.

## 4.0 PERFORMANCE EVALUATION AND MECHANISTIC ANALYSIS

By the end of HVS testing, Section 543 had been subjected to 236.6 $\times 10^3$ applications of the 40-kN load, 331.8 $\times$ $10^3$ applications of the 80-kN load, and 629.3 $\times$ $10^3$ applications of the 100-kN load. The number of applied loads was converted to equivalent 80-kN single axle loads (ESALs) using a load equivalency exponent of 4.2 according to Caltrans procedure, resulting in a total of 35.8 million ESALs. According to the failure criterion established for the project, the number of ESALs to failure for surface rutting was 18.7 million while that for surface cracking (2.5 $m/m^2$) was 35.8 million. It is evident that Section 543 failed by surface rutting before reaching the surface cracking criterion.

As discussed in Chapter 3, Section 543 failed because of stripping and intrusion of fines into the ATPB layer. In the following paragraphs, estimates of pavement responses at the beginning and end of HVS testing, based on the layer moduli obtained during the back-calculation process, are provided together with a discussion of the impact of the response on the performance of the pavement section. Three cases were considered for the analyses. For Cases I and II, the stiffness characteristics of the pavement structure were defined by the FWD back-calculation process (see Section 3.4.3). For Case III, the ATPB layer was replaced by an equivalent layer of dense graded asphalt concrete. While direct comparison of Cases I and II with Case III is not possible because the expected mode of failure of the pavement structure for Case III is fatigue cracking rather than rutting failure due to stiffness degradation in the ATPB, Case III has been included to question the necessity of using an ATPB layer.

### 4.1 Pavement Responses

Pavement responses considered for the analyses are tensile strain at the bottom of the asphalt concrete (ATPB is not included), and vertical compressive stresses at the top of the

ATPB, aggregate base, and subgrade layers. Layer moduli values were obtained from FWD testing by back-calculation. For Case III, the 75-mm ATPB layer was replaced with an equivalent thickness of DGAC obtained using the Odemark method. For a modulus of 1,600 MPa for the intact ATPB and 10,000 MPa for the intact DGAC layer, the equivalent thickness would be about 40 mm of DGAC.[2] Materials, thicknesses, and moduli for the pavement structures used for the three cases are summarized in Table 13.

**Table 13 Summary of Pavement Structures for Analysis**

| Case | Layer | Thickness, mm | Modulus before HVS Trafficking, MPa | Modulus after HVS testing, MPa |
|---|---|---|---|---|
| Case I | AC + ATPB | 247 | 8,500 | 950 |
| | AB | 368 | 300 | 70 |
| | SG | | 170 | 100 |
| Case II | AC | 178 | 12,000 | 1,900 |
| | ATPB + AB | 477 | 470 | 140 |
| | SG | | 160 | 120 |
| Case III | AC | 218 | 10,000 | - |
| | AB | 268 | 300 | - |
| | SG | | 170 | - |

Table 14 summarizes calculated pavement responses under a 40-kN load for the three cases considered. Tensile strains at the bottom of the AC layer have been used to estimate the fatigue performance of the pavement structures.

**Table 14 Summary of Pavement Responses under 40-kN Load**

| Case | Before or After HVS Trafficking | Tensile Strain, Bottom of AC | Vertical Stress, Top of ATPB, kPa | Vertical Stress, Top of AB, kPa | Vertical Stress, Top of SG, kPa |
|---|---|---|---|---|---|
| Case I | Before | - | - | 32 | 19 |
| | After | - | - | 50 | 46 |
| Case II | Before | 46 | 63 | - | 17 |
| | After | 222 | 91 | - | 37 |
| Case III | Before | 42 | - | 36 | 21 |
| | After | - | - | - | - |

[2] $h_{DGAC} = h_{ATPB}\sqrt[3]{\frac{E_{ATPB}}{E_{DGAC}}} = 75\sqrt[3]{\frac{1600}{10000}} \cong 40\,mm$

## 4.2 Fatigue Analysis

The fatigue analysis and design system used in this report is shown in Figure 51.(*10*) For the analysis, a design reliability of 50 percent, corresponding to a reliability multiplier of 1.0, was assumed. The laboratory fatigue life equation for the mixes used in the simulation is:

$$\ln N = -21.9295 - 0.106663\,AV - 4.14248 \ln \varepsilon$$

where $N$ is the number of repetitions to failure obtained from laboratory fatigue beam tests using the controlled strain mode of bending, $AV$ is the percent air-void content of the mix, and $\varepsilon$ is the tensile strain at the bottom of the asphalt concrete. The shift factor (*SF*) equation, which has been calibrated using pavement designed according to the Caltrans procedure, is:

$$SF = 3.1833 \times 10^{-5}\,\varepsilon^{-1.3759}$$

The temperature conversion factor (*TCF*) equation used for this simulation[3] is:

$$TCF = 1.754 \ln(d) - 2.891$$

where $d$ is the thickness of the asphalt concrete layer in centimeters.

The results of the simulation process are summarized in Table 15 for the information obtained from the three cases. Cases I and II represent the same pavement structure using pavement responses measured at different locations.

**Table 15 Summary of Calculation of ESALs Using UCB Fatigue Analysis System**

| Case | Microstrain | Air-Void Content, % | ln N | N, $\times 10^6$ | Shift Factor | AC thickness ($t_{AC}$), cm | Temperature Conversion Factor (*TCF*) | *M* | ESALs, millions |
|---|---|---|---|---|---|---|---|---|---|
| I-II | 46 | 4.6 | 18.95 | 170.5 | 29.5 | 17.8 | 2.16 | 1 | 2,333 |
| III | 42 | 4.6 | 19.33 | 248.6 | 33.5 | 21.8 | 2.51 | 1 | 3,310 |

[3] The equation for TCF is for the region along the California Coast in the vicinity of Santa Barbara. It tends to provide more conservative estimates of traffic than other areas of California

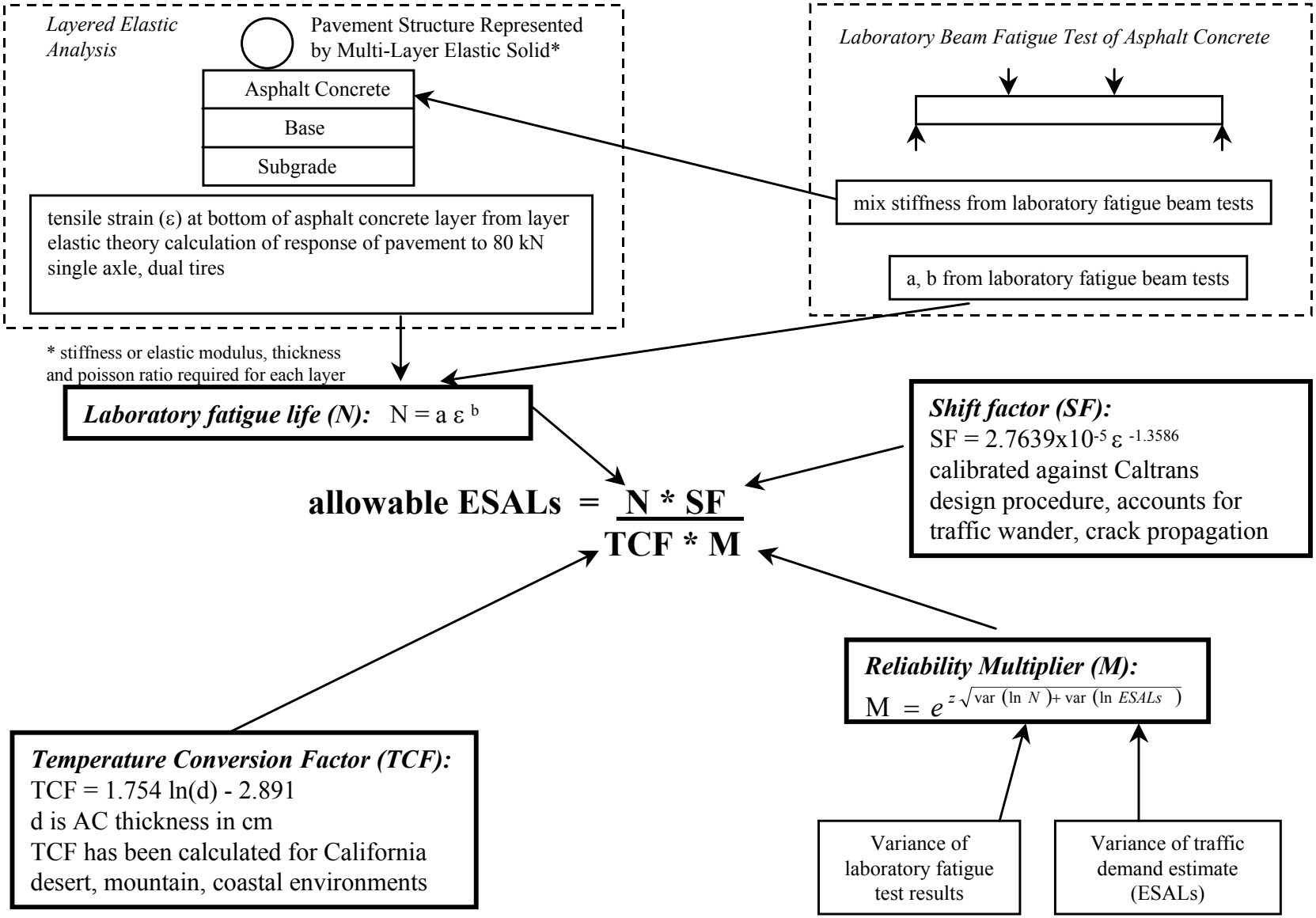


**Figure 51. Methodology followed in the fatigue analysis system to determine ESALs.**

The simulations suggest that if fatigue failure were the distress mode, the sections would sustain at least $2{,}000 \times 10^6$ ESALs (for a reliability level of 50 percent). However, the results of HVS testing of Section 543 indicated that the fatigue performance of this type of section can be severely affected if the ATPB strips. While little fatigue cracking was observed in the section up to the point that the ATPB started to strip, rapid development of surface cracking was observed after this point. It should be noted that if the ATPB is designed in such a way that it does not strip, then the performance of this type of section would be excellent. To improve ATPB performance requires that an improved mix design procedure be developed for the ATPB and that a filter layer (fabric) should be used at the interface between the ATPB and untreated base to prevent the intrusion of fines into the ATPB.

The simulations also suggest that the pavement structure for Case III will outperform the pavement structure of Cases I and II. Replacing the ATPB with an equivalent thickness of asphalt concrete provides an improved fatigue life and reduction in stresses in the unbound layers.

### 4.3 Economic Analysis

Selecting a pavement structure with the ATPB layer or one with an additional thickness of AC would depend on which pavement structure is the most cost-effective. Based on Caltrans construction data, between 1994 and 1998, the cost of ATPB averaged $56 per cubic meter for an average annual production of 81 thousand cubic meters. For the same period, the cost of Type A dense graded asphalt concrete was $35 per tonne, or about $83 per cubic meter, about 1.5 times the cost of ATPB. The cost savings achieved by replacing the 75-mm ATPB layer with a 40-mm DGAC lift would be $880 per kilometer per meter width of pavement. This cost savings plus the benefit of eliminating a potential stripping layer makes the 40-mm DGAC lift attractive.

However, it must be emphasized that to achieve this cost savings while maintaining performance, the asphalt concrete lifts must be properly compacted.

## 4.4 Rutting Analysis

Rutting failure in Section 543 has been attributed to stripping of the ATPB layer. As indicated in the previous section, the failure in the ATPB and subsequent fatigue cracking in the asphalt concrete layers increased stresses at the top of the aggregate base. In addition, because of intrusion of fines from the aggregate base into the ATPB, the permeability of the ATPB was reduced, causing water to be retained in the ATPB layer. The retention of water allowed the aggregate base to increase in water content, thus making it more susceptible to rutting. While criteria for unbound layer rutting are still under development because of the complex state of stresses in the unbound materials, a relatively straightforward method is to determine the ratio of the applied stress to the stress required to cause shear failure in the material.

Based on preliminary laboratory triaxial compression test data for untreated granular materials, stresses to cause failure are in the range of 250 to 800 kPa for confining pressures ranging from 0 to 105 kPa. These results are based on tests conducted on specimens compacted to a relative compaction of 95 percent and optimum moisture content based on California Test Method 216. Since computed vertical stresses were in the range of 30 to 50 kPa for a 40-kN load (see Table 14), stress ratios of applied stress to stress to failure were in the range of 0.03 to 0.2. Ratios below about 0.8 are not expected to cause failure in untreated aggregate base.(*13*)

The significant amount of rutting in the aggregate base (10 mm at the end of HVS trafficking) was due to the increased stress produced by the 100-kN load. Computed vertical stresses on top of the aggregate base were in the range of 70 to 120 kPa before HVS trafficking. Due to the progressive failure of the ATPB, it is believed that the lack of confining pressure, loss

of fine particles, and increase in moisture content significantly reduced the required stress to failure in the aggregate base, thereby increasing the stress ratios and making the aggregate base susceptible to rutting.

A similar approach was used to assess subgrade performance. Estimated stresses to failure under unconfined conditions were approximately 200 kPa for a moisture content of 16 percent. Compute stresses were in the range of 20 to 50 kPa. Therefore, stress ratios were in the range of 0.1 to 0.25. For cohesive subgrades, rutting failure is not expected to occur if stress ratios are below 0.5.(*13*)

Recommendations to improve the rutting performance of unbound materials include increasing the in-place density of these materials. The laboratory tests conducted on the unbound materials used in the Goal 5 project substantiate the improvement in performance due to increase in density.(*14*)

## 5.0 SUMMARY AND CONCLUSIONS

This report has presented the results of the accelerated pavement testing program for Section 543 of the Goal 5 research project. This section is a flexible pavement which includes 75 mm of an ATPB layer between the asphalt concrete and the aggregate base layers. Included in the report are the analyses of the four stages of testing considered in the Goal 5 test plan. Test program results provide recommendations relative to the use of ATPB layers in flexible pavement structures.

The test program for Section 543 started in May 1999 and was completed in March 2000. Under HVS trafficking, a total of $1.197 \times 10^6$ repetitions were applied on the section, including $236 \times 10^3$ repetitions of the 40-kN dual wheel load, $332 \times 10^3$ of the 80-kN load, and $629 \times 10^3$ of the 100-kN load. Trafficking was performed under "wet base" conditions accomplished using a water infiltration system. The wet conditions were considered representative of infiltration associated with precipitation during an average peak week of 51.3 mm, typical for Eureka, CA (California North Coast climate region).

Initial rutting and deflection data collected during HVS trafficking under the 40- and 80-kN loads indicated that the pavement performed about the same as similar sections tested under dry conditions. During the 100-kN loading, section performance deteriorated significantly as evidenced by an increased rate of surface rutting and fatigue cracking. The section initially failed according to a surface rutting criterion of 12.5 mm. Associated forensic data attributed the failure to a reduction in stiffness in the ATPB layer, which resulted from stripping of the ATPB caused by its saturated state and traffic loading as well as intrusion of fines from the untreated aggregate base.

In-depth elastic deflection and permanent deformation measurements obtained during traffic loading indicated a problem in the area above and below the interface of the ATPB and

the aggregate base. Subsequent sampling of materials during the forensic study indicated that the ATPB exhibited significant stripping in some locations in the trafficked areas. At other locations, air-void contents of the ATPB in the trafficked area were less than obtained from cores extracted in the non-trafficked areas.

Percolation tests conducted on the trafficked areas and outside the trafficked areas indicated a significant reduction in the desirably high initial permeability of the ATPB layer. Examination of the open trench during the forensic study confirmed that fine particles from the aggregate base had infiltrated and clogged the ATPB layer.

FWD testing conducted before and after HVS trafficking indicated that the ATPB exhibited a significant loss in stiffness with the stiffness approaching that of the unbound material. Due to the reduced stiffness of the ATPB, significant rutting occurred on top of the aggregate base due to the lack of confinement resulting from the reduced stiffness of the ATPB together with cracking of the asphalt concrete layers. The increase in rutting in the aggregate base resulted from an increase in the bending stresses at the bottom of the asphalt concrete layers producing an accelerated increase in surface cracking. The limited number of cores extracted along the centerline of HVS trafficking indicated that cracking occurred in all asphalt concrete lifts. These cores also indicated that no bond existed between asphalt concrete lifts.

## 5.1 Conclusions

From the results of the tests on Section 543 and associated response and performance analyses, the following conclusions are drawn:

1. The stiffness of the ATPB was significantly reduced due to stripping, which resulted from high stresses (both pore water and interparticle) and the presence of water during traffic loading. Moreover, the prime coat on the untreated aggregate

base was ineffective in preventing the migration of fines from the aggregate base into the ATPB.

2. Intrusion of fines from the aggregate base into the ATPB reduced the permeability of the ATPB layer by about three orders of magnitude (from about 1 cm/s to $10^{-3}$ cm/s). This filling of voids in the ATPB resulted in a system in which additional water was retained in the ATPB; the higher degree of saturation resulted in reduced stiffness which led to accelerated deterioration of its load carrying capability.
3. Section 543 failed by rutting due to reduced stiffness in both the ATPB and the aggregate base. The rapid increase in rutting also contributed to acceleration in surface cracking because of the significant increase in tensile strains in the asphalt concrete layer.

## 5.2 Recommendations

1. While the ATPB can provide an increased structural capacity to asphalt concrete pavement when loaded under dry conditions, it is imperative that the ATPB be designed to be resistant to stripping and consequent loss in stiffness, should water be retained in the ATPB due to a blocked drainage system.
2. Improved ATPB performance necessitates an improved mix design procedure, improved drainage design, and improved construction and maintenance procedures. In terms of mix design, use of an increased asphalt content and the use of a modified binder may reduce the susceptibility of the ATPB to water damage.

3. Improved drainage design requires the use of a filter layer (e.g., filter fabric) adjacent to the ATPB to minimize the intrusion of fines from the untreated base since the prime coat is not sufficient. In addition, edge and transverse drains must be maintained to prevent becoming clogged with fines.
4. The use of ATPB to intercept water entering through the pavement surface should be reconsidered. As an alternative, if the permeability of the asphalt concrete is reduced by means of improved compaction, a sufficient thickness of asphalt concrete is provided to mitigate the potential for load associated cracking, and the degree of compaction of the aggregate base is increased, the need for the ATPB between the asphalt concrete and the aggregate base could be eliminated.

## 6.0 REFERENCES


1. Harvey, J., M.O. Bejarano, A. Ali. *Test Plan for Goal 5: Performance of Drained and Undrained Flexible Pavement Structures under Wet Conditions.* Pavement Research Center, Cal/APT Program, Institute of Transportation Studies, University of California, Berkeley.

2. Harvey, J., Chong, A., Roesler, J. *Climate Regions for Mechanistic-Empirical Pavement Design in California and Expected Effects on Performance*. Draft report prepared for California Department of Transportation. Pavement Research Center, CAL/APT Program, Institute of Transportation Studies, University of California, Berkeley. June 2000.

3. Harvey, J., B-W Tsai, F. Long, and D. Hung. *CAL/APT Program: Asphalt Treated Permeable Base (ATPB), Laboratory Tests, Performance Predictions and Evaluation of Caltrans and Other Agencies Experience.* Report prepared for the California Department of Transportation. Pavement Research Center, CAL/APT Program, Institute of Transportation Studies, University of California, Berkeley. June 1999.

4. Bejarano, M., J. T. Harvey, A. Ali, M. Russo, D. Mahama, D. Hung, and P. Preedonant. *Performance of Drained and Undrained Flexible Pavement Structures under Wet Conditions: Test Data from Accelerated Pavement Test Section 544-Undrained.* Report in process for the California Department of Transportation. Pavement Research Center, Institute of Transportation Studies, University of California, Berkeley. Expected date of publication: June 2004.

5. Bejarano, M., J. T. Harvey, A. Ali, M. Russo, D. Mahama, D. Hung, and P. Preedonant. *Performance of Drained and Undrained Flexible Pavement Structures under Wet Conditions: Test Data from Accelerated Pavement Test Section 545-Undrained.* Report in process for the California Department of Transportation. Pavement Research Center, Institute of Transportation Studies, University of California, Berkeley. Expected date of publication: June 2004.

6. Harvey, J. T., L. du Plessis, F. Long, S. Shatnawi, C. Scheffy, B-W. Tsai, I. Guada, D. Hung, N. Coetzee, M. Reimer, and C. L. Monismith. *Initial CAL/APT Program: Site Information, Test Pavement Construction, Pavement Materials Characterizations, Initial CAL/APT Test Results, and Performance Estimates.* Report prepared for the California Department of Transportation. Report No. RTA-65W485-3. Pavement Research Center, CAL/APT Program, Institute of Transportation Studies, University of California, Berkeley, June 1996, 305 pp.

7. Ullidtz, P. *Pavement Analysis.* Elsevier Publishing Company, 1987.

8. Harvey, J., J. Prozzi, J. Deacon, D. Hung, I. Guada, L. du Plessis, F. Long, and C. Scheffy. *CAL/APT Program: Test Results from Accelerated Pavement Test on Pavement Structure Containing Aggregate Base (AB)--Section 501RF.* Report prepared for the California Department of Transportation. Pavement Research Center, CAL/APT Program, Institute of Transportation Studies, University of California, Berkeley. Draft submitted September 1997. Final submitted April 1999.

9. Harvey, J., M. O. Bejarano, A. Fantoni, A. Heath, and H. C. Shin. *Performance of Caltrans Asphalt Concrete and Asphalt-Rubber Hot Mix Overlays at Moderate Temperatures – Accelerated Pavement Testing Evaluation.* Draft report submitted to California Department of Transportation. Pavement Research Center, CAL/APT Program, Institute of Transportation Studies, University of California, Berkeley. July 2000.

10. Harvey, John T., Louw du Plessis, Fenella Long, John A. Deacon, Irwin Guada, David Hung, Clark Scheffy. *CAL/APT Program: Test Results from Accelerated Pavement Test on Pavement Structure Containing Asphalt Treated Permeable Base (ATPB) Section 500RF.* Report No. RTA-65W485-3. Report Prepared for California Department of Transportation. Pavement Research Center, CAL/APT Program, Institute of Transportation Studies, University of California, Berkeley. June 1997.

11. Harvey, J., I. Guada, C. Scheffy, L. Louw, J Prozzi, and D. Hung. *CAL/APT Program: Test Results from Accelerated Pavement Test on Pavement Structure Containing Asphalt Treated Permeable Base--Section 502CT.* Draft report submitted to California Department of Transportation. Pavement Research Center, CAL/APT Program, Institute of Transportation Studies, University of California, Berkeley. February 1998.

12. Harvey, J., D. Hung, J. Prozzi, L. Louw, C. Scheffy, and I. Guada. *CAL/APT Program: Test Results from Accelerated Pavement Test on Pavement Structure Containing Untreated Aggregate Base--Section 503RF.* Draft report submitted to California Department of Transportation. Pavement Research Center, CAL/APT Program, Institute of Transportation Studies, University of California, Berkeley. December 1997.

13. Bejarano, M. *Subgrade Soil Evaluation for the Design of Airport Flexible Pavements.* Ph.D. thesis, University of Illinois, Urbana-Champaign. 1999.

14. Heath, A. C. *Modelling Unsaturated Granular Pavement Materials using Bounding Surface Plasticity.* Ph.D. thesis, University of California, Berkeley. 2002.